NOTE TO USERS

BOND BETWEEN PORTLAND CEMENT PASTE AND AGGREGATE

39

by

Elmer Lewis Munger

A Dissertation Submitted to the
Graduate Faculty in Partial Fulfillment of
The Requirements for the Degree of
DOCTOR OF PHILOSOPHY

Major Subject: Theoretical and Applied Mechanics

Approved:

Signature was redacted for privacy.

In Charge of Major Work

Signature was redacted for privacy.

Head of Major Department

Signature was redacted for privacy.

Dean of Graduate College

Iowa State College

1957

TABLE OF CONTENTS

	Page
INTRODUCTION	1
DISCUSSION OF THE PROBLEM	16
Solid State Forces	16
Amorphous Materials	28
Setting and Hardening of Portland Cement	35
Concrete Aggregate Minerals	43
Surface Phenomena	50
HYPOTHESIS OF BONDING MECHANISM	58
TEST PROCEDURES AND RESULTS	69
Principal Test Data	69
Tension briquet	69
Materials	69
Fabrication and test	74
Supplemental Test Data	78
Specific gravities and absorption	78
Mortar tension specimen	78
Effect of surface smoothness	89
Spherical inclusion	89
INDEPENDENT DATA	99
DISCUSSION OF RESULTS	101
Tensile Strength Test	101
Oxygen Numbers	116
Correlations	123
Tensile Test Stress Component/Modulus of Rupture Ratio	130
Effect of Surface Smoothness	135
Spherical Inclusion	138
CONCLUSIONS	141
RECOMMENDATIONS FOR FURTHER STUDY	142

TABLE OF CONTENTS (Continued)

	Page
REFERENCES CITED	148
ACKNOWLEDGMENTS	151

LIST OF FIGURES

Figure		Page
1	Per cent ionic character bonding	20
2	Ion adsorption diagrams	34
3	Silicate polymerization	36
4	Afwillite-basal plane	38
5	Quartz-unit cell, β form	46
6	Orthoclase feldspar - one-eighth unit cell, sanidine	48
7	Calcite-unit rhombohedron	51
8	Polarization and surface distortion of crystal lattice at free space surface	53
9	Geometry of tensile test specimen	70
10	Photographs of tensile test specimen molds and testing apparatus	76
11	Electron micrographs, 5600X, Sawn feldspar	92
12	Electron micrographs, 5600X, Sawn feldspar	94
13	Electron micrographs, 5600X, polished feldspar	96
14	Tensile test stress components - sepiolite	102
15	Tensile test stress components - mortar	103
16	Tensile test stress components - glass	104
17	Tensile test stress components - calcite	105
18	Tensile test stress components - chert	106
19	Tensile test stress components - feldspar	107
20	Tensile test stress components - quartz	108
21	Tensile test stress components - beryl	109

LIST OF FIGURES (Continued)

Figure		Page
22	Tensile test stress components - spodumene	110
23	Effective oxygen ions vs average tensile strength	128
24	Effective oxygen ions vs tensile strength (Thorvaldson's data)	129
25	Average tensile test strength/modulus of rupture ratios	132

LIST OF TABLES

Table		Page
1	Electronegativity values of the lighter elements	21
2	Effect of concentration of reactants on the physical character of barium sulfate (L = 0.002 g/l)	33
3	Hydration of Portland cement	40
4	Setting, hardening, and ageing of Portland cement	41
5	Mortar-aggregate tensile test stress components	79
6	Mortar flexural test moduli of rupture	83
7	Specific gravities and absorptions	88
8	Mortar tensile strengths	90
9	Supplemental tensile test series (3-4 day strengths, glass aggregate)	98
10	Tensile strengths (psi) of briquets made with various minerals as aggregates (1:4 by volume) (Thorvaldson's data)	100
11	Chemical compositions of aggregate materials, oxygen atom numbers, and percentages ionic character bonding	117
12	Oxygen numbers, rates of absorption, and average tensile strengths	121
13	Oxygen numbers and tensile strengths (Thorvaldson's data)	122
14	Product moment correlations and t values	124
15	Average tensile test strength/modulus of rupture ratios	131

INTRODUCTION

In a general way the behavior of Portland cement and the properties of the hardened water-cement paste have been known since the formal designation of the material by Joseph Aspdin, as recorded in his British patent 5,022, dated December 18, 1824. The behavior of the new material differed primarily in degree from that of the earlier natural cements and hydraulic limes. The importance of the argillaceous ingredients of the calcined mixture had already been noted by J. F. John (1819), L. J. Vicat (1818), Descotel (1813), James Frost (1811), Joseph Parker (1796), and John Smeaton (1791). To the latter belongs not only the credit for the first clearly recorded understanding of the importance of including clay in the raw mixture, but also credit for the first noted comparison of the concrete produced to "the best merchantable Portland stone in solidity and durability". (4, pp. 6-11)[1]

The material known as Portland cement has varied somewhat from time to time. A recent definition of long standing is that of ASTM Designation C9-30 (1, p. 25):

---

[1] Numbers in parenthesis refer to the list of references cited.

> Portland cement is the product obtained by finely pulverizing clinker produced by calcining to incipient fusion an intimate and properly proportioned mixture of argillaceous and calcareous materials, with no additions subsequent to calcination excepting water and calcined or uncalcined gypsum.

The latest definition, recognizing current practices in the cement industry of the United States, is that of ASTM Designation C150-49 (3, p. 1):

> Portland cement is the product obtained by pulverizing clinker consisting essentially of hydraulic calcium silicates, to which no additions have been made subsequent to calcination other than water and/or untreated calcium sulfate, except that additions not to exceed 1.0 per cent of other materials may be interground with the clinker at the option of the manufacturer, provided such materials in the amounts indicated have been shown to be not harmful by tests carried out or reviewed by Committee C-1 on Cement.

The material so defined may be mixed with water and appropriate amounts of inert filler, or aggregate, in water-cement ratios by weight varying from about four-tenths to somewhat over unity, and produce a hardened paste which binds the aggregate together into concrete of dependable properties.

The development of these properties takes place in two more or less clearly defined steps. First, within a few hours after the addition of the mixing water, there is the complex of phenomena described as "setting", during which the paste alters from its initially plastic state to become a rigid mass of appreciable strength. The rate of development

of this strength is measured empirically in terms of the time required for the neat-cement paste to develop resistance to the penetration of calibrated needles of specified size, shape, and weight in the standard tests for initial and final set. (ASTM Designation C191-49. 2, p. 188) Following this process of setting, the water-cement paste will continue to gain strength, or "harden", for an extended period of time, so long as a favorable temperature is maintained, and moisture is available. While the rate of overall strength gain decreases rapidly after the first few weeks, measurable strength gain persists for many months.

Once the constituent raw materials of Portland cement were clearly established, the study of the material continued with an effort to identify the chemical compounds and the crystal forms present in the hardened clinker. For several years these efforts were largely speculative, and depended primarily on the chemical formulas of the constituent materials, and chemical analyses of the resultant clinker. Two independent studies, those of Henri Le Chatelier, 1882-1887, and A. E. Tornebohm, 1897, are generally accepted as having first taken full advantage of a consideration of the physical characteristics of the materials involved, as indicated by microscopic study and, in the second case, by specific gravity separations of the clinker particles.

Le Chatelier describes the constituents of the clinker as follows (18a, and in 4, pp. 65-67):

> (1) Colorless crystals, with weak double refraction, with square or hexagonal cross sections and very clear borders much resembling those of the cube. It is by far the most abundant constituent.
>
> (2) In the space between these crystals, a ground mass, the color of which is always dark and varies from a yellow red to a greenish brown. Its double refraction is stronger than that of the preceding material, but it does not possess any clear crystalline contours.
>
> (3) Beside these two essential elements, accessory elements are frequently found, varying in different samples:
>
> (a) Crystalline sections of forms and dimensions analogous to those first given, but which are distinguished from them by a light brownish, slightly yellowish color, a complete absence of transparency, and by very fine striae inclined to each other at about 60°. This constituent, although scarcely plentiful, is found, however, in almost all samples of cement of good quality.
>
> (b) Very small crystals of sufficiently strong double refraction to give polarization colors. This constituent is always in small quantity and is sometimes entirely absent. It is found especially in underburned cements.
>
> (c) Certain forms without action upon polarized light and of negative character which do not give any distinguishing test.

On the basis of chemical studies, Le Chatelier concluded that the principal hydraulic constituent of Portland cement was $3CaO \cdot SiO_2$.

Tornebohm, on the other hand, following up his microscopic examination and specific gravity separation by chemical analysis, gave characteristic names to the several constituents as he identified them, and concluded that

alite, which he called the most common crystalline material, had the formula $9(3CaO \cdot SiO_2) + 9CaO \cdot 2Al_2O_3$. Other formulas were more involved, to the point of being considered indeterminate. The various materials were named as follows (in 4, p. 68):

(1) Alite, referred to above as the most common crystalline material, consisted of colorless crystals of weak birefraction, rectangular or hexagonal. These crystals showed a high index and biaxial interference figures.

(2) Belite consisted of small rounded grains with no definite crystal form, biaxial, and often striated. It was characterized by a high index, a greasy yellow color, and bright interference colors.

(3) Celite was often present in the form of rods, especially in underburned clinker, while in well burned clinker it formed the filling material and magma from which alite separated. Tornebohm stated that it was easily recognized by its dark orange-yellow color and its strong birefraction.

(4) Felite consisted of usually rounded grains, sometimes elongated, and usually striated perpendicular to elongation. A colorless biaxial compound with strong birefringence, it was found in variable quantity, and was often absent. The index was high, nearly that of belite, which material it seemed to replace.

(5) Isotropic residue was described as a colorless amorphous material of an index as high as or higher than that of alite. It constituted a filling material which was not always easily distinguished from alite.

A general sort of agreement may be found between the constituents of clinker as described by Le Chatelier and by Tornebohm. However, the descriptions are not generally considered precise enough to be of other than historical value. (4, pp. 68-69)

Numerous other investigators studied the constitution of Portland cement during this general period. Clifford Richardson, 1904-1905; Wilhelm Michäelis, 1867-1909, and E. D. Campbell and A. H. White, 1902-1922, all contributed in one way or another to a body of thought which favored the general theory of solid solutions in Portland cement clinker. Others, particularly W. Asch and D. Asch, and Ernest Martin, prepared elaborate structural formulas for the constituents of Portland cement. The former based their work on a hexite-pentite theory for which little support appears to have been offered. The latter based his work on the assumption of a normal silicic acid, $Si(OH)_4$, of rather special characteristics, and either acidic or basic valences for silicon. Neither the early approach to solid solution theories nor the use of structural formulas appears to have made useful contributions to the presently

accepted views on the subject. (4, pp. 72-81)

Modern information on the constituents of Portland cement clinker has been developed, in a generally chronological order, by extension and refinement of the microscopic methods initiated by Le Chatelier and Tornebohm, by X-ray diffraction techniques, and by correlation and analysis of the combined data available from these two methods of investigation. The application of these methods to the multiphase systems encountered in Portland cement has been facilitated by concurrent advances in chemical techniques, and by improved techniques and instrumentation of high temperature phase research. The techniques and findings are presented in The Chemistry of Portland Cement, by Robert Herman Bogue (4), and The Chemistry of Cement and Concrete, by F. M. Lea (17). These books are generally recognized as definitive works in the field and each contains, in addition to an extensive survey of the subject, detailed references to source material.

The principal constituents of modern Portland cement clinker are:

(1) Tricalcium silicate, $3CaO \cdot SiO_2$, generally designated in the literature as C_3S. The grains are usually well defined, relatively large hexagonal crystals, and have been identified as the alite of Tornebohm's classification. Recent crystallographic studies conducted by Jeffery (15b)

indicate a structural arrangement which may be represented by a formula of the form $Ca_3O(SiO_4)$ for the pure C_3S. The irregular coordinations involved in this grouping are considered to produce a triclinic structure. By the substitution of two aluminum ions for two silicon ions, with the addition of a magnesium ion to maintain the valence balance, an asymmetric unit is formed consisting of $54CaO \cdot 16SiO_2 \cdot Al_2O_3 \cdot MgO$ ($C_{54}S_{16}AM$). The aluminum and magnesium are considered to produce a symmetrical distortion in a structure which cannot adopt a fully stable rhombohedral configuration. Other recent studies by Trömel (26) indicate the possibility of solid solutions between C_3S and C_2S as an explanation for some of the continuing problems concerning the behavior of alite which, for example, has a much higher rate of solution than pure C_3S.

(2) Dicalcium silicate, $2CaO \cdot SiO_2$, generally designated as C_2S. The grains are usually rounded in outline, relatively large, and striated in one or two directions by fine polysynthetic twinning bands. This material is polymorphous, occurring in α, α', β, and γ forms. Depending on the form, it has been identified as the belite or felite of Tornebohm's classification.

(3) Tetracalcium alumino ferrite, $4CaO \cdot Al_2O_3 \cdot Fe_2O_3$, generally designated as C_4AF. Occurring in the matrix surrounding the calcium silicates, and sometimes spoken of a

"light interstitial material", its crystal form is often difficult to distinguish. It has been identified as the celite of Tornebohm's classification.

(4) Tricalcium aluminate, $3CaO \cdot Al_2O_3$, generally designated as C_3A. Also occurring in the matrix surrounding the calcium silicates, and sometimes spoken of as "dark interstitial material", its crystal form is rectangular or prismatic.

Other phases commonly observed are an amorphous dark interstitial material which has been identified as an undercooled liquid (often referred to as glass), free calcium oxide (CaO), and free magnesium oxide (MgO).

Concurrently with the above outlined studies of the compound composition of the Portland cement clinker, studies were made of the hydration process, its products, and the general mechanism by which these products develop the cohesive forces which bind the hardened mass together.

Here, again, the first significant studies are credited to Le Chatelier, during the period 1882 to 1887. (18a, and in 4, pp. 464-470). Beginning by establishing the inadequacy of earlier theories by Lavosier (1765) and Vicat (1837), which theories depended primarily upon a felting together of rigid acicular crystals, Le Chatelier postulated three phases:

(1) The chemical phenomenon of hydration,

(2) The physical phenomenon of crystallization,

and

(3) The mechanical phenomenon of hardening.

The chemical phenomenon of the hydration of Portland cement was assumed to be similar to the simpler, better understood hydration of plaster of Paris.

Carrying the analogy with plaster of Paris into the second phase of the analysis, Le Chatelier concluded that the crystallization of Portland cement takes place from supersaturated solutions, the metastable state of which is the result of marked differences between the solubility of anhydrous or partially hydrated salts and the more completely hydrated salts. As the less soluble material precipitates out the solution is left unsaturated with respect to the anhydrous material, which then dissolves. Eventually all of the cement will have transcrystallized, or passed through the solution phase into the crystalline hydrate. These processes may take place in systems involving several compounds, the more soluble salts going through the sequence first. Materials which affect the degree of solubility will then affect the sequence and the rate of set.

The hardening of the set mass was considered by Le Chatelier to depend on the cohesion of the crystals and their mutual adhesion. The fundamental process of hardening he considered to be due to a splitting up of tricalcium silicate to form monocalcium silicate and calcium hydroxide.

The cohesion of each crystalline product was considered a specific property of that product. The adhesion was considered a variable dependent upon the chemical nature of the bodies in contact, the extent of the contact surface, and the percentage of voids. The effect of excess mixing water in increasing void space was recognized.

Meanwhile Michäelis (in 4, pp. 471-473) was conducting experiments which led him to develop the theory that the hardening and water resistance of cements is due principally to the formation of colloidal hydration products. He considered that essentially monocalcium compounds such as calcium sulfoaluminate, calcium sulfate, and perhaps calcium aluminate and calcium hydroxide, form an initial crystalloidal product. Following this the residual lime enriched saturated solution reacts with the silicates, coagulates rather suddenly, and completes the setting.

Initially low in lime, the hydrogel formed by the sudden coagulation of the cement paste was considered by Michäelis to take up more lime by adsorption. Remaining water is taken up by the interior of the cement grain as hydration proceeds, raising the density of the hydrogel and finally rendering it impermeable. The "inner suction" of the cement grain, by which the hydrogel is hardened, is an important aspect of this theory.

These divergent theories of cement hydration provided

the basis for a continued discussion of their relative merits. Each has had able supporters. The most promising contributions, however, indicate that both crystallization and the formation of colloidal substances are involved in the total hydration process.

M. von Glasenapp (27a, p. 1217) developed an analysis indicating that polycrystalline aggregates must grow from the gel mixtures because of their thermodynamic instability, forming really stable end products of hardening. By this analysis the crystallized end products are probably calcium silicate hydrates. The physical characteristics of the systems involved are such that the alterations described are rather sluggish.

Kühl (16) gave general support to the gel theory as an explanation of the initial setting, but considered that the gel formed by precipitation from supersaturated solutions rather than by swelling of an insoluble material. He further regarded the formation of the gel as a transition phase, followed by the long term process of replacement by a finely crystalline material. He found evidence for the alteration in studies of hydrating samples over many years.

Desch (10, pp. 5, 67-68) pointed out, in discussion before the Faraday Society in 1918, that Le Chatelier worked with dilute solutions, while Michäelis worked with concentrated solutions, and stated further in his concluding

remarks that much of the conflict between the two theories which these men advanced was a difference of terms. He did not consider it especially important

> . . . whether one regards the jelly as a mass of extremely minute interlacing particles or not. . . the essential point is that in the colloidal substance the particles are extremely small, and therefore the surface forces are very important.

Le Chatelier, by his presentation of a paper by Baycoff to the French Academy of Sciences in 1925, may very possibly have intended tacit concurrence in this view, since this paper recognized three stages of hardening of cements as (1) solution, (2) colloidation, and, finally, crystallization. (4, p. 480)

Recent developments in instrumentation are permitting substantial refinements in the observation of the structure of hydrated Portland cement. In the hydration of the separately prepared cement compounds of the clinker, C_3S has been observed to develop: (1) numerous C_2SH_x projections which alter into gel-like globules in a few hours, with faint birefringence after several weeks, and (2) rhombic crystals of $Ca(OH)_2$. C_2S develops a few small projections of C_2SH_x which alter slowly, after several days, to gel-like material. C_3A develops (1) small plates, probably C_4AH_{12-13}, which tend to disappear in a few hours, (2) isometric particles of C_3AH_6, and (3) gelatinous masses of C_3AH_6. C_4AF develops (1) hexagonal plates similar to those

formed by C_3A, (2) trapezohedrons of C_3AH_6 which develop into other isometric forms, (3) vermiform particles believed to be C_3FH_6, and (4) a reddish-brown gel, probably hydrated ferric oxide.

Set cements are observed to have larger proportions of gel, as described above, of composition C_2SH_x.

Electron microscopy and electron diffraction techniques have confirmed the presence of crystalline material in the gel masses. Observed diffraction patterns have included those identified as the completely hydrated afwillite, $C_3S_2H_3$, and the partially hydrated hillebrandite, C_2SH, and tobermorite, CSH(B). Electron diffraction patterns indicating the presence of crystalline material are observed even from masses which have the appearance of amorphous flocs. The developing forms of such flocs, from 1 to 3 microns in diameter, have a tendency to orient themselves, and to develop both concentric and radial thickenings across boundaries, forming interconnecting cross links through the mass. It has been suggested that this mechanism is a possible origin of bonding action. (4, pp. 627-645) Alternatively, it has been reported that crystalline hydration products grow outward from the hydrating cement grains. Consisting individually of foils and ribbons which become folded and buckled, these crystal structures tend to fill the voids between the cement grains and make contact with

each other. Solid state intergrowth at these points of contact has been suggested as the bonding mechanism. (17, p. 223)

DISCUSSION OF THE PROBLEM

Solid State Forces

Consideration of the bond between the paste and the aggregate of Portland cement concrete involves the solid state forces which provide the strength and rigidity of natural minerals. The various types of forces which give rise to these natural solids form the basis for a classification of such solids into five types, which are listed by Seitz (24, p. 1,2) as follows:

a. Metals, characterized by good electrical and thermal conductivity, and formed by the combination of the atoms of electropositive elements.

b. Ionic crystals, characterized by good ionic conductivity at high temperatures, strong infrared absorption spectra, and good cleavage; and formed by a combination of highly electropositive and highly electronegative elements.

c. Valence crystals, characterized by poor electronic and ionic conductivity, great hardness, and poor cleavage; and formed by combinations of the lighter elements in the middle columns of the periodic chart.

d. Semi-conductors, characterized by feeble

electronic conductivity which increases with increasing temperature, crystallize most often in the ionic type of structure, and are generally halides, oxides, sulfides, or selenides. They display a tendency to favor addition of impurities and to disobey simple valence rules.

e. Molecular solids, characterized by low melting and boiling points, and formed by inactive atoms and saturated molecules. They generally evaporate in the form of stable molecules.

Many solid substances have properties that overlap two or more of these ideal types. Classification in any one type is therefore not necessarily unique. Furthermore, many substances casually referred to as solid are more accurately described as supercooled liquids or as gels, so that they may not be adequately classified under any of the above types.

Concrete aggregates are usually natural minerals. Referring to such materials, Palache *et al.*, in their seventh edition of Dana's classic *Mineralogy*, state (20, pp. 1,2):

> Most minerals have the ionic type of bonding, that is, the interatomic binding force consists of an electrostatic attracting force between oppositely charged ions. A small portion of the total number of minerals has a metallic type of bonding, that is, the positive ions are enmeshed in a field of electrons. The native elements (of the metallic type) and perhaps certain of the sulfides are the only minerals having this type of bonding. Diamond, sphalerite, and a number of the sulfides

> have the homopolar type of bonding; that is the atoms are held together by the sharing of electrons from their outer shell. With the exception of the metals and a few sulfides, then, all minerals are predominantly ionic. These latter have been subdivided on the basis of the variation in the strength of the binding force into (1) isodesmic, (2) mesodesmic, and (3) anisodesmic compounds. Most of the minerals (with the exception of the metals and the homopolar compounds) in this volume are isodesmic compounds, that is, the strength of the bondings of the cations with the anions are qualitatively the same, and no discrete units are formed by particular cation-anion groups. In the silicates, which are to be described in Volume III, the silicon-oxygen bond is stronger than that between oxygen and the other cations, and they fall, therefore, into the second division of the crystallochemical classification (mesodesmic). The phosphates, sulfates, arsenates, etc., are in the third division (anisodesmic) because the PO_4, SO_4, AsO_4 groups are discrete units in the structure. All these are grouped in Volume II.

Eitel, in discussing the development of the physical chemistry of the silicates, refers to the variation in type of bonding as follows (12, pp. 8,9):

> The more detailed knowledge of the crystal structures of many compounds showed convincingly that between the purely heteropolar (ionic) and the purely homopolar (covalent) binding in the crystal edifice the transition may be <u>gradual</u>.

In support of this statement, Eitel refers to Pauling (21). Working with the halides, Pauling considers the resonance states of these diatomic molecules, and develops expressions for their various percentages of ionic character bonding. The values obtained are shown to bear a relationship to the electronegativity of the elements involved, electronegativity being "the power of an atom in a

molecule to attract electrons to itself". This relationship is expressed in the equation (21, eq 12-1, p. 69):

$$\% \text{ ionic character bonding} = (1 - e^{-c(x_A - x_B)^2}) \times 100 \quad (1)$$

in which: $c = 0.25$

$(x_A - x_B)$ = electronegativity difference.

It is indicated that this relationship was so evaluated by fitting an appropriate curve to the calculated values for the compounds HI, HBr, HCl, and HF. These values as determined by Pauling are plotted as open circles on the graph of Figure 1, and the curve defined by the above equation is shown as a broken line. Electronegativity values according to Pauling alone (21, Table 11-3, p. 64) are underlined in Table 1.

A later treatment of this same relationship is given by Coulson (8). This author cites Hannay and Smyth for an improved mathematical expression of the relationship of equation (1) above (8, eq 33, p. 134):

$$\% \text{ ionic character bonding} = 16(x_A - x_B) + 3.5(x_A - x_B)^2 \quad (2)$$

This equation is given with the comment that Pauling's equation does not fit the large values of the electronegativity difference $(x_A - x_B)$ as well. Electronegativity values according to Coulson and Pauling are given in Table 1, without underlining. This table is patterned after the

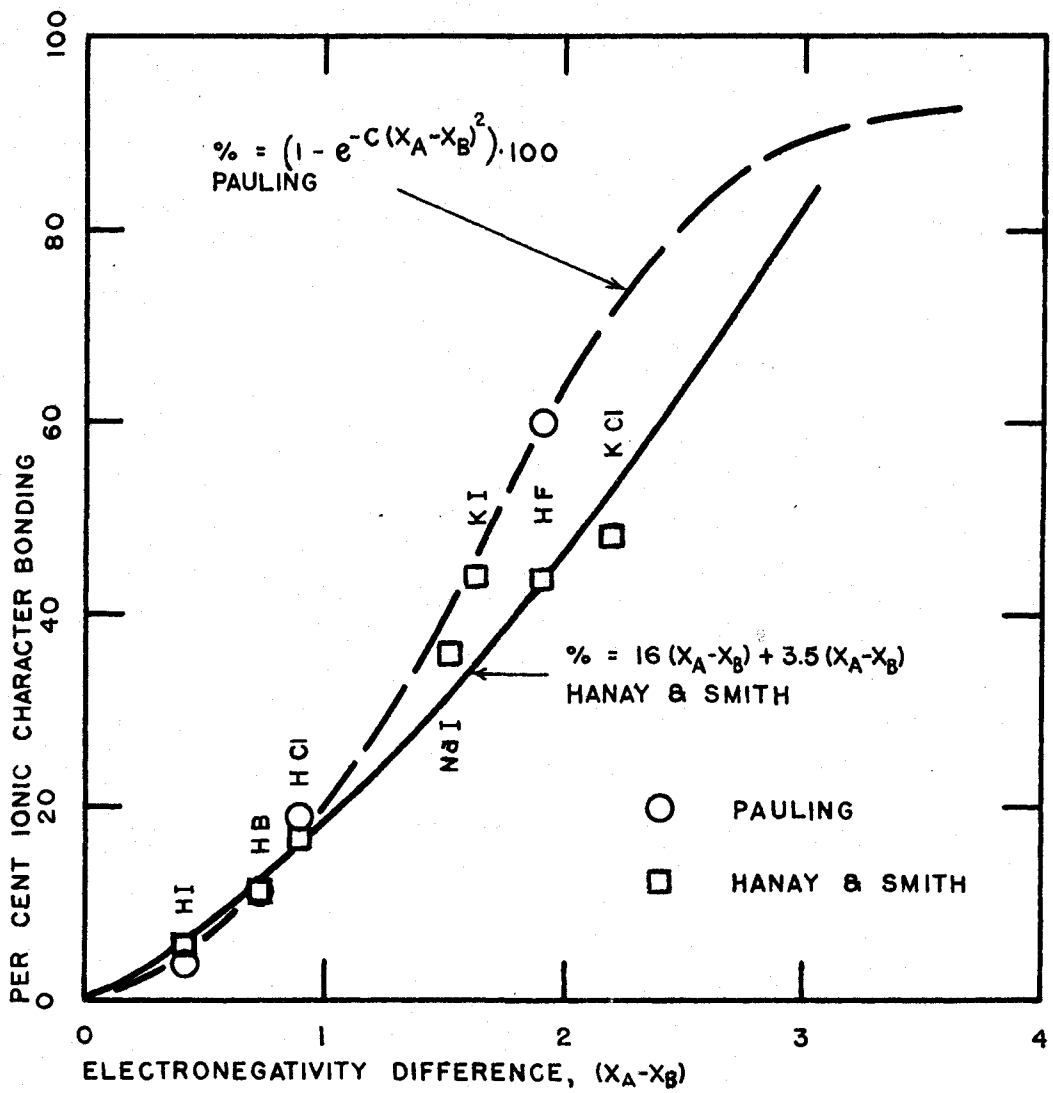

FIG 1 - PER CENT IONIC CHARACTER BONDING

Table 1. Electronegativity values of the lighter elements (see text for references to sources)

H										
2.1										
Li	Be	B	C	N	O	F				
1.0	1.5	2.0	2.5	3.0	3.5	4.0				
Na	Mg	Al	Si	P	S	Cl				
0.9	1.2	1.5	1.8	2.1	2.5	3.0				
K	Ca	Sc	Ti	V	Cr	Mn	Fe	Co	Ni	
0.8	1.0	1.3	1.6	(1.6)	(1.6)	(1.7)	(1.7)	(1.7)	(1.7)	
Cu	Zn	Ga	Ge[a]	As	Se	Br				
(1.8)	(1.8)	(1.8)	1.8	2.0	2.4	2.8				
Rb	Sr	Y	Zr	Cb	Mo	Ma	Ru	Rh	Pd	
0.8	1.0	1.3	1.6	(1.6)	(1.6)	(1.6)	(1.6)	(1.7)	(1.7)	
Ag	Cd	In	Sn	Sb	Te	I[b]				
(1.7)	(1.7)	(1.7)	1.7	1.8	2.1	2.5				
Cs	Ba									
0.7	0.9									

E
n.n value according to Coulson and Pauling

E
n.n value according to Pauling

E
(n.n) value interpolated between values from above sources

[a] Value according to Coulson, 1.7 according to Pauling.

[b] Value according to Coulson, 2.4 according to Pauling.

arrangement of Table X, Coulson (8, p. 134), concerning which it is stated that "Table X shows the expected increase in electronegativity values from left to right along any row of the periodic table, and a decrease down any column." On the basis of these characteristics, values for additional elements have been interpolated. These are enclosed in parentheses in Table 1. It is noted that two elements are given different electronegativity values by Pauling and by Coulson. These are indicated by footnote in Table 1. Coulson's values are given preference because they reflect additional work since the date of Pauling's publication.

Hannay and Smyth's equation is indicated to include consideration not only of calculated values for the hydrogen halides, but also for sodium and potassium iodides, and potassium chloride. The calculated values according to Hannay and Smyth are plotted as open squares on the graph of Figure 1, and the curve defined by equation (2) is shown as a solid line.

The consideration of the resonance relationships by which Pauling analyzes the hydrogen halides is extended by him to include evaluation of the percentage of ionic character bonding of the more complex two-element compounds which have several resonance states. Reasonable agreement with the values obtained from equation (1) is indicated. Since rigorous solutions of the functions involved are not

available, exact agreement cannot be expected.

Eitel applies equation (1) to the more complex compounds of the silicates by computing the electronegativity difference value on the basis of the average electronegativity value of the cations involved. All of the compounds with which he is concerned at this point have the single element, oxygen, as the anion.

A concise discussion of the character of the ionic binding energy as it occurs in natural solids is given by Seitz (24, pp. 77-94). Referring to the relatively simple diatomic halides, sulfides, and oxides, the classical theory of ionic crystals is developed in terms of three energies: (1) electrostatic interaction, or coulomb forces; (2) repulsive interaction, and (3) multipole interaction. The electrostatic interaction energy for two-element crystals is:

$$E_e = \frac{-N_A A_{ro} e_+ e_-}{r_o} \qquad (3)$$

in which: E_e = electrostatic interaction or coulomb force energy,

N_A = Avogadro's number, 6.02×10^{23},

A_{ro} = Madelung constant in terms of r_o,

e_+ = absolute value of positive ion charge,

e_- = absolute value of negative ion charge, and

r_o = cation - anion distance.

The Madelung constant may also be expressed in terms of the cube root of molecular volume or, for cubic crystals, the cube edge length. In using these other expressions the dimensional parameter r_o is replaced by the applicable equivalent dimension. Typical values of the Madelung constant are: for NaCl, $A_{ro} = 1.7476$; for rutile, TiO_2, $A_{ro} = 4.816$; and for corundum, Al_2O_3, $A_{ro} = 25.0312$.

The repulsive interaction energy is:

$$E_r = \frac{b}{r^n} \qquad (4)$$

in which: E_r = repulsive interaction energy,

b, n = empirical constants, and

r = distance between nearest unlike ions.

This expression is due to Born (in 24, p. 76). Setting the total energy of the crystal equal to the sum of equations (3) and (4), expressions for b and n may be developed, and the above equations may be combined:

$$E = \frac{N_A A_{ro} e_+ e_-}{r_o} \left(1 - \frac{1}{n}\right) \qquad (5)$$

in which: E = total crystal energy.

Equation (5) is a statement of the classical theory. However, the application of quantum mechanics to interionic forces has indicated that equation (4) cannot be rigorously correct. Born and Mayer (in 24, pp. 82-94) have replaced this equation by an expression of the type:

$$(r) = ae^{-\frac{r}{\beta}} \qquad (6)$$

in which: (r) = repulsive interaction energy, and

a, β = empirical constants.

These workers have added another expression evaluating the van der Waals interaction attractive force. This expression, also referred to as the dipole-dipole term, involves series limit frequencies of the discrete spectra of the two atoms or ions, and their polarizabilities. Depending upon the data used to evaluate the quantities involved, a considerable range of numerical values is obtained. The total effect of this expression is small in any event, but it is of significance in determining the relative stability of two different lattice types. Further, this term is actually the first of an infinite series. The second term, referred to as the dipole-quadrupole term, was first investigated by Margenau (in 24, p. 86). The third term is referred to as the quadrupole-quadrupole term, and is negligible in cases considered by Seitz.

Finally, the mechanical motion of the atoms or ions in a crystal may be treated as though the atoms or ions were oscillators of various frequencies. According to quantum mechanics, such an oscillator retains energy at the absolute zero of temperature. This retained energy is called the zero point energy, and must be included with other energy terms when considering cohesive energy.

The total energy of the above outlined terms, using the quantum mechanics expression for repulsive interaction energy, is expressed in the Born-Mayer equation. Values of the separate terms, and the totals, are given for various compounds in Table XXIX, p. 88, Seitz (24). These values, together with the experimentally determined energy from Table XXIV, p. 80, Seitz (24), are listed below for sodium chloride which, because of its wide occurrence and excellent conformance to type, is one of the most accurately evaluated minerals of the ionic crystal classification. Energy values are expressed in kilogram calories per mole.

Madelung, or electrostatic interaction energy	204.3
Repulsive interaction energy	- 23.5
van der Waals, or dipole-dipole energy	5.2
Dipole-quadrupole energy	0.1
Zero point energy	- 1.7
Total	184.4
Experimentally determined energy	182.8

The principles of quantum mechanics as they relate to the character of valence bonding forces are outlined by Cartmell and Fowles (7). The fundamental concept involved is that of the energy quantum, which was formulated by Planck in 1900, and used by him in deriving an expression for black-body radiation. This same concept was used by

Einstein in 1905 to explain the photoelectric effect, and by Bohr in 1913 to explain the spectrum of the hydrogen atom.

Bohr's model of the atom postulates discrete, quantized circular orbits for the movement of the electron about the nucleus of the hydrogen atom. In the application of this model it is necessary to apply four rather arbitrary quantum numbers. A more formal model is described by the Schrödinger wave equation, which defines the statistical probability of the occurrence of the electron at any point in space about the isolated nucleus. The distribution defined by this equation is sometimes referred to as the electron cloud surrounding the nucleus.

The solutions to the Schrödinger equation are rigorous only for the single electron of the hydrogen atom. Approximations have been worked out, particularly by Hartree and his colleagues, to describe the more complex multi-electron atoms. A characteristic arrangement of electrons in concentric shells is indicated. The mechanism of valence bonding is explained by the overlap of orbitals defined in these approximate solutions. In terms of the electron cloud concept, this amounts to an interpenetration of the electron clouds of the nucleii involved so that, by sharing electrons, they build up complete, stable electron shells. Evidence for this phenomenon is provided in the electron densities

determined by the methods of Bragg (5). A valence crystal such as diamond is found to have relatively high electron densities between atoms. An ionic crystal such as sodium chloride shows large areas of relatively low electron densities between atoms. Quartz, which is intermediate between these two type crystals in bonding characteristics, shows some interpenetration of electron shells, together with some areas of low electron density. (12, pp. 4-7)

Amorphous Materials

In addition to the five types of solids as classified by Seitz, there are two other groups of natural materials which may have substantial structural stability. These are the glasses and the gels.

Technically, a glass may be described as a super-cooled liquid. From the definitions of the crystalline solids, this means that the atoms present in the glass are random in orientation. The liquid has cooled into the solid state without opportunity for crystallization. Various radicals may, and in some cases practically always do occur as distinct forms; for example, the SiO_4 group is believed to be present even in molten silicate glass (12, p. 251). However, the periodic regularity which characterizes the crystalline materials is absent, even in the essentially pure SiO_2 composition of fused silica.

Glass occurs in nature as obsidian, a rapidly cooled silicate volcanic rock of varying composition, which may form the entire mass of a body of rock, or the interstitial matrix of a partially crystalline body. Obsidians are not geologically stable. They tend to form spherulites, centers of crystallization about which the elements present take up more or less regular crystal patterns. This same phenomenon is observed in old man-made glass, especially when it has been subject to the action of ground water. The presence of strong alkalis may also lead to a relatively rapid chemical action with the glass. These characteristics of glass make it unsuitable for a permanent concrete aggregate.

Physically, a gel differs from a glass principally in its manner of formation. Glasses are, as a rule, the products of the cooling of a molten mass. Gels are the products of gelation, which may be due to such causes as increase of concentration because of evaporation of a liquid phase, chemical precipitation of a solid phase, or alteration of phase stability due to some other change, such as change of temperature. The gel is initially characterized by a random orientation of particles of a solid phase, interconnected through and enclosing a liquid phase. The solid phase may be locally molecular or crystalline in character. As the gel undergoes syneresis the arrangement may become more regular, resulting, in some cases, in the formation of

crystalline masses. In other cases the random orientation persists. The denser forms of opal, for example, in which there is essentially no water, are in many ways equivalent to glass.

The formation of sols and gels by condensation or precipitation from solution depends upon a condition of supersaturation. The rate of precipitation and the character of the precipitate are functions of two velocities. The first of these, the initial velocity of condensation of nuclei, or nucleation, is expressed by the Von Weimarn equation (eq (1), (2), 27b, p. 136):

$$W = KJ \frac{(Q-L)}{L} = KJ \frac{P}{L} = KJU \qquad (7)$$

in which: W = initial velocity of condensation of nuclei,

K = empirical constant,

J = variable multiplier, other than following factors,

Q = total concentration of substance to be precipitated,

L = solubility of coarse crystals,

P = absolute supersaturation, and

U = P/L = percentage supersaturation.

The term J accounts for such factors as the viscosity of the reacting medium, the variation in solubility with the size of primary particles, polymerization of the reactant

molecules, molecular complexity of the reactants, adsorption, presence of dust particles, extent of agitation on mixing, specific tendency to form nuclei, and specific tendency to grow on nuclei.

The second velocity, the velocity of growth on nuclei, is expressed by the Nerust - Noyes equation (eq (3), 27b, p. 137):

$$V = \frac{D}{S} \cdot O \cdot (Q - L) \qquad (8)$$

in which: V = velocity of growth on nuclei,

D = diffusion coefficient,

S = thickness of adhering film, and

O = extent of surface.

Equation (7) expresses the velocity of nucleation. The character of the precipitate depends upon the values of both the absolute supersaturation P, and the percentage supersaturation U = P/L. If P is relatively small, discrete crystalline particles tend to be formed. As P becomes larger, the crystal forms become skeletal, and finally give place to sols, amorphous precipitates, or jellies. For any specific two phase system, as the value of P increases, the U = P/L value will increase correspondingly, and the velocity of precipitation will increase. The relative values of Q and L will indicate whether a gel or a sol may be expected. If the solubility is high, a sol cannot be obtained, since

a value of Q sufficient to produce the amorphous form will produce a jelly.

Table 2 is taken from Table 37, p. 138, Weiser (27b), and shows the effect of concentration of reactants on the physical character of barium sulfate precipitates.

The relationships of equations (7) and (8), as illustrated in Table 2, offer an explanation for the fact that early investigators working with dilute solutions of the compounds of Portland cement tended to obtain well defined crystal forms. Investigations with the heavily supersaturated solutions comparable to normal water-cement pastes have produced gel forms. This is also in accordance with these colloid relationships.

The hydrous oxides and silicates are developed in aqueous solutions by stepwise processes. (9, p. 241 et seq.) The polyvalent ions of the transition metals attract and hold water molecules by ion-dipole attractive forces. A representation of the hydrated $Cu(H_2O)_4^{2+}$ ion is shown in Figure 2(a). The number of water molecules which can be attached is determined by the coordination number of the ion and depends, to a considerable extent, on the size of the ion.

The attractive forces between the oxygen atoms of the water and the metallic ion resemble covalent bonds, and are so strong that the bonds holding the hydrogen atoms are

Table 2. Effect of concentration of reactants on the physical character of barium sulfate (L = 0.002 g/l)[a]

Normality of $Ba(CNS)_2$ and $MnSO_4$	P	$U = \frac{P}{L}$	Nature of precipitate
0.00005 to 0.00014	0.000 to 0.006	0 to 3	No precipitate in a year. Microcrystals would be expected in a few years and macrocrystals from large amounts of solution.
0.00014 to 0.0017	0.006 to 0.096	3 to 48	Slow precipitation at U = 8. Momentary sol stage at U = 25. Complete separation in months to hours.
0.0017 to 0.75	0.096 to 43.8	48 to 21,900	Crystal skeletons and needles precipitate in a few seconds at U = 48; Beyond this instantaneous precipitation. Crystals barely recognizable at U = 21,900.
0.75 to 3.0	43.8 to 175.1	21,900 to 87,500	Precipitates, which appear amorphous, form immediately.
3.0 to 7.0	175.1 to 409.0	87,500 to 204,500	Clear cellular jellies.

[a]Table 37, Weiser (27b), p. 138

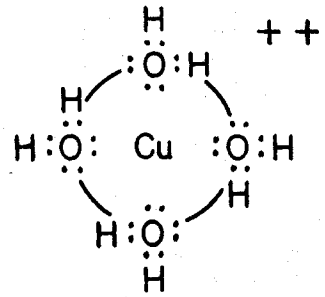

FIG 2 (a) - THE HYDRATED $Cu(H_2O)_4^{2+}$ ION

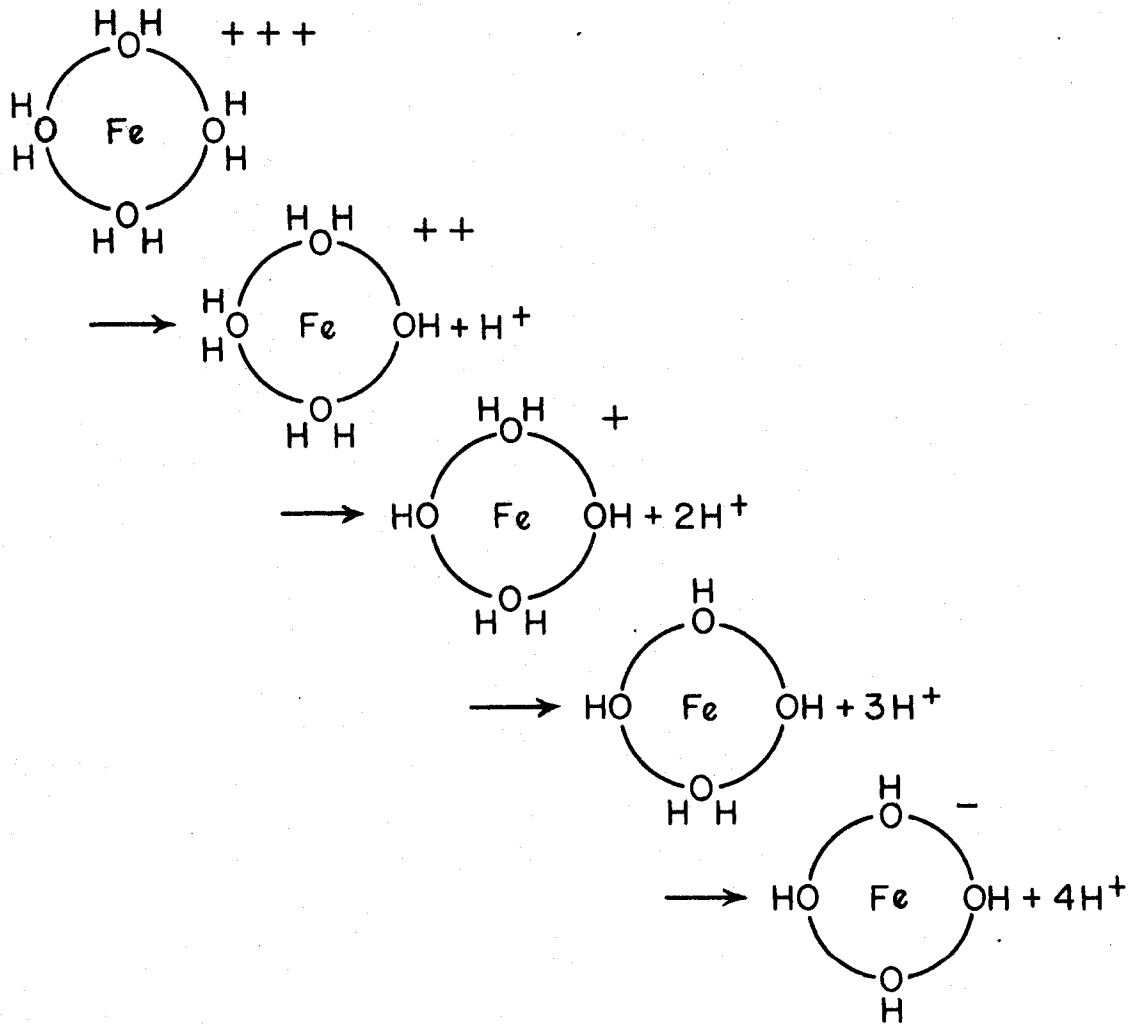

FIG 2(b) - IONIZATION OF THE HYDRATED $Fe(H_2O)_6^{3+}$ ION (ONLY FOUR OF SIX H_2O MOLECULES ARE SHOWN)

FIG 2 - ION ADSORPTION DIAGRAMS

loosened and the hydrated ion becomes acidic. This process is indicated schematically for a ferric ion in Figure 2(b). Only four of the six covalently bound water molecules are shown. The remaining two would be located above and below the ferric ion. The neutral $Fe(OH)_3(H_2O)_3$ is unstable and tends to polymerize with loss of water.

In an anologous manner the silicon ion will become surrounded by four hydroxyl groups, and may also adsorb two H_2O dipoles. The neutral $Si(OH)_4(H_2O)_2$ is also unstable, and polymerizes in the manner indicated schematically in Figure 3(a) (14, Figure 15, p. 58). This process leads to a cross linked high polymer of the composition SiO_2, with uncombined OH and H_2O groups around the margins, schematically indicated in Figure 3(b). Depending upon the conditions of precipitation, the crystal form may be that of cristobalite (9, p. 248), or quartz (6, p. 67).

Setting and Hardening of Portland Cement

Relatively recent x-ray examinations, and electron microscopy and diffraction studies indicate that the optically amorphous gel masses of the hydrated calcium silicates are actually microcrystalline in structure. However, the particle size, in the order of 85 to 100 Å dimension, is that of colloidal particles present in such materials as pure silica gel or organic gelatine. The

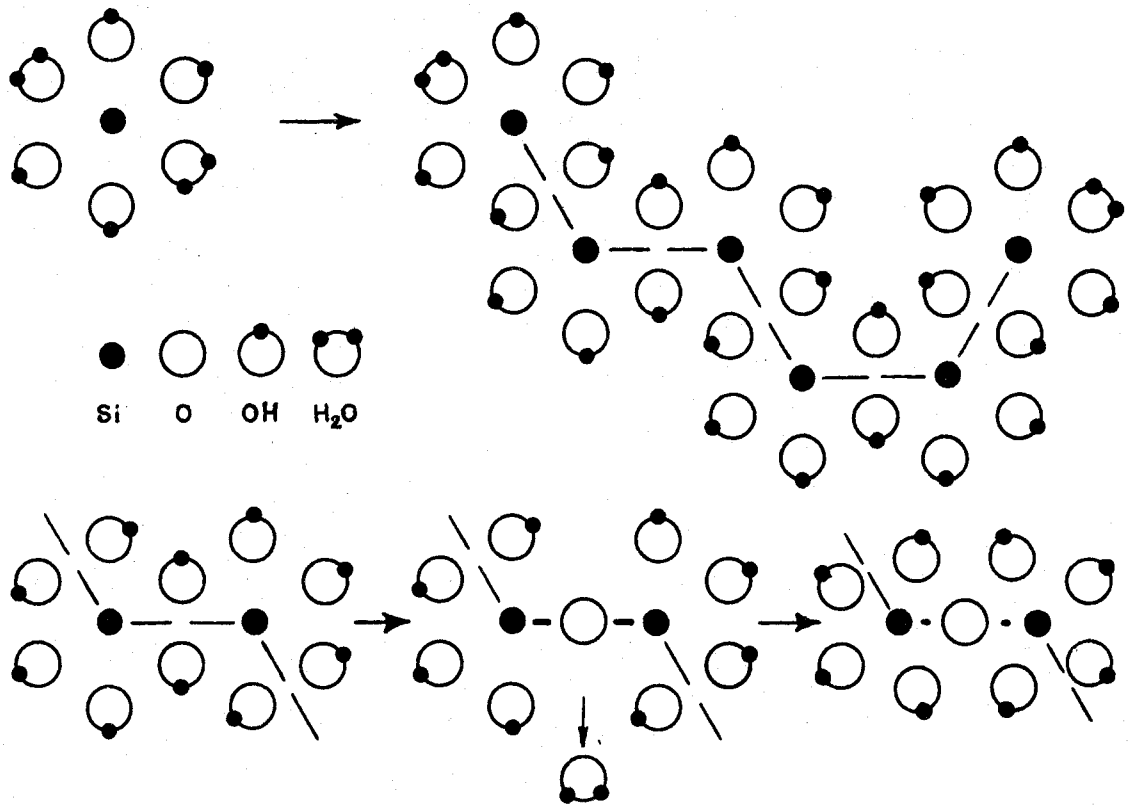

FIG 3(a) - POLYMERIZATION OF ORTHOSILICIC ACID

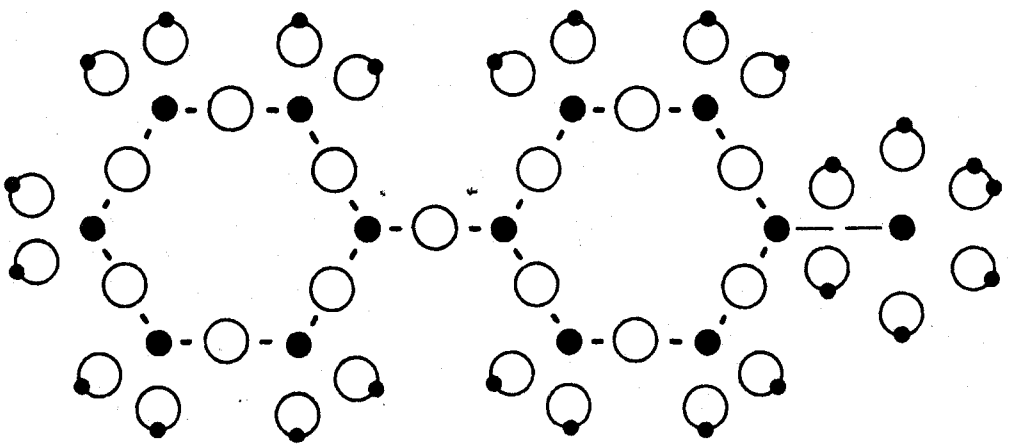

FIG 3(b) - SCHEMATIC REPRESENTATION OF CROSS LINKED SiO_2 POLYMER
(ONLY THREE-FOLD COORDINATION IS SKETCHED, FOURTH
OXYGEN WOULD BE ABOVE OR BELOW CENTRAL SILICON IONS)

FIG 3 - SILICATE POLYMERIZATION

surface area of the set mass is thus very large. This large surface area has a major effect on the properties of the hardened paste.

One of the several natural hydrous calcium silicates, which has been studied in considerable detail, is afwillite, also recorded as a hydration product of Portland cement under special conditions (17, p. 185). It has the formula $3CaO \cdot 2SiO_2 \cdot 3H_2O$, which may be written structurally in the form $Ca_3 \cdot 2H_2O \cdot SiO_3(OH)_2$. The structure of the basal crystal plane of this material is sketched in Figure 4. The oxygen ions, hydroxyl groups, and water molecules are not differentiated. The silicate tetrahedra, in this case, have been identified as $SiO_3(OH)$. (19b, p. 282)

The calcium aluminates, calcium ferrites, and calcium sulphates tend to develop larger crystal forms, appearing under the optical microscope in favorable conditions as discrete crystalline particles of various characteristic patterns, although some of the calcium aluminates are characterized by amorphous gel structures under usual magnifications. Calcium hydroxide is also released as distinct crystals in the hydration of tricalcium silicate and tricalcium aluminate. These materials, both in terms of percentage of material present, and in strength developed, are probably less significant than the calcium silicates in the properties of the hardened water-cement paste. However, it

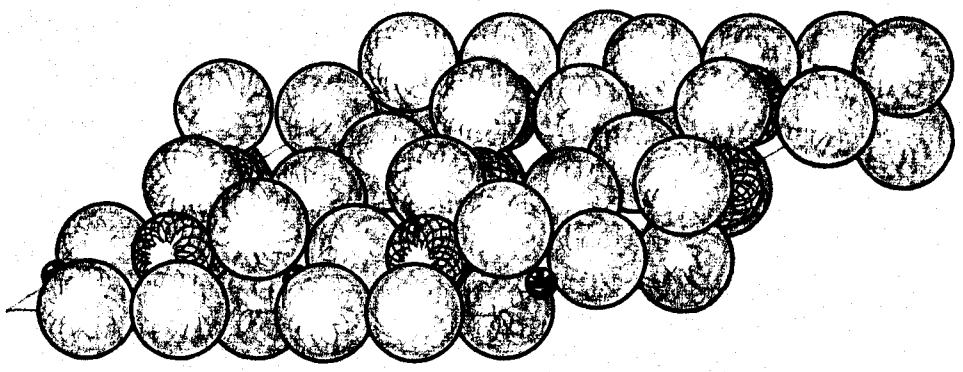

SILICON

CALCIUM

OXYGEN, HYDROXYL ION, OR WATER MOLECULE

FIG 4 - AFWILLITE - BASAL PLANE

AFTER MEGAW (1961)

is significant that the presence of the various ions of these other compounds in the environment of the hydrating cement will affect the equilibrium of the possible end products. It is also fairly well established that numerous complex solid solution phases exist among these various compounds. (4, p. 571-588; 17, p. 170-225)

Lea (17) has tabulated the setting and hardening processes in outline form from two points of view. The hydration of Portland cement is schematically represented in terms of the chemical compounds and mineralogically stable end products in Table 3, which is reproduced from page 208, Lea (17). Stages I, Ia, IV, and IVa belong to the early reaction period, followed by stage II. Stages V and Va will not commence until all of the gypsum is used up, a matter of several hours. Finally, stages III, VI, and VIa are very slow reactions, for which completely descriptive evidence is not available.

The setting, hardening, and aging processes are schematically represented in terms of physical systems and conditions in Table 4, which is reproduced from page 224, Lea (17). The changes from state I to states IIIa and IIIb take place during the setting process. It is possible that an initially hydrous gel is formed, which then undergoes syneresis with the separation out of water to form the metastable gel of state IIIa. Alternatively, it has been

Table 3. Hydration of Portland cement

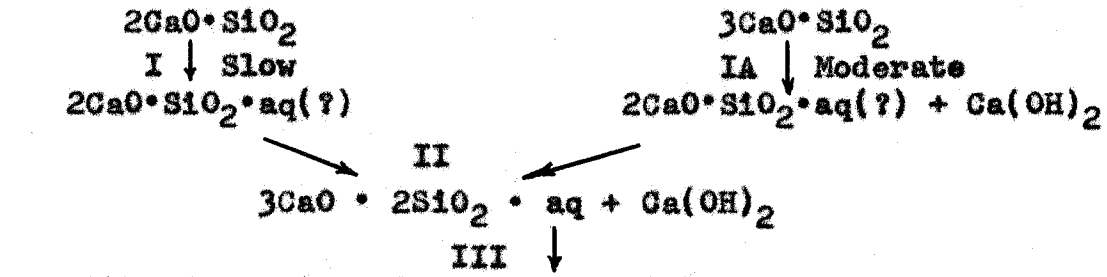

Possible formation of hydrated calcium aluminosilicates and of some silica passing into the aluminaferric oxide solid solutions

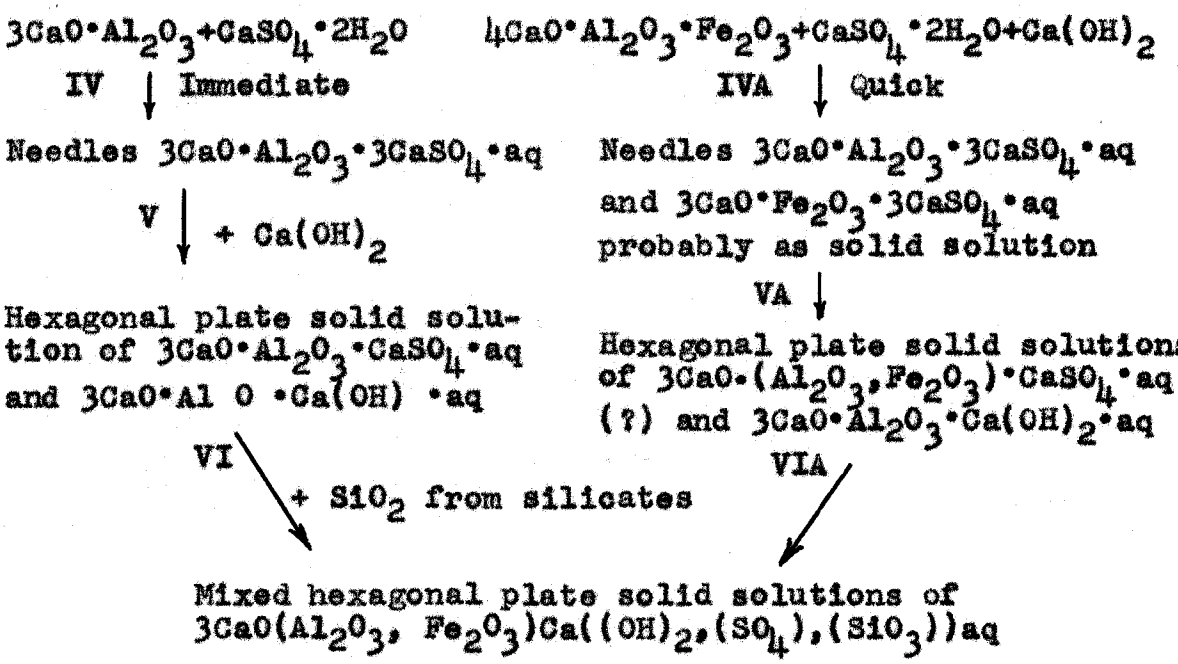

Table 4. Setting, hardening, and ageing of Portland cement

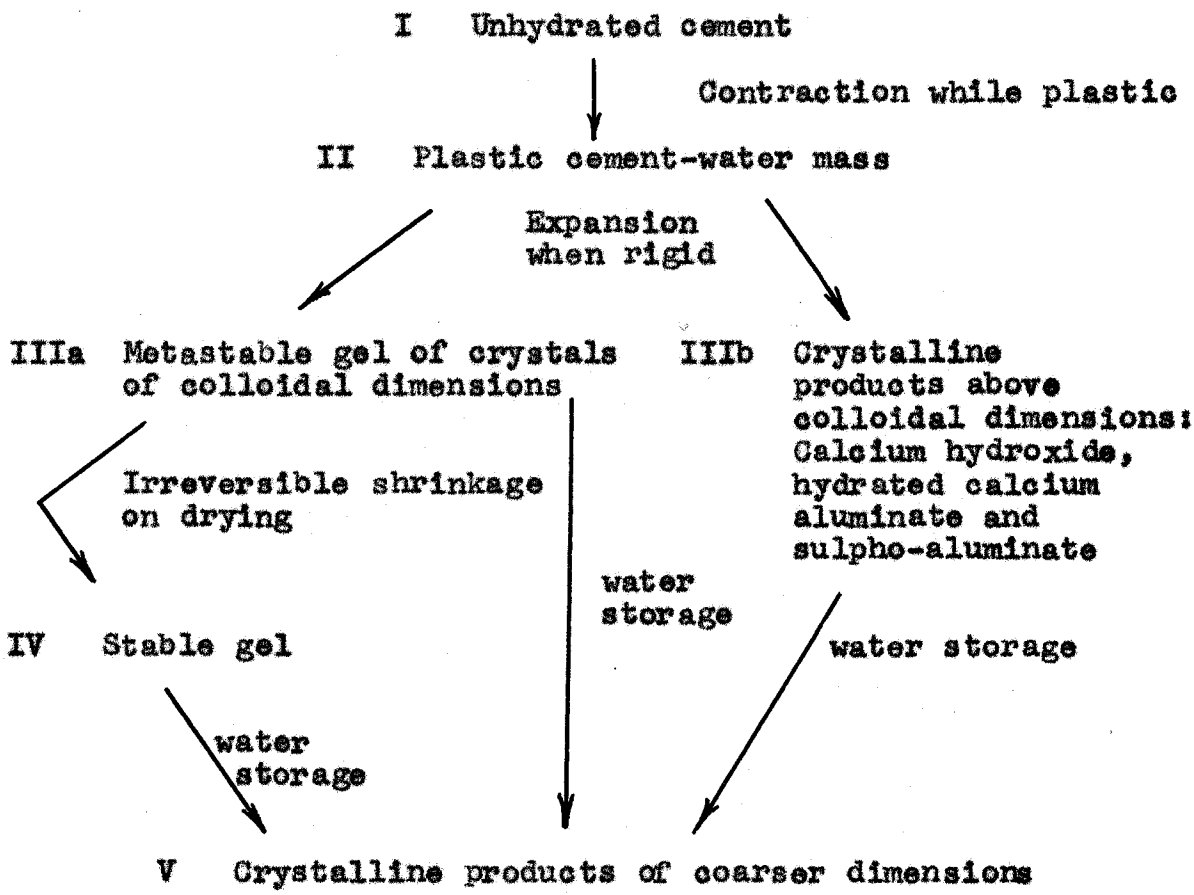

suggested that the calcium silicate gels as originally formed in the hydrating cement mass are in a form more comparable to that reached by a silicate gel only after syneresis. Very possibly a combination of these processes is present.

State IV of Table 4 occurs when the set cement is allowed to dry in air, and may not be fully present in case of continuous water storage. In this latter case, it is probable that the metastable gel of state IIIa persists, at least in part, until the transformation to state V. This latter change, from either states III or IV, is the slow process of stages III, VI, and VIa of Table 3.

The bonding together of the individual particles of the hydrating cement paste has been explained in two general ways. The first, restated in recent years by English workers (Lea, 17, p. 223), is essentially an extension of the interlocking crystal theory of Le Chatelier. The set cement is pictured as a matted felt or meshwork of calcium silicate hydrate crystals consisting individually of foils or ribbons. These grow outward from the hydrating cement grain, and become folded and buckled. At some points of contact between the crystals growing out from adjacent cement grains there exist similarly oriented lattices, so that there is intergrowth by solid state reactions, and a welding together of the mass. The number of such welds, and

the strength of the individual welds, increase as the hydration proceeds, thereby strengthening the entire mass. The growth of these crystal forms fills the voids between cement grains and aggregate particles, binding the whole together. There remain within the mass interstitial voids and capillary channels filled with water, which may be lost upon drying.

Bogue (4, p. 645), representing the general approach of American workers, interprets the available data somewhat differently by giving more emphasis to minute spherical particles which have been observed to form throughout the hydrating mass. Because of their high surface energies, these particles are considered to be subject to strong mutual attraction. This causes coalescence of the individual particles into aggregations up to a few microns in diameter. Favorable orientation of these aggregations leads to cross linkage bonds. The formation and development of these bonds binds the whole mass together. The interstitial voids will persist as a capillary network.

Concrete Aggregate Minerals

The silicate and aluminate minerals constitute the great bulk of the usual concrete aggregates. A brief review of the crystal structure of the concrete aggregates may then begin with a consideration of the structure of these

groups of minerals.

The principles of silicate structures as currently understood are based on the observation that one silicon cation predominantly enters into tetrahedral coordination with four oxygen anions, forming a tetrahedron shaped complex anion $(SiO_4)^{4-}$. This anionic group and, especially in the two dimensional sheets and the three dimensional networks, the geometrically similar $(AlO_4)^{5-}$ anionic group, form the basic geometric building blocks for silicate structures. The general rules by which these tetrahedra are bound together in complex silicates were developed by W. L. Bragg (5). Fundamentally, the tetrahedra are joined at corners only by the powerful primary Si-O-Si bond or, alternatively, in the aluminum silicates, by the almost equally powerful Al-O-Al bond.

On the basis of the number of $(SiO_4)^{4-}$ tetrahedra which are linked together, these structures are classified as nesosilicates (isolated tetrahedrons), sorosilicates (tetrahedrons in pairs, or trigonal, square, or hexagonal rings), inosilicates (tetrahedrons in single, double, or, in rare cases, triple chains), phyllosilicates (tetrahedrons in two dimensional sheets), or tectosilicates (tetrahedrons in three dimensional networks). A unique complex of a central tetrahedron with a tetrahedron linked to each corner occurs in zunyite.

The fundamental silicate mineral is silica, which crystallizes as a tectosilicate. There are various forms, stable under different conditions. The form stable at ordinary temperature and pressure is usually designated as α-quartz. This transforms into the somewhat more symmetric β-quartz at 573° C. A unit cell of the hexagonal crystal of β-quartz is sketched in Figure 5. This crystal lattice, being composed of silicon and oxygen in the proportions SiO_2, linked together in a three dimensionally continuous network of (SiO_4) tetrahedra, is chemically balanced and geometrically stable. It has the highest percentage of valence bonding of any silicate mineral computed in this study and, with one exception, magnesite, the highest valence bonding of any mineral computed. These considerations offer an explanation of its well known rigidity, hardness, and resistance to weathering.

When aluminum ions are substituted for silicon ions in the tetrahedra of this lattice, the basic unit is distorted somewhat because of the larger diameter of the aluminum ion. Perhaps more important, the chemical equilibrium is disrupted. In the simplest case it is restored by the incorporation of alkali cations located in the lattice interstices in coordination with the unbalanced anionic charges of the (AlO_4) tetrahedra. Thus the plagioclase feldspar series contains varying proportions of sodium and calcium, and orthoclase

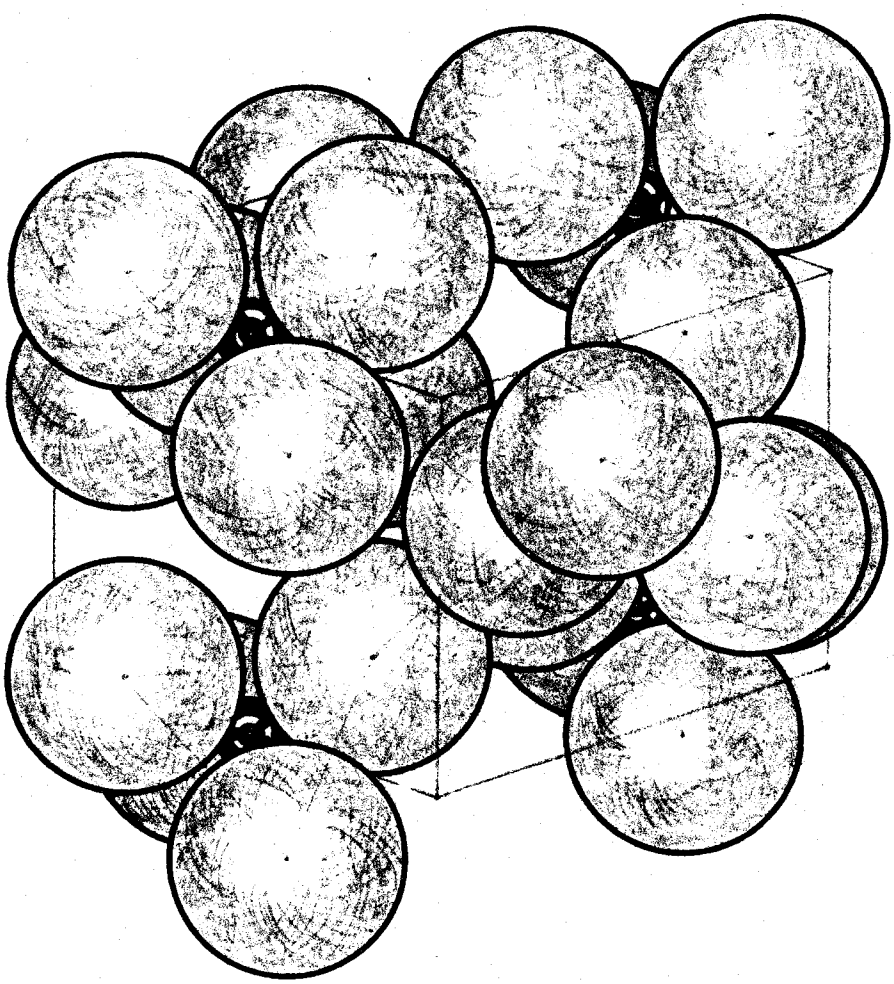

SILICON

OXYGEN

FIG 5 - QUARTZ - UNIT CELL, β FORM

AFTER EITEL (12)

feldspar contains potassium. One eighth of a unit cell of orthoclase feldspar, in the high temperature sanidine form, is sketched in Figure 6. The relatively diffuse binding of the alkali cations leaves them subject to removal by solution, and the distortion of the lattice reduces its rigidity and hardness. The feldspars as a group are not as hard as quartz, and are less durable, geologically speaking. They are, none the less, good concrete aggregate materials unless severely weathered.

More complex modifications of the tectosilicate lattice, and phyllosilicates, inosilicates, sorosilicates, and nesosilicates involve other and more numerous cations, frequently including iron and magnesium, and additional anions, such as the sulfides, halides, carbonates, and hydroxyl ions. Among the more common minerals the structural modifications of the crystal lattice arising from these substitutions lead to increased solubility, decreased hardness, and generally reduced durability. Thus crystalline silicates other than quartz and feldspar are relatively less important as concrete aggregate materials.

An important qualification on this generalization must be made in many regions to cover the locally abundant chert rocks. Chert, a microcrystalline variant of silica, is often an important residual material resulting from the weathering of limestone. The structure consists essentially

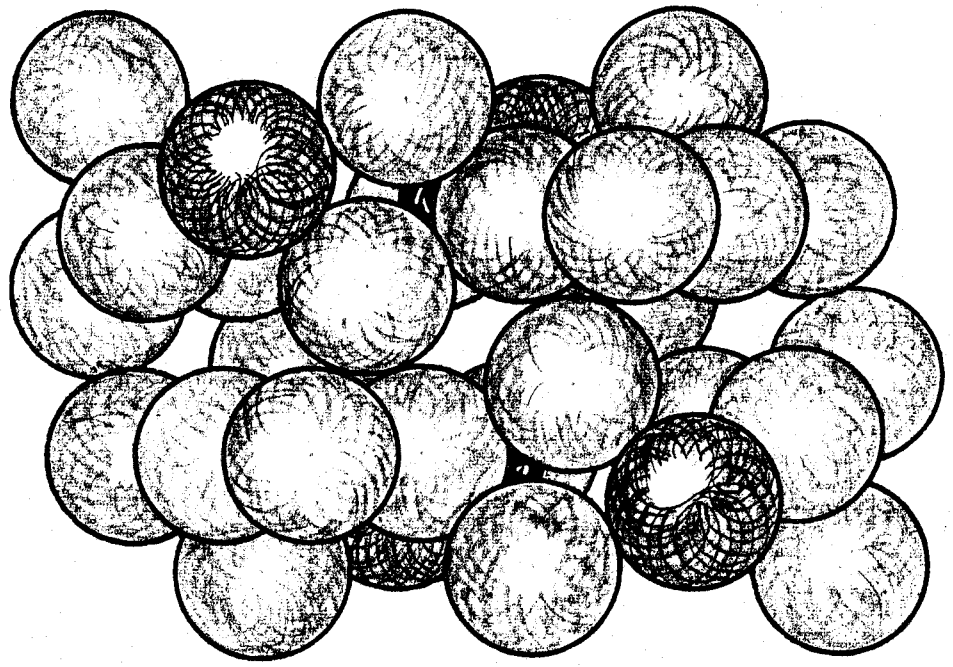

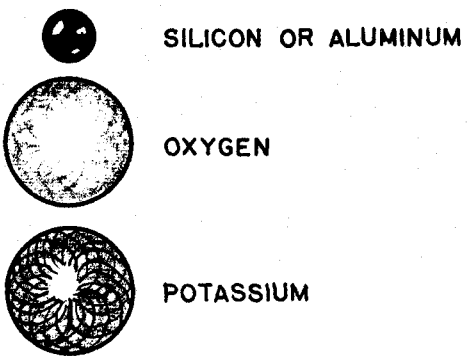

FIG 6 - ORTHOCLASE FELDSPAR - ONE-EIGHTH UNIT CELL, SANIDINE

AFTER WYCKOFF (31)

of an interlocking network of microscopic quartz crystals which unite to form a rock mass of considerable strength. The scratch hardness is equal to that of quartz. However, the individual quartz granules frequently do not completely fill the rock space. The resulting voids may be filled with amorphous silicate material, or they may be open. This leads to a wide range of properties. Weathering may produce significant variation in a single hand specimen.

In the event of substantial proportions of amorphous material the chert properties may include reactivity with the relatively small amounts of free lime present in Portland cements. If such materials must be used as concrete aggregate especially strict limitations on the amount of free lime of the cement may be required. This is a special problem beyond the scope of this study.

Another important group of concrete aggregate materials is the carbonates, especially calcium carbonate. This mineral occurs in the form of limestone or marble in many areas in sufficient quantity and of such properties as to be an excellent concrete aggregate. Its structure may be compared to that of quartz by noting that instead of the tetrahedral anionic group $(SiO_4)^{4-}$, the calcite has the triangular planar anionic group $(CO_3)^{2-}$. These groups are bound together by the action of calcium ions which balance the valence and form the relatively weak C-O-Ca-O-C bond.

A sketch of the unit rhombohedron of calcite is shown in Figure 7. This network is less rigid, softer, and less durable than those joined by the relatively stronger Si-O-Si or Al-O-Al bonds. As a result limestone and marble do not have the structural strength, hardness, and resistance to weathering of quartz and the feldspars. However, when not so porous as to lose all useful strength, or so contaminated with undesirable impurities such as pyrite (FeS_2) and amorphous silica as to develop undesirable chemical effects, they are good concrete aggregate materials. The closely related double carbonate dolomite $CaMg(CO_3)_2$ also forms a good concrete aggregate material. It is often loosely referred to as limestone or marble.

Surface Phenomena

Consideration of the bonding of the cement products to the aggregate surface involves not only the chemical elements present on that surface, but their exact physical arrangement as well. Weyl (28, p. 147) discusses surface phenomena in some detail, with particular attention to quartz, fused silica, and glass as examples. The surface phenomena are considered to be governed by the polarization and deformation of the ions because the surface involves the asymmetrical groups cation-anion-space or anion-cation-space. The screening of the cations is reported as a basic

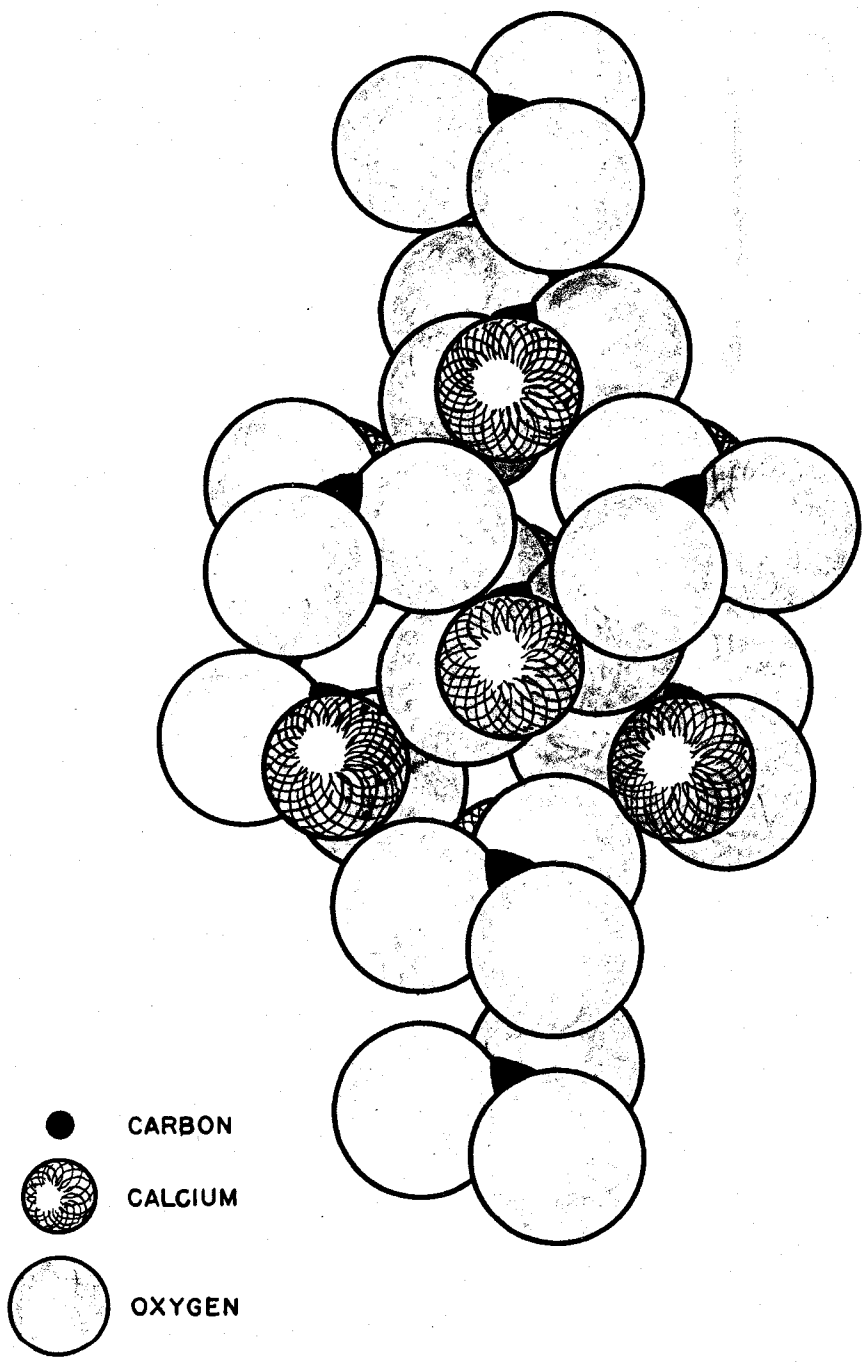

FIG 7 - CALCITE - UNIT RHOMBOHEDRON

AFTER WYCKOFF (31)

principle of these phenomena. The degree of screening depends on the number, size, and polarizabilities of the surrounding ions, and on the cation-anion distance. In silica, as in most silicates, four O^{2-} ions can screen the Si^{4+} ion. However, the orthosilicic acid molecule is tightened because of the absence of the attractive forces provided by surrounding cations in the usual lattice structure. The acid is therefore unstable as a monomer, and polymerizes to increase the effective screening power of the surrounding oxygen atoms. The instability of this SiO^{4-} group, and its tendency to polymerize, were noted above in the discussion of colloidal phenomena.

Because of the unbalanced character of the cation-anion-space and anion-cation-space groups, a fresh surface of an ionic crystal will have a rather high energy. Four general mechanisms are available by which this surface energy may be reduced.

The first mechanism is a polarization of the surface ions. The idealized 100 surface of a freshly fractured simple cubic cation-anion lattice is indicated in Figure 8(a). The figure is reproduced from Weyl (28, p. 153). Each ion now has a coordination number of five instead of six, which causes strong unbalanced forces as indicated schematically by arrows. The unbalanced attractive force of the cation in the cation-anion-space group polarizes the

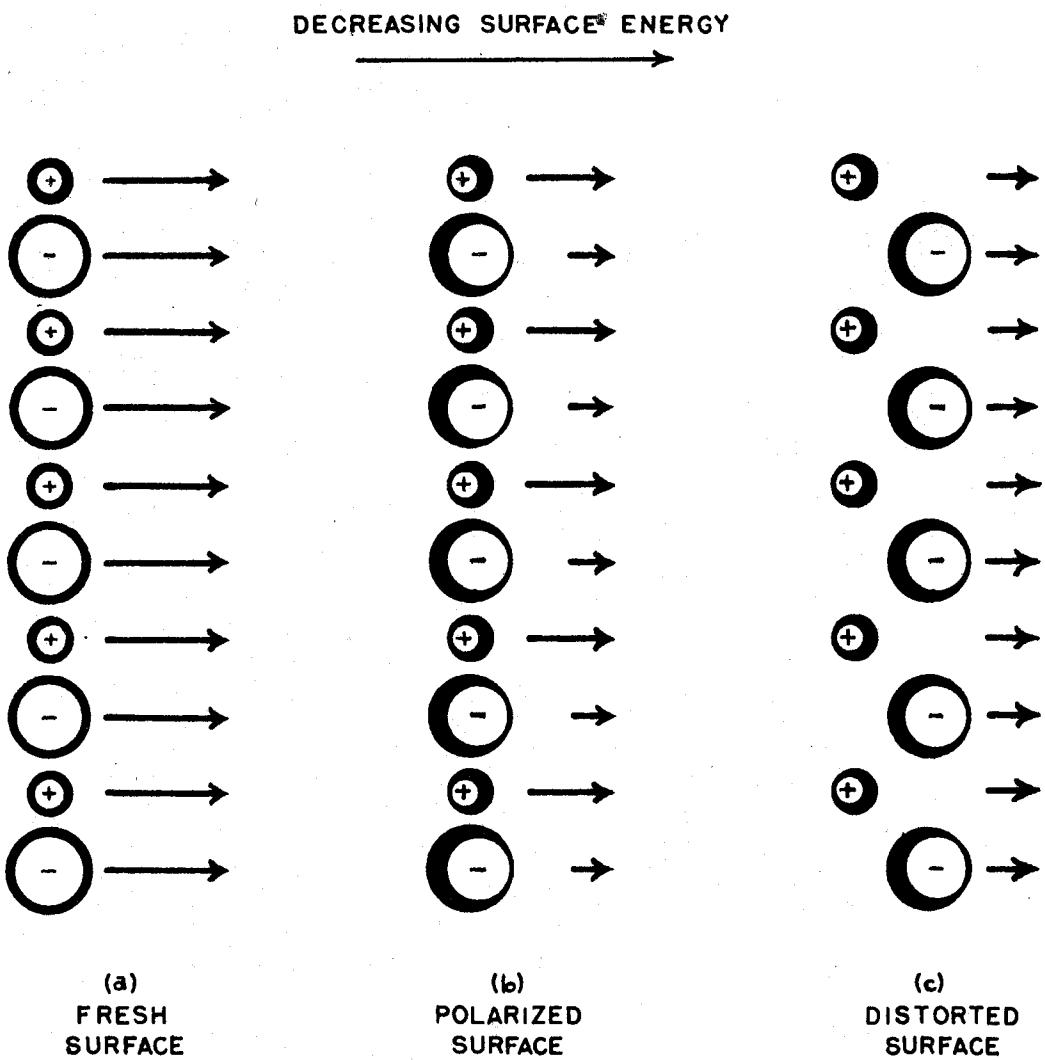

FIG 8 - POLARIZATION AND SURFACE DISTORTION OF CRYSTAL LATTICE AT FREE SPACE SURFACE

anion, pulling the electron cloud over toward the cation, and decreasing the negative field of the crystal. In general the polarization of the smaller surface cation is less significant. The situation produced by the polarization of the surface ions is indicated in Figure 8(b).

The second mechanism is the formation of a surface structure of non-stoichiometric proportions such that the outer layer consists of anions. All cations are thus screened. This characteristic lowers the surface energy, and is of importance in the formation and stability of colloids.

The third mechanism is the distortion of the surface structure and the formation of an electric double layer. This may or may not follow the polarization of surface ions described as the first mechanism above. It is shown schematically in the transition from Figure 8(b) to Figure 8(c). The deformed surface consists of oriented dipoles, and will develop the phenomena of an electric double layer. The distortion of the surface layer will disturb the force pattern acting on the second layer, producing distortion in that layer also; this effect will extend a considerable depth into the crystal.

The fourth mechanism is the sorption of molecules and of ions. This process for the lowering of the surface energy becomes important for solids containing cations of

low polarizability, and having a low anion-to-cation ratio, such as Al_2O_3 and SiO_2.

Weyl concludes that the first and second mechanisms above have little effect in reducing the surface energy of fractured quartz, while the third and fourth mechanisms are quite important. Various studies indicate a strongly distorted surface zone on quartz particles with a thickness in the order of 0.3 to 0.5 micron, while minor distortion extends much deeper. The chemisorption of the fourth mechanism is strong enough to break up some oxygen molecules in dry air. In the presence of a polar liquid the surface energy is substantially reduced by the adsorption of molecules or ions, lowering the resistance to scratching or cutting. This same effect, although somewhat less pronounced, is present in glass--a fact which is taken advantage of by glass cutters who wet their cutting tools immediately prior to scribing the glass surface.

Handy (13, p. 88 et seq.), in studies of the use of Portland cement to stabilize Iowa loess, considers the bonding of the paste to quartz and feldspar surfaces. Referring to Weyl (28), Handy advances the hypothesis that quartz adsorbs OH ions due to insufficient polarization screening. These ions are supplied by the surface of the hydrated cement gel, thus forming a bond. As ion adsorption takes place, the unbalanced forces producing the distorted

surface layer of the mineral are neutralized, and the structural polarization screening is progressively replaced by further ion adsorption. This leads to an increase of bond strength. Such a progressive effect is suggested as more likely to take place with quartz than with feldspar, because of a probable lower polarization screening of the latter material. It is suggested that on the other hand this lower polarization, which results from a larger number of cations in the feldspar lattice, will result in a relatively rapid bond strength gain on the feldspar surface due to more rapid chemical bonding.

Handy also suggests that because of the very fine size of the cement gel crystals and their poorly defined crystal structure the bonding will follow almost any ionic pattern exposed in the face of a mineral crystal. Differences in the pattern are considered to arise from variation in the lattice pattern for different minerals, or from different patterns of polarization screening attained.

Another surface phenomenon of importance in a consideration of the bonding of cement products to aggregates is epitaxy, that is, the production of crystal growth on a dissimilar substrate from solution or from the vapor phase. Seifert (23, p. 318 et seq.), discusses several natural and artificial cases of such crystal growth. In general, he concludes that if two crystalline materials have similar

types of bonding forces, and possess geometrically similar lattice patterns on well defined crystal faces (which will probably have small Miller index numbers), they may develop intergrowth on a common plane. This is in general possible if the geometrically similar faces do not produce matching of ions of opposite sign, and if the environment provides sufficient energy to accomplish any required minor distortion of the interface. A natural example is kyanite-staurolite, $(100)_K//(010)_{St}$; and a synthetic example is niter-mica, $(001)_N//(0001)_M$. There appear to be further requirements for such growth, for which full explanation is not yet available.

HYPOTHESIS OF BONDING MECHANISM

An hypothesis of the bonding mechanism between Portland cement paste and aggregate is developed in five steps.

First, the somewhat different American and English views concerning the internal cohesion of the hardening Portland cement paste are compared with respect to colloid phenomena.

The American view, summarized by Bogue (4, p. 465), emphasizes the coalescence of minute individual particles into spherical aggregates in the order of a few microns in diameter. Favorable orientations of such aggregates at points of contact lead to the development of cross linkages which bind the mass together, including the cement grains. The interstitial voids persist as a capillary network.

The English view, summarized by Lea (17, p. 223), is an elaborated form of the simple mechanical interlocking crystal theory of Le Chatelier. A matted felt or fine meshwork of crystalline foils and ribbons grows outward from the cement grains, becoming folded and buckled in the process. The developing crystals make contact and, at points of favorable orientation, intergrow by solid state reaction to become welded together. The growth of these crystals fills the

voids between cement grains and aggregate particles, binding them all together. Voids and capillaries filled with water remain.

The two approaches give essentially the same result, but by significantly different methods. In either case the end product is a microcellular network of calcium silicate hydrate material. The initial connecting links are tenuous contacts between growing aggregates of crystalline structure and colloidal dimensions. However, the first view postulates the spontaneous origin of new centers of growth in the solution surrounding the cement grains, without precluding the simultaneous development of crystalline structure from the surfaces of the grains themselves. The second view postulates the progressive outward growth of this crystalline structure from the hydrating grains of cement.

A consideration of the colloid principles expressed in equations (7) and (8), and illustrated by the data of Table 2, indicates that the first of these mechanisms is the more probable. The preferential growth of crystalline structure as such would be expected in more dilute solutions. The strongly supersaturated solutions produced in the normal water-cement paste would be expected to favor the development of additional growth centers and the formation of a more finely divided or amorphous gel structure.

Bogue's summary of the American view of the nature of

the internal bond of the cement paste is accordingly chosen as a basic premise (4, p. 645).

Second, the mechanism by which the development of this gel structure is accomplished is considered, again with respect to colloid phenomena.

There appears to be no particular limitation on the polymerization process of the silicate ions described by Hauser (14, Figure 15, p. 58), insofar as the presence of the other elements of Portland cement or the usual aggregate minerals are concerned. Natural hydrous calcium silicate minerals exist, and analogous compounds have been identified as hydration products of Portland cement. The neutralization of the acidic SiO^{4-} radical may be accomplished by the adsorption of either hydrogen or calcium ions. The cross linked polymer is then expected to contain calcium ions, in proportions depending upon the composition of the solution at the time of formation. Hydroxyl ions and water molecules are included in the developing structure in accordance with the valence and coordination requirements of the silicon and calcium ions.

Thus the hardening of the Portland cement paste is described as a polymerization process of silicate ions. This permits initial contact points to form structural bonds without the necessity of any rigid correlation of orientation.

Third, Handy's hypothesis (13, p. 88 et seq.) of the bonding of Portland cement to quartz and feldspar surfaces is considered with respect to this polymerization hypothesis. Handy considers that the OH ions adsorbed as screening by the unbalanced surface cations of the fractured mineral are provided on the surface of the hydrating cement grain, giving rise to a bond. Ion adsorption causes a local relaxation of structural polarization, leading to further ion adsorption and a developing bond. Because of the small size of the crystal aggregates involved in the gel, and their poorly defined structure, Handy considers that the ion adsorption bonding described in his hypothesis can follow almost any ionic pattern exposed on the aggregate.

Consideration of the polymerization behavior of the silicate radical suggests an extension of this hypothesis. Rather than the bond with the mineral being developed through the direct adsorption of OH ions attached to the cement grains, the gel particles are developed spontaneously on the face of the mineral, on the cement grains, and in the void spaces by the polymerization of the silicate tetrahedra. As this polymerization proceeds the developing gel masses intersect, and form multiple bonds through continued cross polymerization. The calcium ions present in the solution, together with their adsorbed ions, are incorporated in the developing lattice. This lattice will be

formed in stoichiometric ratios conforming to the particular equilibrium conditions prevailing in the liquid phase.

The bonding between the hardening cement gel structure and the surface of the mineral aggregate is described as an extension of the polymerization of the silicate tetrahedra by the development of Si-O linkages between the silicon ions of the tetrahedra and the oxygen ions of the mineral lattice. There is also the possibility, under favorable conditions, of Ca-O linkages.

The calcium ions are less firmly held in the lattice, and are subject to leaching out if the concentration of the calcium in the liquid phase is sharply reduced. This will alter the equilibrium conditions of the remaining materials. In the continued presence of water, the calcium silicate hydrates formed earlier will tend to redissolve and repolymerize in new lattices. The formation of this rearranged material accounts for the autogenous healing of cracked Portland cement concrete. Relatively lime-free water enters the crack, decreasing the lime content of the interstitial water and leaching out lime in the region adjacent to the crack. As more calcium is leached from the material, the reformed structure becomes increasingly resistant to further leaching. Equilibrium is reached and, due to the increased proportion of silicate bonding, the new material is stronger than the original.

Thus, when a structurally competent mass of concrete develops surface cracks which then heal, and are subsequently subjected to moderate abrasion, there develop what may be called "protruding cracks". This phenomenon may be observed in the service drive ramps of the Iowa State College Library. Although showing clear evidence of surface abrasion, the concrete in the region of the former cracks, traces of which cracks still appear, is definitely higher than the surrounding material. This is distinct from the deposition of the leached calcium as calcium carbonate at the surface of the crack as a projecting bead. This related phenomenon is also evident in these ramps, near the side walls where the exudation is protected from abrasion.

Fourth, the development of the polymerizing calcium silicate hydrate crystal structure is a potentially more ordered process than suggested by Handy. Seifert (23, p. 318 *et seq.*) concludes that if two crystalline materials have similar types of bonding forces and geometrically similar lattice patterns on simple, well defined crystal planes, they may develop epitaxic intergrowth on a common plane. Apparent further requirements for such intergrowth are as yet undefined. However, the electron techniques which are currently expanding the knowledge of cement compounds and products also indicate the possibility of submicroscopic phenomena of epitaxic character in several cases

not previously identified.

Lea (17, p. 186 et seq.) classifies the calcium silicate hydrates as fibrous and non-fibrous. While afwillite, taken as an example (Figure 4), is non-fibrous in habit, its selection is rather a matter of available information than of a completely typical pattern--the investigation of finely fibrous materials is quite difficult. Many of the cement products are finely fibrous, and many of the non-fibrous materials form thin sheets or foils. Epitaxic growth of such materials on mineral aggregates would thus tend to be limited to very small surfaces in any case. A comparison of the general pattern of the afwillite lattice of Figure 4 and the lattices of some of the more typical aggregate minerals of Figures 5 to Figure 7 indicates the possibility of a considerable measure of such ordered overgrowth.

In this connection it is further noted that mineral compositions, and hence mineral lattice patterns, are not fixed. In other words, there is not necessarily any one exact formula or structural pattern for the composition of a mineral. Rather, nearly all minerals vary somewhat in composition; many of them vary a great deal (29, p. 3). The limiting consideration is that of an orderly, gradual, continuous change in composition and crystal structure throughout a well defined range. The calcium silicate

hydrates are minerals possessing this variation in composition to a marked degree. For example, calcium silicate hydrate I (CSH(I) by Taylor's notation, CSH(B) by Bogue's notation) is given by Lea (17, p. 180) with a formula range of $(CaO)_{0.8-1.5}SiO_2(H_2O)_{2.5-1.0}$. Variations within the ranges indicated reflect conditions of stability in a range of lime concentrations. Thus as the materials in solution precipitate out in the setting water-cement paste mass, continuously varying crystal lattices are available from place to place and from time to time from which to develop epitaxic overgrowth wherever the original random polymer orientation comes within the required degree of fit for growth of the calcium silicate hydrate upon the aggregate surface.

Finally, as a result of the probable epitaxic character of nucleation on the aggregate surface, the type of bonding force which holds the mineral together has a bearing on the character and strength of the cement paste-aggregate bond. The energies of some of the oxide bonds, in kilogram calories per gram atom of oxygen, are listed by Houwink (15a, p. 28) as follows:

SiO_2	1550	kg cal/gm atom O
Al_2O_3	1200	" " " " "
MgO	940	" " " " "
CaO	830	" " " " "

The high energy of the Si-O bond supports the observation by Weyl that fractured quartz is prone to adsorb oxygen. Feldspars, containing Al-O bonds, will be only somewhat less likely to display this behavior. In suitable environments any cation will tend to adsorb oxygen to some extent.

Most concrete aggregate minerals are oxides, or contain anionic radicals consisting of oxide groups, such as $(CO_3)^{2-}$. Thus the chemisorption of oxygen in the fourth cation shielding mechanism noted by Weyl is to some extent a matter of restoring the original crystal structure on the fracture surface, or extending the crystal structure on an exposed crystal plane. For the oxides this then amounts to an alternate mechanism for the establishment of a non-stoichiometric surface on the mineral--one composed of a disproportionately large number of oxygen atoms. The type of bonding established between the cations and the adsorbed oxygen is generally of the same character as that existing in the original crystal.

In accordance with Seitz's tabulation of solid bonding forces (24, p. 1,2), most minerals are either ionic or covalent crystals. Palache *et al.* (20, pp. 1,2) indicate that ionic bonding is more prevalent in minerals as considered in terms of the number of varieties. However, the more abundant silicon and aluminum minerals, which are of major importance as concrete aggregates, are strongly

covalent, to varying extents. Thus the internal bonding forces of concrete aggregates consist of varying proportions of the two types of forces.

The oxygen atom of the mineral surface will display to the adjoining space a force pattern which will conform to the bonding forces holding it in place. Thus an oxygen atom bonded by strongly ionic forces will tend to behave as an ion, developing ionic bonding with any available cation, while an oxygen atom bonded by strongly covalent forces will tend to develop only covalent bonding, with an inhibiting of ionic bonding. This dual character of available bonding forces will tend to produce two more or less distinct types of strength gain.

In the initial solution environment of the developing cement gel a substantial ion concentration exists. It is therefore postulated that the relatively mobile ions of the solution will be attracted to the ionic oxygen of the mineral face, leading to an early bond strength gain by the formation of polymerization bridges in some proportion to the amount of ionic oxygen present. As the polymerization proceeds and the coagulating gel, assuming a more regular structure, begins to develop an expanding crystal lattice, atoms will tend to be drawn into regularly coordinated positions in which covalent bonds may be expected to develop. This will lead to a later bond strength gain in some

proportion to the amount of covalently bound oxygen present.

TEST PROCEDURES AND RESULTS

Principal Test Data

Tension briquet

The principal test data consist of the results of tests on nine series of neat cement mortar tension briquets containing transverse aggregate wafers of various materials, placed at various angles to the applied force. The tension briquet has ends shaped in general accordance with Figure 3, ASTM Designation C 190-49, Test for Tensile Strength of Hydraulic-Cement Mortars. (2, p. 188) Instead of the center section of one square inch in the standard briquet, the specimens used in these series of tests are lengthened to form a uniform rectangular prism ten inches in length. The aggregate wafers are placed across the center of this prismatic section. The geometry of the specimen is indicated in Figure 9.

Materials

The cement used for the specimens of these series was Hawkeye Portland Cement, Type I, obtained through regular commercial channels. Two sacks were purchased, and blended

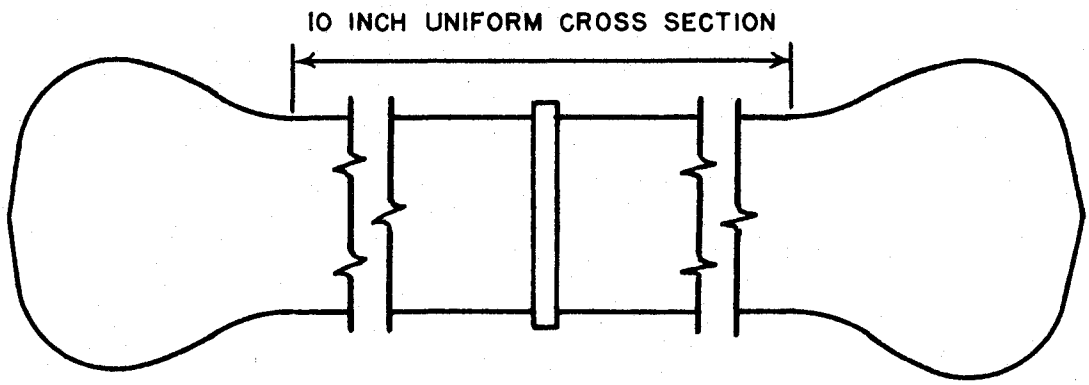

(a) - AGGREGATE WAFER NORMAL TO APPLIED FORCE

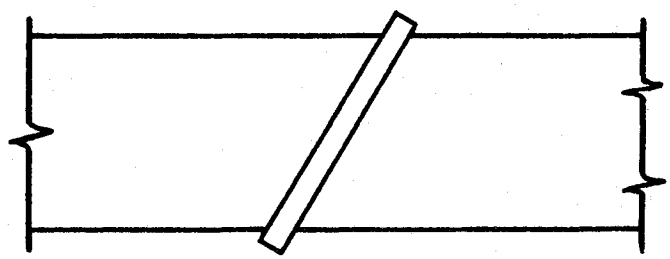

(b) - AGGREGATE WAFER AT 30° TO NORMAL

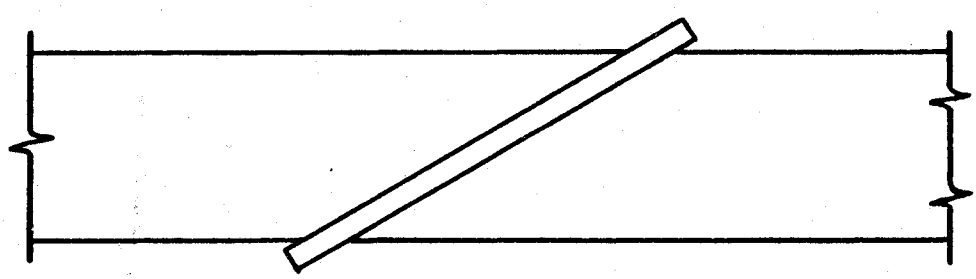

(c) - AGGREGATE WAFER AT 60° TO NORMAL

FIG 9 - GEOMETRY OF TENSILE TEST SPECIMEN

as placed in a single metal container with a reasonably tight fitting friction lid. The cement composition, as indicated in regular mill tests, was obtained from the manufacturer, as follows:

SiO_2	- 22.3%	C_3S	- 50.0%
Al_2O_3	- 4.4%	C_2S	- 26.0%
Fe_2O_3	- 3.5%	C_3A	- 5.6%
MgO	- 2.4%	C_4AF	- 11.0%
CaO	- 64.1%		
SO_3	- 2.1%		

Aggregate wafers were of nine different materials. Arranged in order of increasing effective oxygen ion number, calculated as described below, these were sepiolite, neat cement mortar, glass, calcite, chert, orthoclase feldspar, quartz, beryl, and spodumene. All wafers were cut to shape on a diamond saw running in a cooling lubricant bath of kerosene, except calcite, which was cleaved into thin rhombodrons that were cemented together to required size, and glass, which was cut to size from commercial window glass using ordinary glass cutters.

Of the minerals, calcite and orthoclase feldspar were made available by the Geology Department of Iowa State College, sepiolite, quartz, beryl, and spodumene were purchased through commercial channels, and chert was made available through a personal source. The neat cement

mortar was sawn from specimen No. 83 of the test series, made from the cement described above. Origin and brief description of the mineral specimens follow:

Sepiolite: A rounded block of pure white color, microcrystalline, highly porous, with some variation in porosity through the piece, from Eski-hi-sher, Asia Minor.

Calcite: A roughly rhombohedral block, euhedral faces on three sides, cleavage faces on three sides, clear to faintly tawny, essentially one crystal, although some evidence of irregularity and a few fine inclusions, from Picher, Oklahoma.

Chert: A roughly rectangular block, irregular weathered light gray surface on one side, conchoidal fractured dark gray surface on one side and all edges, microcrystalline, a few small fossil remnants, slightly porous, especially on weathered surface, from Wreford quarry, Kansas. Wafers from unweathered region.

Orthoclase feldspar: Several roughly rectangular pieces, orthogonal cleavage faces in two directions with irregular fractures across the ends, buff to orange pink, essentially single crystals but with some irregularity in cleavage planes, and with some perthitic intergrowth, from Fountain, Colorado. Wafers parallel to basal cleavage plane.

Quartz: An aggregate of essentially parallel, somewhat

intergrown crystals varying from approximately three quarters of an inch transverse thickness down to approximately one quarter inch, with smaller crystals filling interstices, mostly clear, some milky areas, some flawing and inclusions at interfaces; from Ouray, Colorado. Wafers at approximately 45° inclination to a axis.

Beryl: An irregular, roughly rectangular fragment, uneven to somewhat conchoidal fractures on all faces, apparent euhedral face on one end with striations, essentially single crystal, with intergrowth of perthitic character, milky white color with blue-green shading to varying extent, from Labelle Co., Quebec. Wafers parallel to basal plane.

Spodumene: An elongated cleavage fragment of rhombic cross section with irregular fractures across the ends, essentially single crystal with some small inclusions uniformly distributed, light gray color, fibrous to pearly luster, from Keystone, South Dakota. Wafers parallel to cleavage plane.

The aggregate wafers were located in three positions: normal to the applied tensile force, at 30° inclination from the normal, and at 60° inclination from the normal. These positions are indicated in Figure 9.

Fabrication and test

The molds for the tensile test specimens are of birch wood, shaped to the proper form by planing, sawing, and sanding, and finished by several applications of boiled linseed oil. As a bond break material which would not contaminate the aggregate wafer surface with oil or wax, the molds were lined with aluminum foil through the center prism section for the specimens of these series. The molds prepared for casting specimens are shown in Figure 10(a).

The cement mortar was mixed with a water-cement ratio by weight of four tenths. This was chosen after experimentation as a ratio within the practical range for concrete mixes--4.5 gal. per bag, with an expected compressive strength at 28 days of 5,500 to 6,800 psi, using modern cements--and a workable consistency for the specimens of the test series. Cement weight was determined using laboratory balances to 0.1 gram, tap water was measured volumetrically at room temperature. Water was poured into the cement, in an enamelware bowl, and allowed to stand 30 sec. The mortar was then mixed vigorously for 1 min., and placed in the molds in two equal layers, each layer being worked into place to eliminate bubbles. The surface of the specimen was trowelled smooth, and it was placed in a moist room to cure until test. The molds were removed at 24 hours.

Figure 10(a). Molds prepared for casting tensile test specimens

Figure 10(b). Tensile test specimen mounted for application of test load

Figure 10(c). End of tensile test specimen mounted for flexural test

Figure 10. Photographs of tensile test specimen molds and testing apparatus

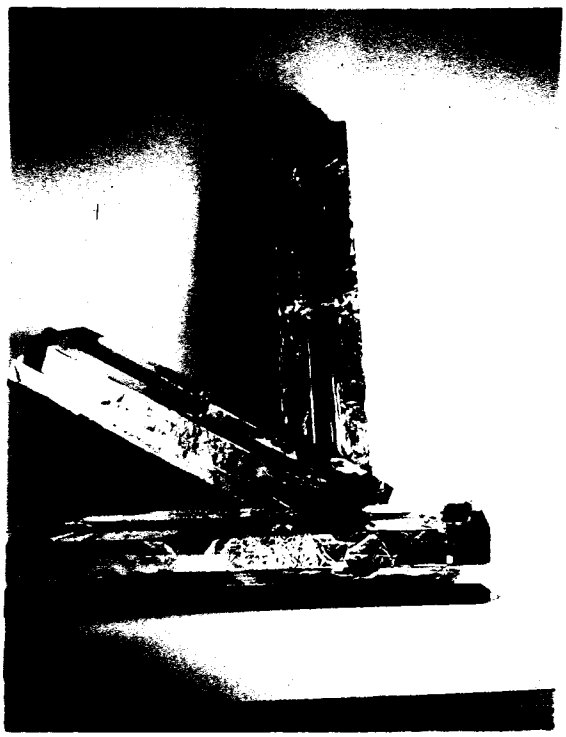

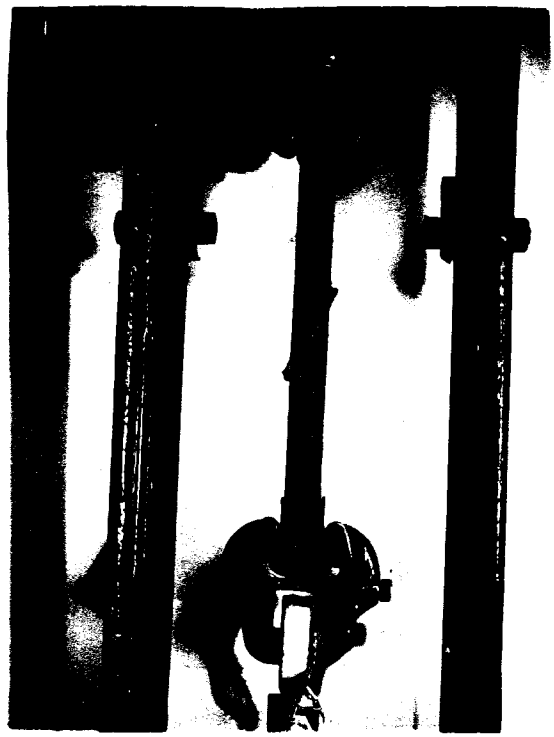

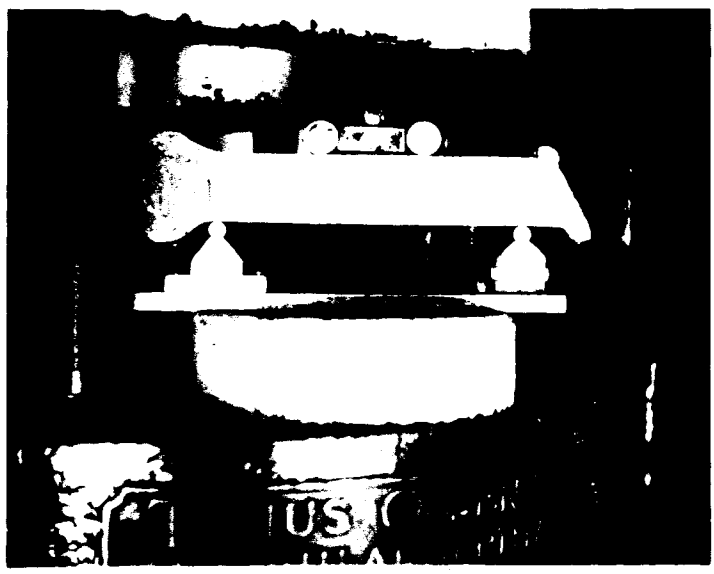
US

The specimens were tested at 7 or 28 days. First, the tensile strength was determined using a 20,000 lb. capacity lever type testing machine with a one-tenth nominal weight poise giving load readings to 0.5 lb. The specimens were held in a pair of end grips meeting the requirements of ASTM Designation C 190-49, adapted for use in this machine by fittings which maintain the ball point suspension provided for in Figure 2, ASTM Designation C 190-49. To minimize the effects of surface irregularities on the specimens, pads of rubber were inserted between the specimen face and the rollers of the grips. A specimen ready for tensile test is shown in Figure 10(b).

Following the tensile test, the two ends of the prism section described above were tested in flexure in the same machine, using a compression head, and a load rig which applied a flexural load at the third points of a 4.5 in. span of the uniform nominal one inch square section. A specimen ready for flexural test is shown in Figure 10(c).

Measurements of all fracture surfaces were taken to the nearest one-hundredth of an inch. On the basis of these measurements, and the observed loads, normal and tangential stress components were computed for the mortar-aggregate surfaces of the tensile test, and the modulus of rupture was computed for the flexural test. Tensile test results were also corrected to account for areas of no bonding, as

discussed below. The mortar-aggregate tensile test stress components are shown in Table 5. The moduli of rupture for useful values of flexural load are shown in Table 6.

Supplemental Test Data

Specific gravities and absorption

The specific gravities were determined by weights taken in air and in water, using a Jolly balance. Percentages of absorption based on oven dry weight at 95° C. were taken after 24 hours in distilled water at 22° C., and again after an additional 5 hours in boiling distilled water. Rates of absorption in grams per square centimeter into plane surfaces in contact with the free surface of distilled water were determined, using a contact time of 60 sec. on oven dry material. A chainomatic type balance was used for all weights involved in the absorption determinations. Values of the specific gravity and of the various absorptions are shown in Table 7. Each value is the average of three determinations.

Mortar tension specimen

Mortar tension specimens were prepared without aggregate wafers for the determination of tensile strengths of the mortar itself. These specimens were tested at 7 and 28

Table 5. Mortar-aggregate tensile test stress components

Aggregate	Surface angle	7 Day strengths		28 Day strengths	
		σ, psi	τ, psi	σ, psi	τ, psi
Sepiolite	Normal	33.08	--	64.07	--
		42.30	--	68.01	--
		42.32	--	73.94	--
	Ave.	39.23		68.67	
	30° to N	22.78	13.16	63.56	36.70
		41.88	24.18	65.16	37.62
		37.17	21.86	55.03	31.78
	Ave.	33.94	19.60	61.25	35.37
	60° to N	24.92	43.15	80.44	139.32
		17.78	30.80	54.73	94.79
		16.92	29.31	94.45	163.59
	Ave.	19.87	34.42	76.54	132.57
	Ave. σ	31.02		68.82	
Mortar	Normal	39.71	--	70.52	--
		42.30	--	52.19	--
		59.18	--	72.48	--
	Ave.	47.06		65.06	
	30° to N	89.93	51.92	50.21	28.99
		63.24	36.51	83.75	48.36
		66.93	38.64	38.37	22.16
	Ave.	73.37	42.36	57.44	33.17
	60° to N	102.71[a]	177.90[a]	107.10	185.49
		76.77	132.96	196.56	340.45
		79.49	137.68	135.08	233.95
	Ave.	86.32	149.51	146.25	253.30
	Ave. σ	68.92		89.58	
Glass	Normal	40.45	--	35.72	--
		42.98	--	213.95[b]	
		27.40	--	52.64	--
	Ave.	36.94		44.18	

[a]Fracture by mortar tension, stresses calculated for aggregate surface

[b]Omitted from average

Table 5. (Continued)

Aggregate	Surface angle	7 Day strengths		28 Day strengths	
		σ, psi	τ, psi	σ, psi	τ, psi
Glass (continued)	30° to N	48.04	27.74	61.03	35.24
		26.32	15.20	71.70	41.40
		17.62	10.18	27.69	15.98
	Ave.	30.66	17.71	53.47	30.87
	60° to N	18.68	32.35	28.74	49.78
		11.75	20.33	57.26	99.17
		23.34	40.42	26.02	56.08
	Ave.	17.92	31.03	37.34	98.01
	Ave. σ	28.51		56.10	
Calcite	Normal	45.34	--	97.71	--
		51.07	--	71.62	--
		50.06	--	75.34	--
	Ave.	48.82		81.56	
	30° to N	29.15	16.83	21.20	12.24
		44.11	25.47	36.89	21.30
		44.90	25.92	45.41	26.22
	Ave.	39.39	22.74	34.50	19.92
	60° to N	36.88	63.88	61.94	107.29
		31.50	54.57	76.54	132.56
		49.64	85.97	92.82	160.76
	Ave.	39.34	68.14	77.10	133.54
	Ave. σ	42.52		64.39	
Chert	Normal	37.74	--	42.98	--
		42.65	--	68.26	--
		29.66	--	76.20	--
	Ave.	36.68		62.48	
	30° to N	41.03	23.69	39.21	22.64
		42.97	24.81	73.17	42.24
		--	--	--	--
	Ave.	42.00	24.25	56.19	32.44
	60° to N	36.08	62.48	41.86	72.51

Table 5. (Continued)

Aggregate	Surface angle	7 Day strengths		28 Day strengths	
		σ, psi	τ, psi	σ, psi	τ, psi
Chert (continued)	60° to N	45.80	79.33	275.26[a,b]	476.76[a,b]
		53.81	93.20	263.02[a,b]	455.56[a,b]
	Ave.	45.23	78.34	41.86	72.51
	Ave. σ	41.22		56.95	
Feldspar	Normal	37.28	--	61.26	--
		33.01	--	87.94	--
		26.73	--	62.50	--
	Ave.	32.34		70.57	
	30° to N	121.66	70.24	96.51	55.72
		91.41	52.78	81.78	47.22
		53.61	30.96	33.77	19.50
	Ave.	88.89	51.33	70.69	40.81
	60° to N	73.95	128.08	58.48	103.03
		87.58	151.69	76.82	133.05
		49.45	85.65	93.15	161.34
	Ave.	70.33	121.81	76.15	132.47
	Ave. σ	63.85		72.46	
Quartz	Normal	59.31	--	117.93	--
		40.70	--	60.54	--
		36.64	--	62.18	--
	Ave.	45.55		80.22	
	30° to N	64.40	37.18	102.34	59.09
		100.23	57.87	67.30	38.86
		7.21[a]	4.16[a]	30.66	17.70
	Ave.	82.32	49.60	66.77	38.55
	60° to N	60.82	105.33	57.07	98.85
		68.48	118.61	59.35	94.13
		30.40	52.66	64.81	112.31
	Ave.	53.23	92.20	60.42	101.76

[a]Omitted from average

[b]Fracture by mortar tension, stresses calculated for aggregate surface

Table 5. (Continued)

Aggregate	Surface angle	7 Day strengths		28 Day strengths	
		σ, psi	τ, psi	σ, psi	τ, psi
Quartz (continued)	Ave. σ	57.62		69.13	
Beryl	Normal	83.42	--	103.80	--
		58.28	--	66.29	--
		54.43	--	70.31	--
	Ave.	65.38		80.13	
	30° to N	44.51	25.70	123.41	71.26
		60.94	35.18	101.69	58.72
		49.54	28.60	120.35	69.48
	Ave.	51.66	29.83	115.15	66.49
	60° to N	48.92	84.74	94.48	163.65
		41.54	71.95	62.15	53.82
		68.34	118.36	83.44	144.53
	Ave.	52.93	91.68	80.02	120.67
	Ave. σ	56.66		91.77	
Spodumene	Normal	50.08	--	92.57	--
		70.75	--	71.86	--
		48.41	--	106.85	--
	Ave.	56.41		90.43	
	30° to N	35.00	20.21	79.24	45.75
		44.56	25.72	97.55	56.32
		36.26	20.94	73.00	42.15
	Ave.	38.61	22.29	83.26	
	60° to N	67.79	117.41	85.60	148.25
		67.56	117.02	122.02[b]	211.33[b]
		43.54	75.42	61.98	107.36
	Ave.	59.63	103.28	89.87	
	Ave. σ	51.55		87.85	

[b]Fracture by mortar tension, stresses calculated for aggregate surface

Table 6. Mortar flexural test moduli of rupture

Spec. no.	Age at test	Modulus of rupture, psi	
		7 day	28 day
27	28		860.72
			892.00
29	28		1034.56
			997.92
31	7	971.42	
		954.72	
32	7	789.73	
		721.14	
34	7	954.45	
		938.84	
35	28		807.54
			830.52
38	28		1105.80
39	7	896.31	
		881.92	
41	7	708.00	
42	7	606.20	
43	7	890.38	
		786.72	
44	7	660.35	
47	7	622.11	
49	7	661.26	
		503.28	
50	28		1405.25
			1118.60
51	28		991.44
52	28		1074.86
			1013.04
53	28		810.02
			894.86
56	7	844.22	
57	7	761.52	
		742.26	
58	28		1101.12
			1073.38
59	28		1017.02
60	28		961.26
			1034.72
61	28		954.80
			894.04

Table 6. (Continued)

Spec. no.	Age at test	Modulus of rupture, psi	
		7 day	28 day
65	7	665.28	
66	28		890.48
67	28		1176.12
			852.93
68	28		1235.32
			999.46
69	28		1212.00
			900.99
73	7	784.00	
74	7	800.04	
75	7	721.52	
76	7	829.15	
		718.56	
78	7	841.75	
79	7	898.56	
81	7	742.00	
		817.19	
82	7	859.74	
		874.38	
84	7	739.50	
		720.44	
86	28		989.94
87	28		921.99
			801.83
88	28		912.00
			972.42
89	28		902.88
			867.84
90	28		959.14
			944.32
91	7	734.70	
		642.96	
92	7	698.56	
93	7	692.16	
		703.38	
94	28		983.04
			839.52
95	28		737.02
97	28		999.57
101	7	908.31	
103	7	715.52	
		861.30	

Table 6. (Continued)

Spec. no.	Age at test	Modulus of rupture, psi	
		7 day	28 day
104	7	699.56	
		816.56	
105	28		1044.60
			1075.80
106	28		734.78
107	28		1018.98
			788.50
109	7	840.14	
110	7	1028.50	
		1082.40	
111	28		1214.40
			1034.40
112	28		1060.98
			1093.68
113	28		1092.70
115	7	710.40	
117	7	821.10	
		785.90	
118	28		1044.00
119	28		1023.36
120	28		841.80
124	28		955.70
			1092.12
125	28		1046.56
			998.46
126	28		853.06
			959.10
127	7	998.22	
		879.66	
128	7	953.22	
		1020.92	
129	7	806.00	
		763.08	
131	28		1055.65
			1021.08
132	28		1130.91
			1071.98
137	28		1118.40
			1109.46
138	7	797.71	
140	7	847.83	
		817.52	

Table 6. (Continued)

Spec. no.	Age at test	Modulus of rupture, psi	
		7 day	28 day
143	28		957.42
145	7	999.60	
146	7	795.80	
		797.30	
147	28		1197.77
			1123.36
149	28		999.88
			947.64
150	7	715.00	
153	28		1101.66
			919.68
155	28		1144.56
			1082.40
159	28		1130.40
			1069.50
160	28		1224.72
			998.97
161	28		1173.90
			1130.29
164	7	719.88	
		696.90	
169	7	723.80	
170	7	703.56	
		750.40	
171	28		813.44
173	28		861.10
			915.80
174	7	646.30	
182	28		894.24
183	28		856.96
			904.26
185	7	654.36	
189	28		849.66
			913.28
190	7	677.70	
192	7	864.43	
		716.13	
193	28		763.50
194	28		921.69
195	28		809.08
			685.86

Table 6. (Continued)

Spec. no.	Age at test	Modulus of rupture, psi	
		7 day	28 day
196	7	719.90	
198	7	680.68	
		665.76	
199	28		922.56
			956.80
200	28		921.20
203	7	750.87	
204	7	736.32	
206	28		897.90
			992.92
207	28		827.97
208	7	681.68	
		626.60	
209	7	632.10	
		820.16	
210	7	658.75	
		730.95	
211	28		891.66
212	28		973.56
213	28		860.94
			930.30
219	7	641.36	
		688.38	
220	7	638.30	
		681.22	
221	7	694.98	
222	7	702.99	
225	7	711.95	
		873.46	
226	7	748.89	
		723.20	
227	7	906.26	
		777.45	
229	28		833.66
Root mean square		781.12	987.48
Probable error		70.38	85.90

Table 7. Specific gravities and absorptions

Mineral	Specific gravity (sat.sur. dry)	Per cent absorption 24 hour 22° C.	24 hour 22° C. + 5 hour boiling	Rate of absorption gm/sq cm in 60 sec.
Sepiolite	1.343	111.431	114.995	0.0441
Mortar	2.010	22.501	23.175	0.0333
Glass	2.556	0.006	0.006	nil
Chert	2.555	1.952	2.050	0.0066
Calcite	2.721	0.019	0.020	nil
Quartz	2.635	0.104	0.137	0.0001
Feldspar	2.556	0.210	0.247	0.0001
Beryl	2.659	0.014	0.017	0.0001
Spodumene	3.159	0.215	0.232	0.0018

days. Results of these tests are shown in Table 8. There are included in this table the mortar test strengths developed by specimens containing aggregate wafers or glass marbles in which the bond developed was strong enough that the specimen failed in mortar tension, with no failure on the mortar aggregate surface.

Effect of surface smoothness

In order to investigate the effect of surface smoothness on the bond strength developed, a set of feldspar wafers were polished on a metallurgical polishing wheel, on one side, and three specimens were prepared with an aggregate wafer orientation of 30° to the normal. These specimens were tested at 7 days, with results as follows:

Specimen no.	σ, psi	τ, psi
256	37.52	21.67
257	16.84	9.72
258	30.31	17.50
Ave.	28.22	16.30

Electron micrographs of the sawn and polished surfaces are shown in Figures 11, 12, and 13, respectively.

Spherical inclusion

Additional tensile test specimens were prepared in which a glass marble was placed in the center of the prism section,

Table 8. Mortar tensile strengths

Specimen no.	Age at test	Tensile strength, psi	
		7 day	28 day
27	28		522.52
31	7	562.50	
39	7	379.55	
49[a]	7	408.16	
53[a]	28		509.58
69[a]	28		577.68
103[a]	7	384.11	
113[b]	28		488.06
132[b]	28		532.82
149[b]	28		550.53
155[b]	28		526.05
227[b]	7	410.85	
	Average	429.03	529.61

[a]Glass marble specimen, fracture by mortar tension.

[b]Aggregate specimen, fracture by mortar tension.

Black elongated areas in upper center, and along right and lower edges, are breaks in replica along general line of sharp relief.

Black streak from lower left corner is break in replica along general line of sharp relief. White object in right center is extraneous material. Note prominence in lower center, representing depression in original surface.

Figure 11. Electron micrographs, 5600X, Sawn feldspar

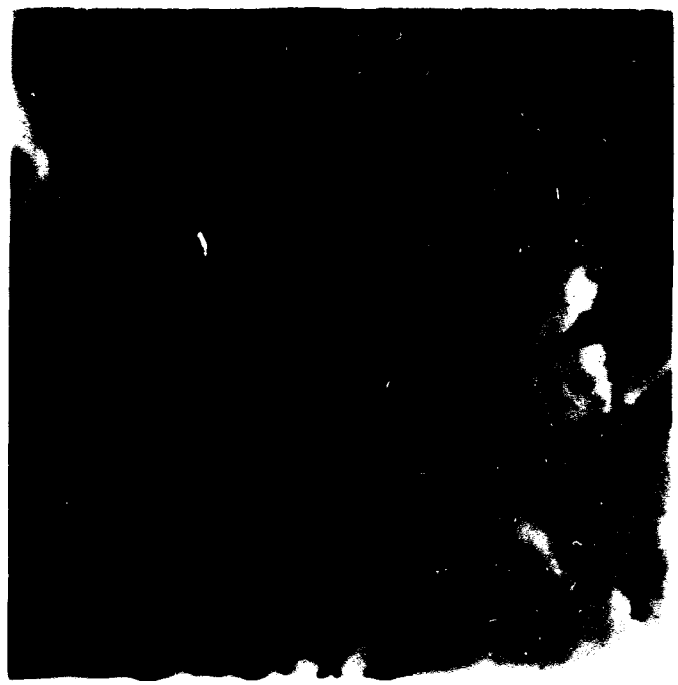

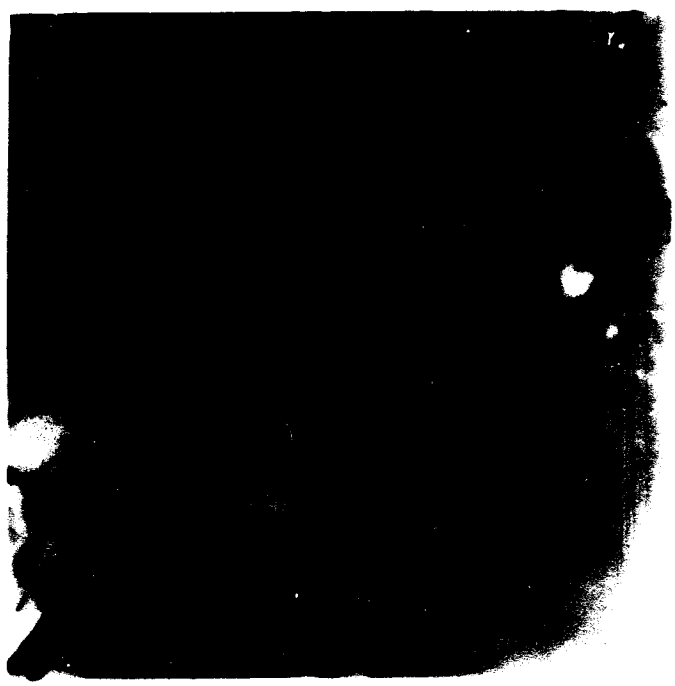

Narrow black areas in lower left corner are breaks in replica along general line of high relief. Note well defined successive levels of plane surfaces.

Heavy black lines in lower corners and along right upper edge are breaks in replica along general lines of sharp relief. Horizontal lines of variation in intensity due to faulty development of original negative.

Figure 12. Electron micrographs, 5600X, Sawn feldspar

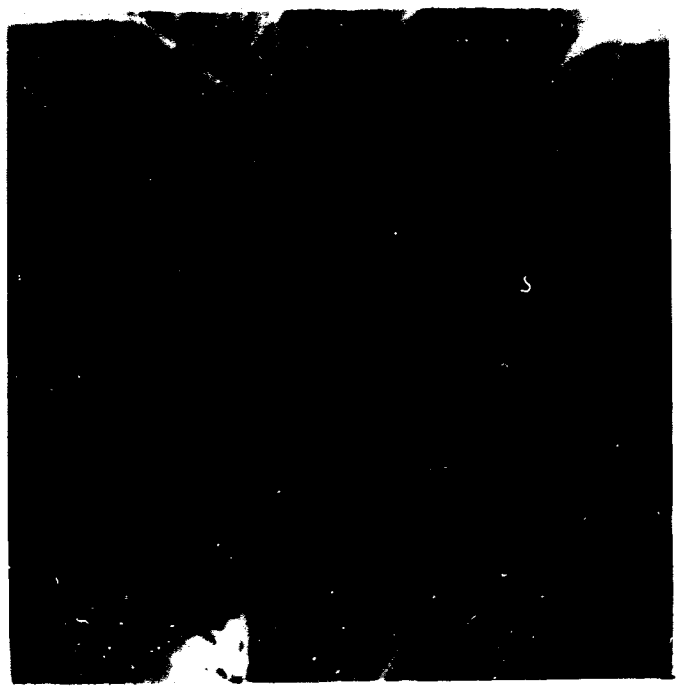

Black lines in upper left corner are random breaks in the replica.

The highlighted irregular line of relief from the lower center upward is one of the most pronounced items of relief observed in the replicas of the polished feldspar.

Figure 13. Electron micrographs, 5600X, polished feldspar

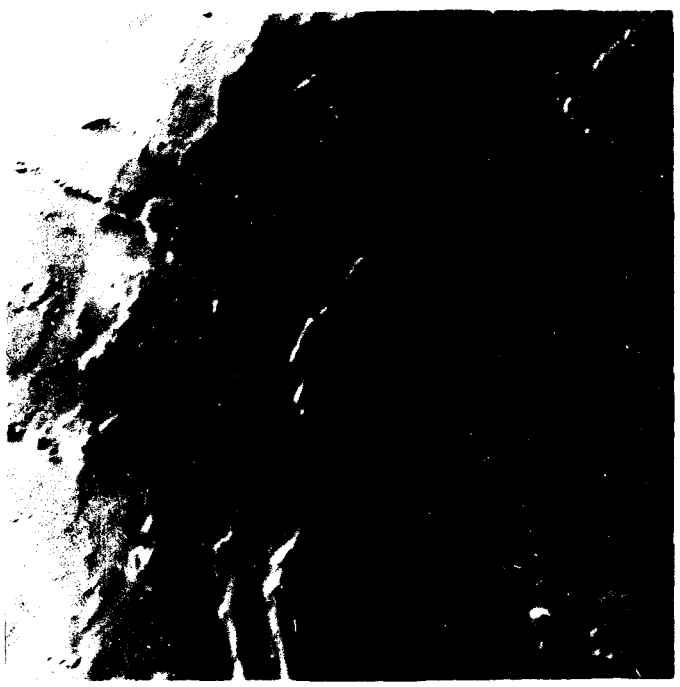

in lieu of the transverse glass wafer. The tendency of these specimens to fail by mortar fracture, without failure at the aggregate surface, is noted in the second paragraph above. It was observed that the tensile test values determined by breaking these specimens were in general disproportionately high as compared with the values determined by breaking the specimens with the transverse glass wafer. To provide data on the effect of orientation of the aggregate surface as cast, a supplemental series of specimens was prepared in which the prism of the tensile test specimen was vertical as cast. The two ends of the specimen were cast on successive days, so that the freshly placed cement mortar rested on the aggregate surface in each case. Because of the above noted tendency of the earlier specimens to break in mortar tension other than at the aggregate surface, this supplemental series was tested when the mortar last placed was three days old. Care was taken that the tests were conducted within an hour, more or less, of 72 hr. from the time of placing the last mortar, which was in turn placed 24 hr. from the time of placing of the initial mortar of the specimen. The test results of this supplemental series are shown in Table 9.

Table 9. Supplemental tensile test series (3-4 day strengths, glass aggregate)

Surface angle	Mortar-aggregate Strength at test σ, psi	τ, psi	Mortar tension P/A, psi	Modulus of rupture psi
Normal	146.76	--	146.76	677.02
				480.59
	109.73	--	109.73	391.28
				612.36
	183.10	--	183.10	590.48
				435.68
Ave.	146.53		146.53	531.24
30° to N	74.35	42.93	99.14	494.73
				838.10
	144.27	83.30	192.37	425.42
				618.76
	68.92	39.79	91.89	553.80
				526.82
Ave.	95.85	55.34	127.80	576.10
60° to N	50.31[a]	95.80[a]	221.25	862.76
				475.48
	32.10[a]	55.60[a]	128.39	624.96
				619.76
	48.77[a]	69.52[a]	195.08	695.52
				472.50
Ave.	43.73	73.64	214.91	625.16
Glass marble	184.60[b]	--	184.60	461.04
				440.64
	105.25[b]	--	105.25	489.30
				451.14
	242.21[a,b]	--	242.21	393.90
				440.96
Ave.	177.35		177.35	446.26

[a]Fracture by mortar tension, stresses calculated for aggregate surface

[b]Average tensile stress in prism section

INDEPENDENT DATA

Independent data of value in checking the hypothesis advanced above were published by Thorvaldson (25b), in a paper concerned with the effect of chemical nature of aggregate on strength of steam-cured Portland cement mortars. The data reported in this publication are based on tests of mortar tension briquets made with pure mineral aggregates. Specimens containing each mineral investigated were tested after damp storage for 52 hr., damp storage for 24 hr. followed by autoclave at 150° C. for 24 hr. with test at 52 hr., and damp storage for 52 hr. followed by water cure for 14 months. Thorvaldson's pure mineral test data (Table 1, 25b, p. 774) are reproduced as Table 10.

Table 10. Tensile strengths (psi) of briquets made with various minerals as aggregates (1:4 by volume) (Thorvaldson's data)

Aggregate	Formula	Stored in damp closet 52 hr.		In damp closet 24 hr.; in autoclave at 150° C. 24 hr.; broken at 52 hr.		In damp closet 52 hr.; in water 14 months	
Rose quarts	SiO_2	92		515		340	
Smoky quartz	SiO_2	84	87	540	545	360	370
Milky quartz	SiO_2	85		575		410	
Flint	SiO_2	98		660		485	
Quartzite	SiO_2	90		740		410	
Chert	SiO_2	110		815		580	
Marble	$CaCO_3$	78		90		370	
Magnesite	$MgCO_3$	155		585		730	
Barite	$BaSO_4$	105		155		340	
Chromite	$FeCr_2O_4$	103		200		460	
Ilmenite	$(FeTi)_2O_3$	90		190		435	
Hematite	Fe_2O_3	108		205		570	
Cyanite (kyanite)	$Al_2O_3 \cdot SiO_2$	84		205		415	
Sillimanite	$Al_2O_3 \cdot SiO_2$	128		290		655	
Wollastonite	$CaSiO_3$	74		155		445	
Chrysolite	$(MgFe)_2SiO_4$	88		185		355	
Nephelite	$NaAlSiO_4$	85		210		455	
Albite (Ab)	$NaAlSi_3O_8$	117		180		425	
Oligoclase	Ab_4An_1	50		235		460	
Andesine	Ab_3An_2	105		240		415	
Labradorite	Ab_1An_1	111		210		405	
Bytownite	Ab_1An_3	95		235		435	
Anorthite (An)	$CaAl_2Si_2O_8$	--		--		--	
Anorthoclase	$(Na, K)AlSi_3O_8$	70		150		360	
Microcline	$KAl\ Si_3O_8$	90		105		450	

DISCUSSION OF RESULTS

Tensile Strength Test

The mortar-aggregate tensile test strengths of Table 5 are shown graphically for each aggregate material in Figures 14 through 22. These data show a substantial range of values for individual specimens of the same test conditions. Several factors contribute to this variation, some of which also affect the test results for the modulus of rupture.

The aluminum foil used for a bond break mold lining was observed to have an effect upon some of the specimens. During the development of the pattern for the test specimen, several mold materials and methods of assembly were investigated. In all the problem of contamination of the surface of the aggregate wafer by oil from the molds was critical. Painting the surfaces of the molds with aluminum paint was tried, with initially good results. This favorable performance was attributed in part to the well known reactivity of aluminum with Portland cement. However, the effectiveness of the paint was rapidly lost. The use of aluminum foil, applied fresh for each specimen, was then tried. Reaction effects observed were limited to a few small gas

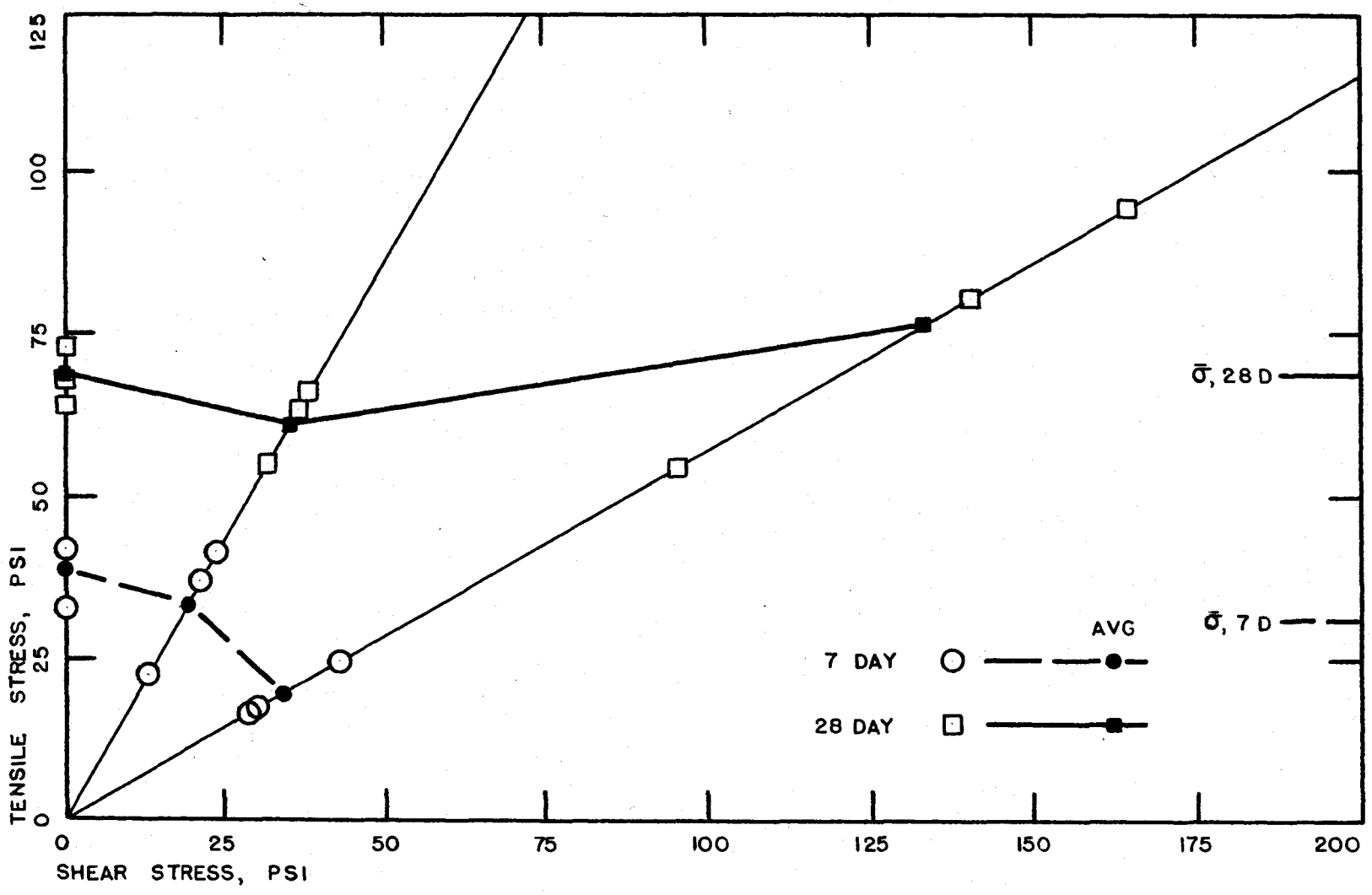

FIG 14 - TENSILE TEST STRESS COMPONENTS - SEPIOLITE

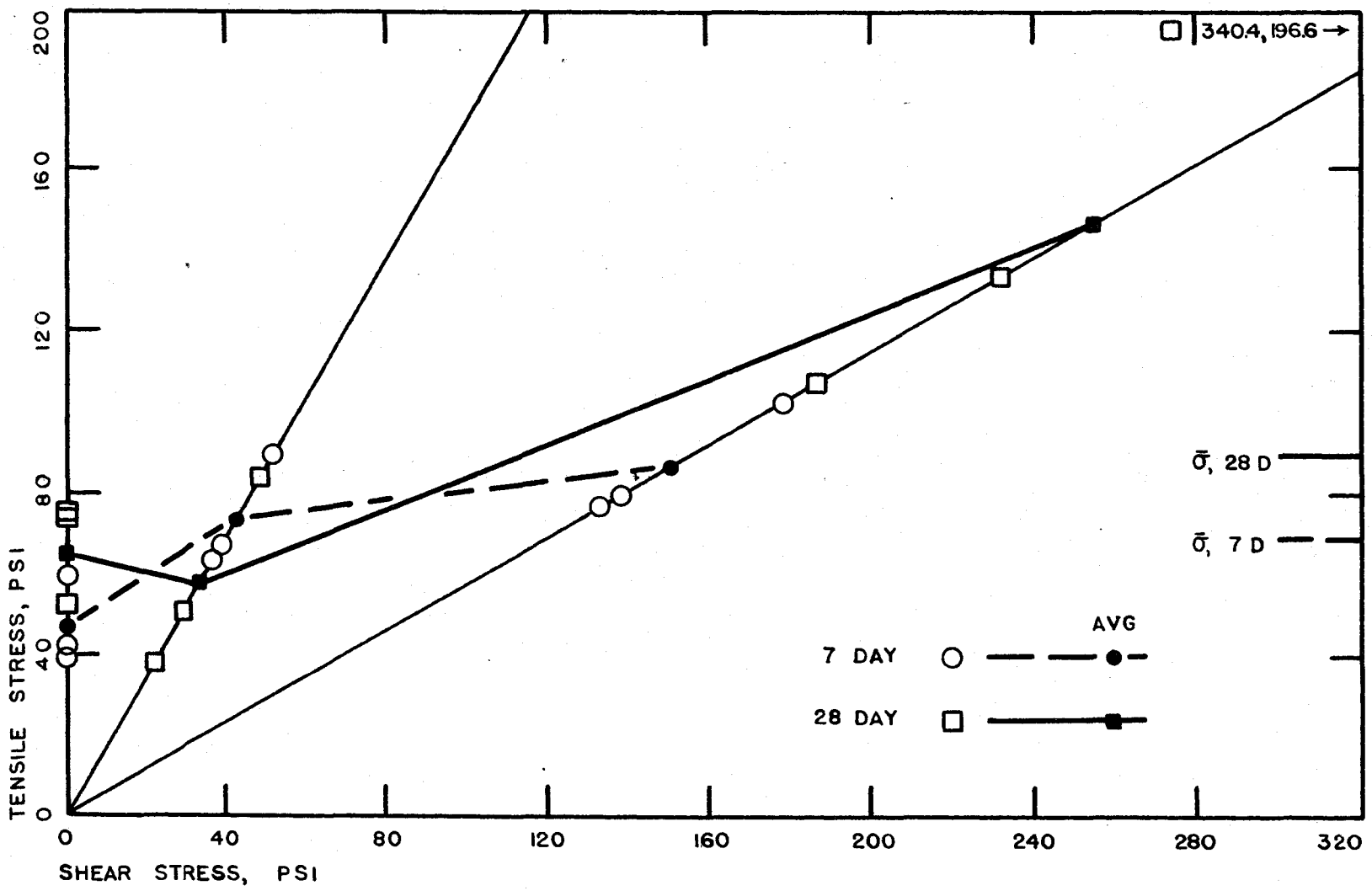

FIG 15 - TENSILE TEST STRESS COMPONENTS - MORTAR

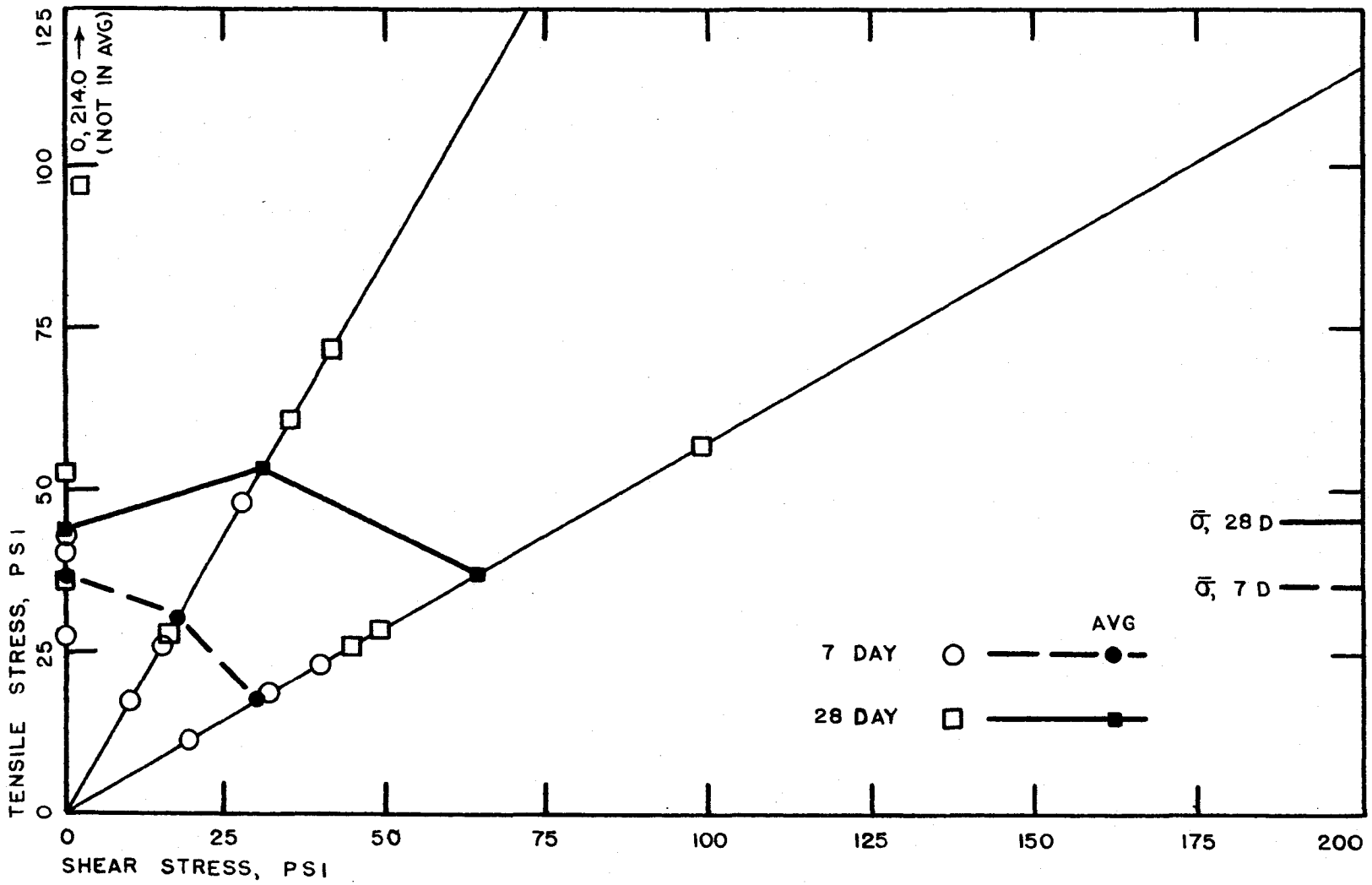

FIG 16 - TENSILE TEST STRESS COMPONENTS - GLASS

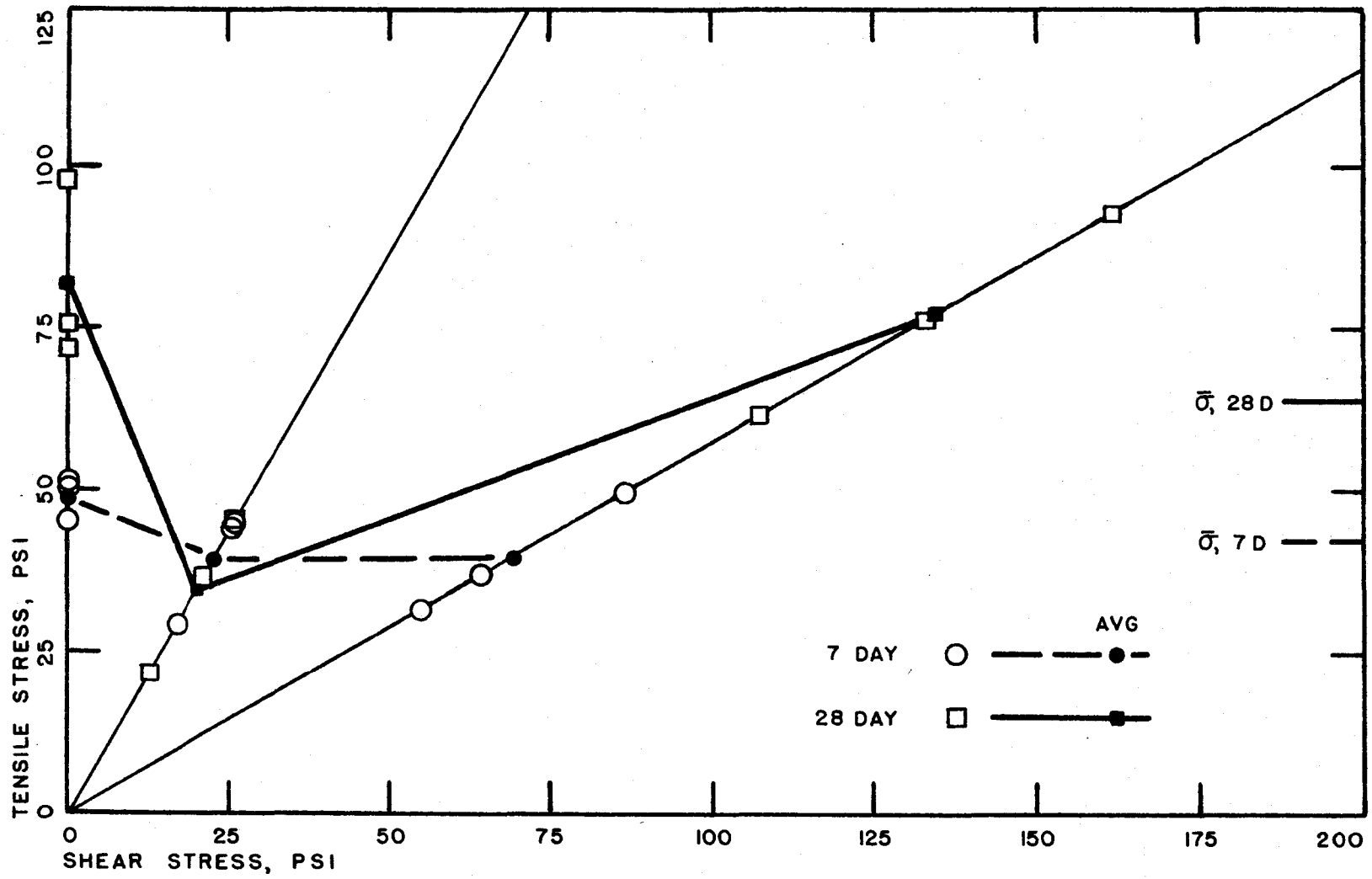

FIG 17 - TENSILE TEST STRESS COMPONENTS - CALCITE

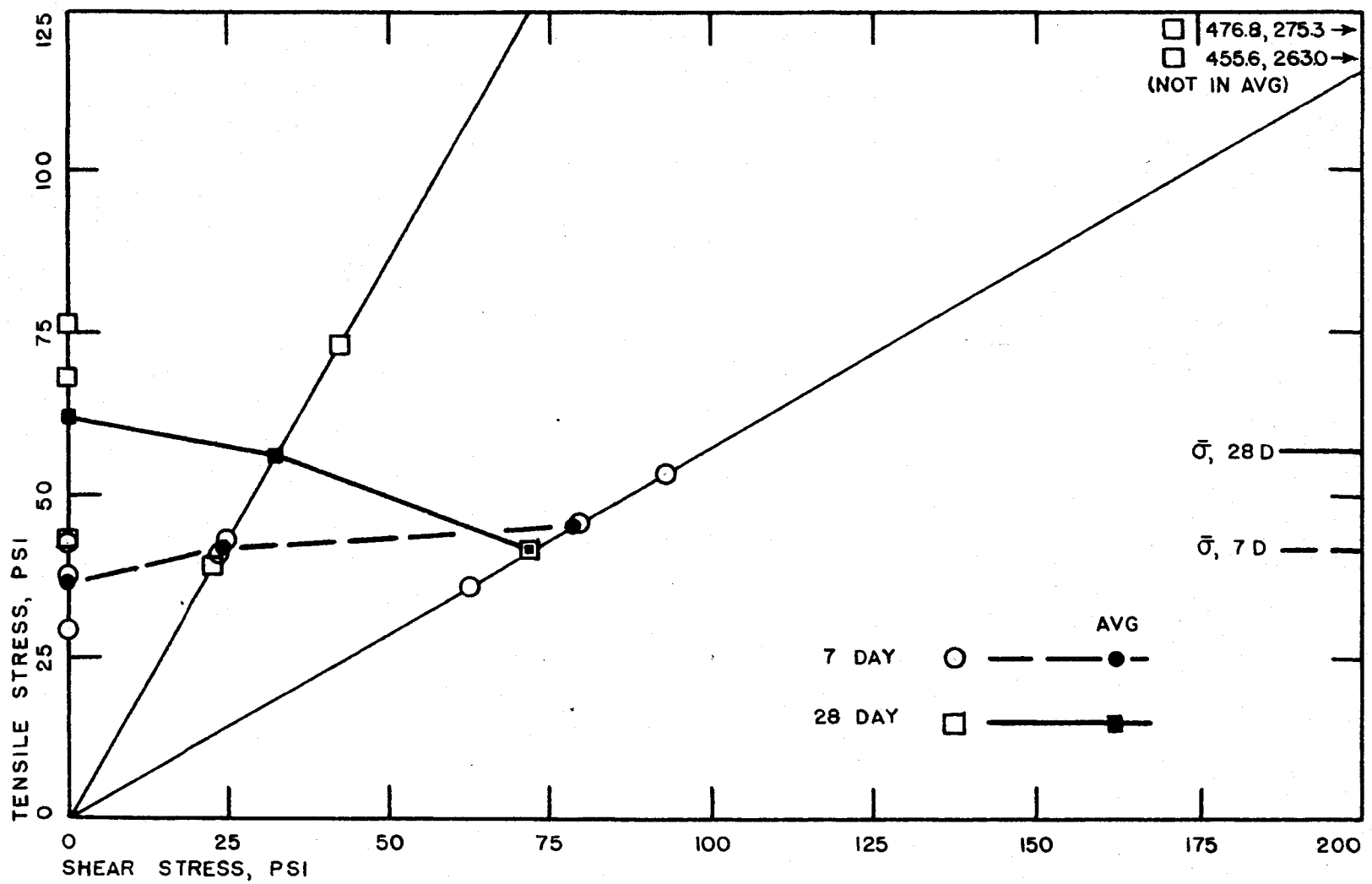

FIG 18 - TENSILE TEST STRESS COMPONENTS - CHERT

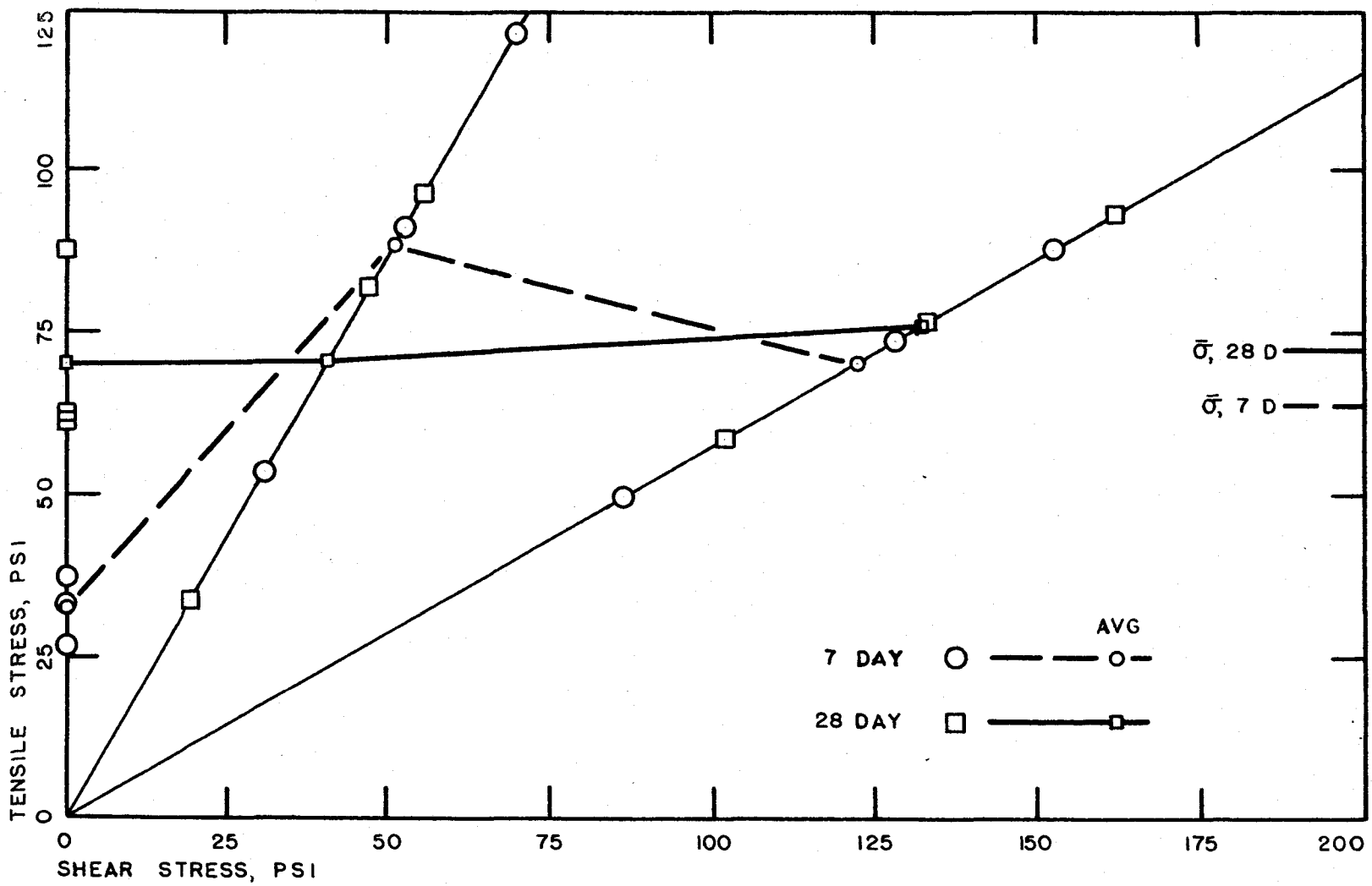

FIG 19 - TENSILE TEST STRESS COMPONENTS - FELDSPAR

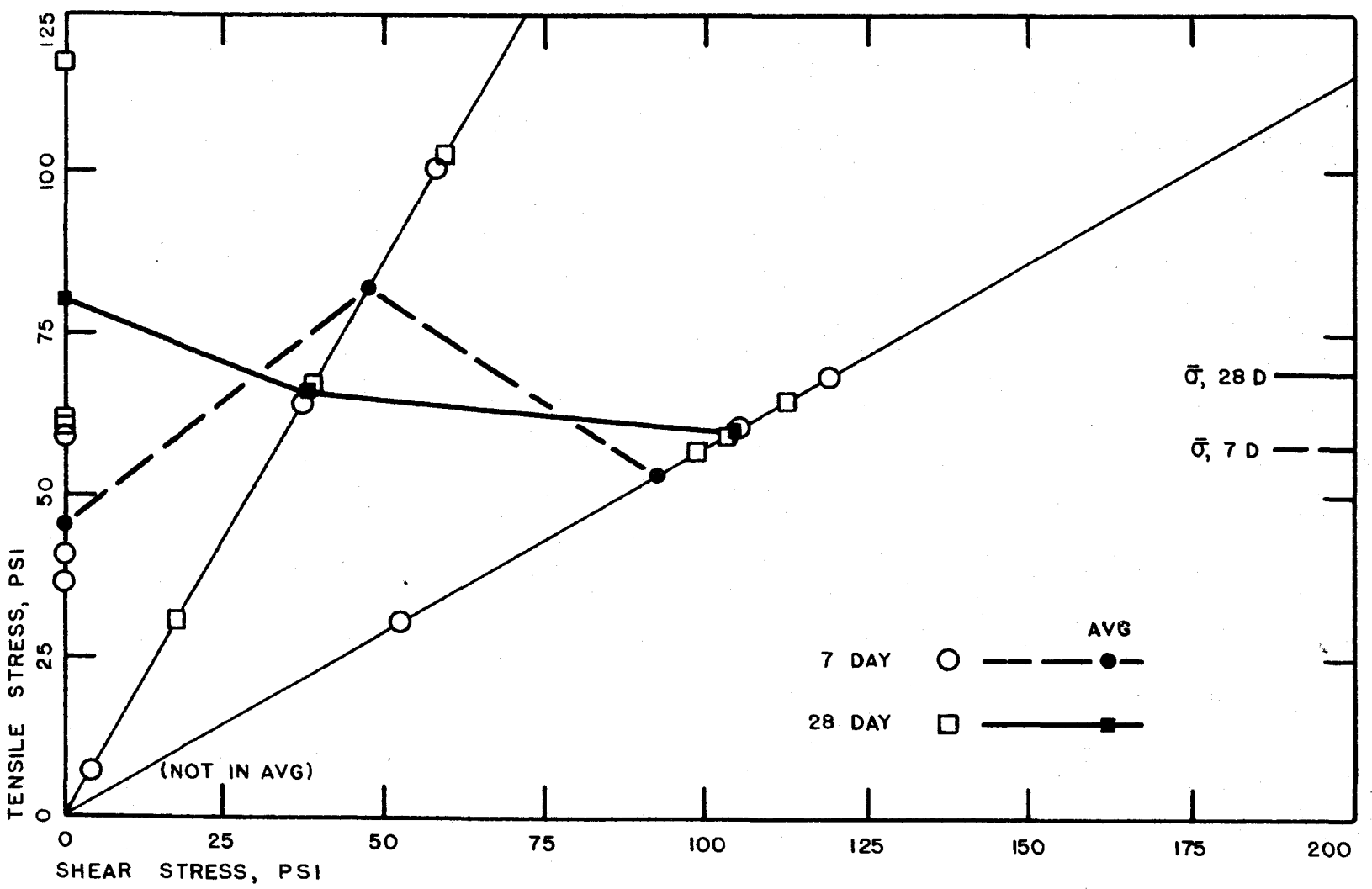

FIG 20 - TENSILE TEST STRESS COMPONENTS - QUARTZ

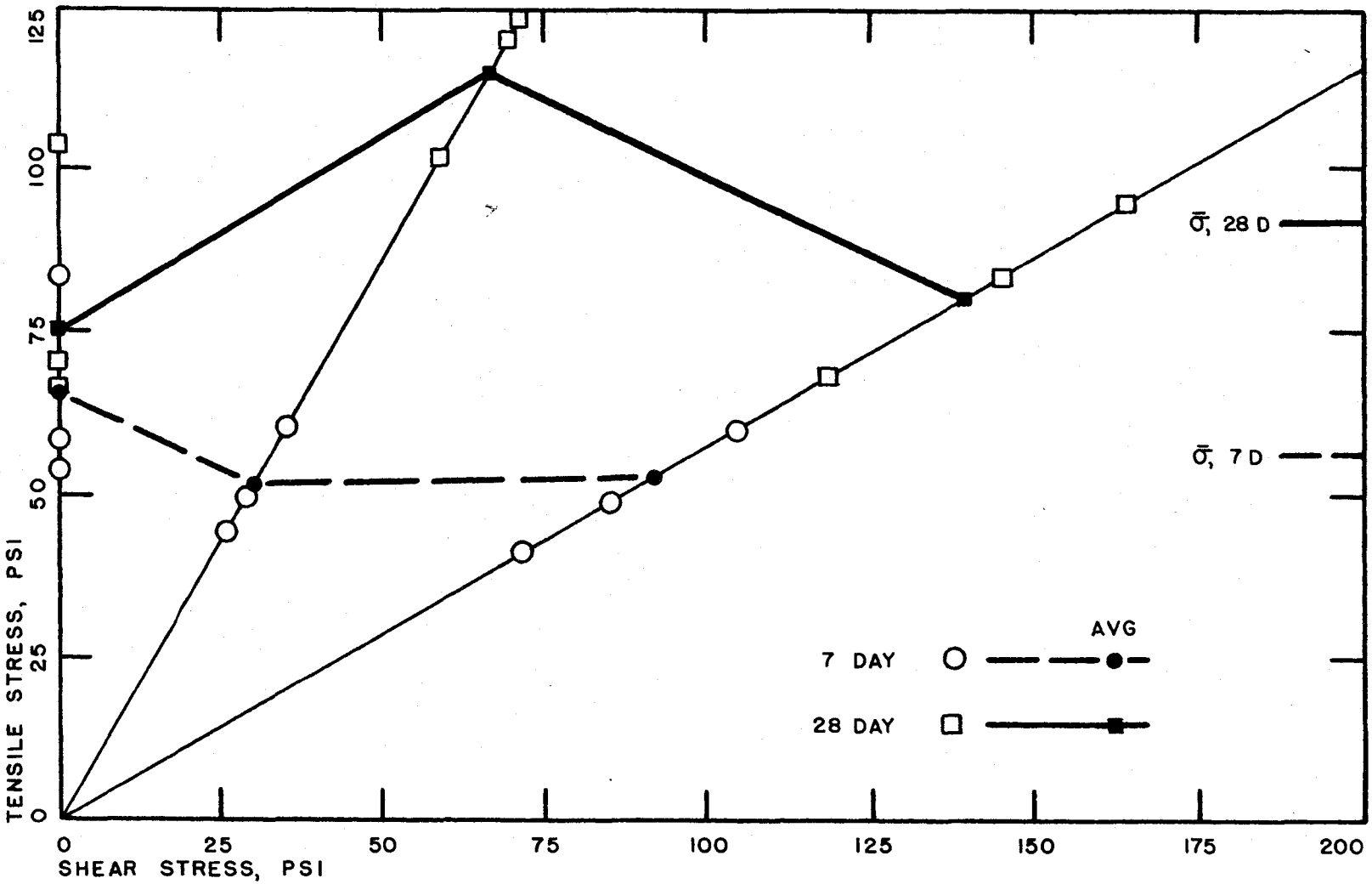

FIG 21 - TENSILE TEST STRESS COMPONENTS - BERYL

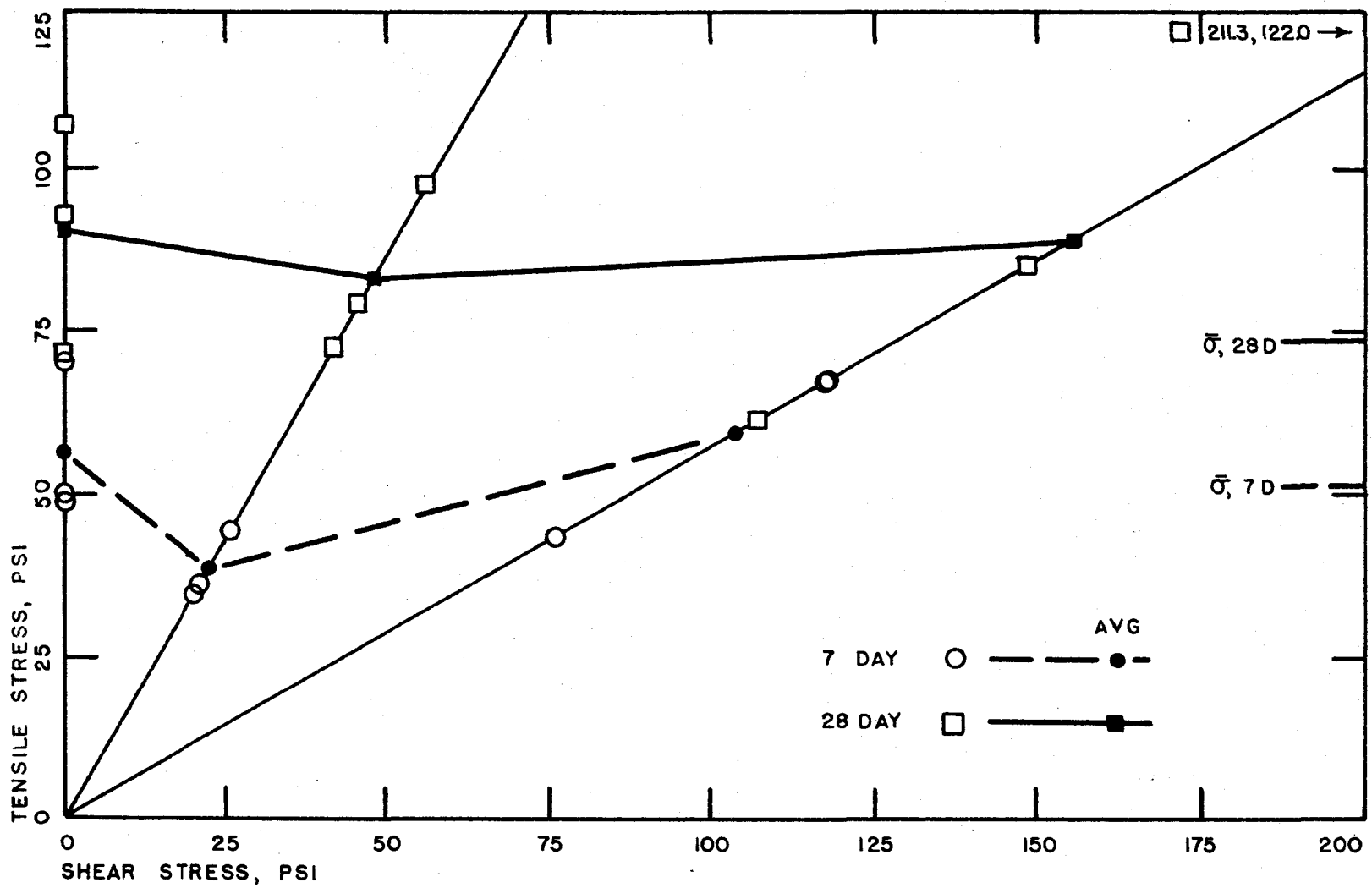

FIG 22 - TENSILE TEST STRESS COMPONENTS - SPODUMENE

bubbles on the specimen surface. On the basis of these preliminary results, this method was adopted. Moist room temperatures during these exploratory tests, made in March and April, 1956, were from 19° to 20° C.

During the course of the summer, temperatures in the moist room, which were controlled manually by adjusting the volume of the spray, were observed to increase to the general range of 21° to 22° C. Variations in water system pressure, or other causes, led to low volume of spray which in four instances permitted temperatures to rise to 24° or 25° C. In each of these instances evidence of increased reaction rate between the aluminum mold lining and the neat cement paste was observed. In one case a noticeable curvature of the prism section of the specimen was developed. Substantial bubble formation on the aluminum-mortar surface was developed, and planes of weakness were formed in the mortar briquet. These led to failure at relatively low values of the modulus of rupture when tested in flexure. Only rarely did this effect appear to influence the tensile strength results directly, but it does account for the lack of useful values of modulus of rupture for many of the specimens, and probably contributes to the large variation in tensile test results.

A second effect apparently arises from the orientation of the aggregate wafers as cast. Whereas the planes of

weakness of the briquet due to the aluminum reaction developed as tensile failures of the incompletely hardened paste, leading to fine cracks across the tops of the specimens, a different phenomenon was observed on the wafer surface. This surface tended to be well bonded across the top of the specimen, but to be poorly bonded, to the point of displaying a film of water, across the lower part of the aggregate wafer surface. The observation of this condition, together with the disproportionately high bond strength developed around the glass marbles, as noted earlier, suggests that a film of water forms on the vertical, smooth surface of the aggregate wafer, and effectively prevents the development of normal bond strength. In some specimens with no free water on the exterior surface, the freshly fractured mortar-aggregate surface would actually release a small drop of water which would run down and drip off of the specimen. No rational explanation is offered for this behavior. It was not observed in the supplemental tensile test series of Table 9, in which the aggregate surface formed the bottom of the mold cavity.

The use of kerosene as the lubricating coolant for the diamond saw on which the aggregate wafers was cut probably had a detrimental effect on the bond strength. Specimens as cut were rinsed in carbon tetrachloride, dried, rinsed in acetone, dried, and placed under water for at least an hour,

generally longer, prior to placing in the mold. Particular care was taken that the more absorbent materials were thoroughly saturated, surface dry at the time of placing the mortar. In addition to the above cleaning procedure, the highly absorbent sepiolite was boiled in carbon tetrachloride to remove all traces of oil. All traces of odor were eliminated, but a light buff staining persisted.

In working with the feldspar wafers, preparing replicas from which the electron micrographs of Figures 11 to 13 were taken, there was evidence that the oil film was not completely removed, even after further scrubbing with detergents. It is accordingly considered probable that traces of oil have contributed to strength variation.

As indicated in Figure 9, the edges of the aggregate wafer extend somewhat beyond the face of the prism section of the tension specimen. This extending portion of the aggregate wafer fits into a slot in the side of the mold, and the wafer is wedged into this slot to hold it in proper alignment during the casting of the mortar. Some irregularity in the thickness of the wafers, and, in a few cases, of the surface smoothness, caused some variation in the surface of the hardened mortar in this region. A reasonably clean, true edge was usually obtained, but in several cases a substantial fillet of mortar was formed between the planes of the specimen side and of the extended surface of the

aggregate wafer. While believed to be minor, these variations probably affected strength values to some extent.

Two other sources of possible variation are the water and the direct effect of curing temperature on strength. Tap water was used. While impurities are measured in parts per million, it is nonetheless possible that variations in the water supply might affect the test results. Somewhat more probable variation in strength might be expected from the 4° to 5° C. variation in curing temperature observed during the course of the test program. This variation was never sudden enough to develop thermal effects, but could have affected strength gain appreciably.

Finally, all test data, from Tables 5, 6, 8, and 9, are the results of tensile tests of brittle materials. Such materials are especially susceptible to stress concentration factors, of whatever cause, and, under tensile test, have no opportunity to fail progressively and adjust to localized excessive stress. Several of the possible sources of variation mentioned above not only vary the effective strength, but introduce stress raisers as well. The variation is then considered to be downward from a true value, rather than about a true value.

Four of the sets of tensile test stress components listed in Table 5 are omitted from the average values, as indicated by footnote. One glass specimen, 28 days old,

with the aggregate wafer normal to the applied load, and two chert specimens, 28 days old, with the aggregate wafer inclined 60° to the normal, gave test results so much higher than the rest of the specimens for these materials as to indicate that a different order of bond strength was involved. One quartz specimen, 7 days old, with the aggregate wafer inclined 30° to the normal, gave a test result so low as to indicate some sort of serious experimental error.

However, it is considered fortunate, in one respect, that the effective bond strength was so sharply reduced throughout the test program. While the variation is serious, and in no way minimized, it is believed that the common pattern among all nine aggregates, excepting only the results of seven day tests on the sepiolite and glass, is sufficiently well defined to support the conclusion that mortar-aggregate bond strength follows the general pattern of the maximum normal stress theory, or Rankine's theory of failure. Failure takes place at a limiting value of the tensile stress on any plane. When the bond strength achieves more normal values as, for example, in the supplemental tensile test series of Table 9, the specimen fails in mortar tension before the tensile stress across the aggregate-mortar surface reaches the limiting value, if the angle of inclination of the aggregate-mortar surface is such that the tensile component of applied stress is small. All three of

the specimens of the supplemental series in which the aggregate wafer was inclined 60° to the normal failed in mortar tension, as indicated in the footnote to Table 9. The tensile test values are not, in this case, breaking strengths.

On the basis of this observation, the average tensile stress of each of the aggregate materials, as indicated in Table 5 for 7 and for 28 days, is taken as the significant aggregate-mortar bond strength.

Oxygen Numbers

Chemical compositions of the aggregate materials are shown in Table 11. The chemical compositions of the pure minerals are taken from Winchell (29), except that for sepiolite, which is taken from Marshall (19a). It is estimated that the perthitic intergrowth present in the feldspar amounts to 5 per cent, as indicated. The oxide analysis of the mortar specimens consists of the cement composition as furnished by the manufacturer, with 16.7 per cent of the mortar weight as combined water (20 per cent of the cement weight). This percentage is based on results reported by Bogue (4, p. 529), indicating about 24 per cent water at complete hydration. The oxide analysis given for the glass is that of Experimental Glass No. 7, Table 3.7, Philips (22,

Table 11. Chemical compositions of aggregate materials, oxygen atom numbers, and percentages ionic character bonding

Material	Chemical composition	Millions of oxygen atoms per sq. μ	Percentage ionic character bonding
Sepiolite	$(OH)_2Mg_5Si_8O_{20}\cdot 8H_2O$	3.72	37.60
Mortar	SiO_2 - 22.3% Al_2O_3 - 4.4% Fe_2O_3 - 3.5% MgO - 2.4% CaO - 64.1% SO_3 - 2.1% 98.8% H_2O - 16.7% of mortar	6.10	49.16
Glass	SiO_2 - 73.8% Na_2O - 10.5% CaO - 7.0% ZnO - 5.0% Al_2O_3 - 3.5%	12.40	42.20
Calcite	$CaCO_3$	13.75	38.72
Chert	SiO_2	14.25	37.32
Feldspar	$K(Si_3Al)O_8$ - 95% $Na(Si_3Al)O_8$ - 5%	12.38	44.77
Beryl	$Be_3Al_2Si_6O_{18}$	14.98	41.29
Spodumene	$LiAlSi_2O_6$	17.11	45.40

p. 54), the composition of which is characteristic of ordinary commercial lime-soda glass.

Gram molecular weights were computed for the various materials. The water of crystallization of sepiolite was included. Equivalent values were computed for the glass and for the mortar on the basis of the oxide compositions. The water of hydration of the cement was included in the equivalent gram molecular weight computed for mortar. It is considered that in the hardened water-cement paste this amount of water is bound in a manner at least analogous to the water of crystallization of natural minerals.

The gram molecular weights were divided by the specific gravities to determine the equivalent volumes. From these volumes the numbers of oxygen atoms per unit volume were computed using Avogadro's number. These were then converted to numbers of oxygen atoms per square micron of surface by calculating the number contained in a volume one micron square and 2.8 Å thick. This last dimension is the approximate diameter of the oxygen ion as it occurs in crystalline minerals. The diameter has been determined by Bragg (5) as 2.64 Å. The slightly larger value was used for these calculations because the oxygen sheets of mineral lattices are subject to slight distortions on account of the varying sizes of the other atoms with which they are combined in making up the crystal structure. For example, the different

sizes of the silicon and aluminum ions in their respective tetrahedra produce different amounts of spreading of the oxygen ions which form the corners of the tetrahedra, leading to minor variations in the generally plane surfaces of the crystal. The dimension used above will enclose essentially all of the volume of the oxygen atoms of such an oxygen sheet.

Finally, the percentage of ionic character bonding of the various materials was computed, using the electronegativity values of Table 1 in equation (2). Equation (2) contemplates diatomic compounds; for the more complex compounds of these materials, the average electronegativity of the cations was computed, following the procedure indicated by Eitel (12). For the glass and mortar, the percentages were computed for each oxide, and then combined as a weighted average.

Values for millions of oxygen atoms per square micron of surface, and for percentages of ionic character bonding, are included in Table 11.

The percentages of ionic character bonding were applied to the numbers of oxygen atoms per square micron to arrive at values designated as effective oxygen ions per square micron. It is assumed that the remainder of the oxygen atoms are bound by covalent forces, which then gives the values designated as effective valence oxygen per square

micron. These three oxygen numbers for the various aggregate wafer materials are shown in Table 12.

The rates of absorption of Table 7, in hundredths of a gram per square centimeter in 60 sec., are repeated for ready reference in Table 12.

The average tensile strengths for each aggregate wafer material, as shown in Table 5 for 7 and for 28 day tests, are also repeated for ready reference in Table 12. An additional strength value, the gain in strength from 7 to 28 day tests, is shown.

The three oxygen numbers described above were also computed for the pure mineral aggregates of Thorvaldson's test data (26), as reproduced in Table 10 above. Flint, quartzite, and chert were omitted, since these materials, while essentially pure chemically, have a wide variation in physical arrangement. Magnesite and sillimanite were omitted since, in response to a discussion by Munger, the author has noted that both of these materials are cryptocrystalline, with varying amounts of impurities. The oxygen values for the minerals studied are shown in Table 13.

For ready reference the applicable strength values of Thorvaldson's data are also repeated in Table 13. The three values given for the different quartzes in Table 10 are averaged in Table 13. The autoclave strength value for quartz, while shown, is omitted from subsequent consideration, since, in the author's closure to the original paper, it is

Table 12. Oxygen numbers, rates of absorption, and average tensile strengths

Material	Oxygen numbers millions per sq. μ			Rates of absorption hundredths of gm/sq cm/min	Average tensile strength, psi		
	Atoms	Effective ions	Effective valence		7 day	28 day	Δ 7-28 day
Sepiolite	3.72	1.40	2.32	4.41	31.02	68.82	37.80
Mortar	6.10	3.00	3.10	3.33	68.92	89.58	20.66
Feldspar	12.38	5.54	6.84	0.01	63.85	72.46	8.61
Glass	12.40	5.23	7.17	--	28.51	45.10	16.59
Calcite	13.75	5.32	8.43	--	42.52	64.39	21.87
Chert	14.25	5.46	8.79	0.66	41.22	56.95	15.73
Quartz	14.70	5.63	9.07	0.01	57.62	69.13	11.51
Beryl	14.98	6.19	8.79	0.01	56.66	91.77	35.11
Spodumene	17.11	7.77	9.34	0.18	51.55	87.85	36.30

Table 13. Oxygen numbers and tensile strengths (Thorvaldson's data)

Material	Oxygen numbers millions per sq. μ			Tensile strengths, psi				
	Atoms	Effective ions	Effective valence	52 hr. Control	52 hr. Autoclave	52 hr. & 14 month	Δ52 C to 52 A	Δ52 C to 14 mo.
Quartz	14.8	5.5	9.3	87	545[a]	370	—	283
Marble	13.7	5.7	8.0	78	90	370	12	292
Barite	12.5	5.4	7.1	105	155	340	50	235
Chromite	11.7	7.0	4.7	103	200	460	97	357
Ilmenite	12.3	7.5	4.9	90	190	435	100	345
Hematite	12.5	6.9	5.6	108	205	570	97	462
Cyanite	19.0	8.2	10.8	84	205	415	121	331
Wollastonite	12.7	6.6	6.1	74	155	445	81	371
Chrysolite	13.7	6.7	7.0	88	185	355	97	267
Nephelite	12.6	6.2	6.4	85	210	455	125	370
Albite	13.5	10.4	3.1	117	180	425	63	308
Oligoclase	13.4	9.5	3.9	50	235	460	185	410
Andesine	13.4	8.6	4.8	105	240	415	135	310
Labradorite	13.3	8.1	5.2	111	210	405	99	294
Bytownite	13.3	7.1	6.2	95	235	435	140	340
Anorthoclase	12.9	5.7	7.2	70	150	360	80	290
Microcline	12.3	5.5	6.8	90	105	450	15	360

[a]Value not included in calculations.

noted that unusual reaction products are formed when mortars containing quartz are autoclaved at 150° C. Two additional strength values are shown, the gains in strength from 52 hour control specimens to 52 hour autoclave specimens, and the gains in strength from 52 hour control specimens to 14 month specimens.

Correlations

Product moment correlations were computed between each of the oxygen numbers tabulated in Table 12, and each of the strength values. Multiple product correlations were also computed between each of the oxygen numbers, the rates of absorption, and each of the strength values, together with t values for the regression of strength on the oxygen numbers independent of the rates of absorption. These values are tabulated in Table 14(a) and 14(b).

Product moment correlations were also computed between each of the oxygen numbers tabulated in Table 13, Thorvaldson's data, and each of the strength values. These are tabulated in Table 14(c).

The product moment correlations of Table 14(a) are so low as to have no practical significance. For seven degrees of freedom (n-2 for two variates), Snedecor tabulates a minimum significant correlation coefficient of 0.666 (25a, Table 7.2, p. 125). None of this first group of values

Table 14. Product moment correlations and t values

Average tensile strengths	Oxygen atoms	Effective oxygen ions	Effective valence oxygen
(a) Oxygen numbers vs. average tensile strengths			
7 day	0.1187	0.2117	0.0499
28 day	0.0049	0.1155	-0.1387
Δ 7-28 day	-0.1586	-0.1066	-0.1900
(b) Oxygen numbers and rate of absorption vs. average tensile strengths ($ty_{1.2}$ values in parentheses)			
7 day	0.1258 (0.2037)	0.2997 (0.7300)	0.1376 (0.2449)
28 day	0.4925 (1.3121)	0.6599 (2.0636)	0.2862 (0.0272)
Δ 7-28 day	0.6651 (1.7793)	0.6598 (1.7452)	0.5818 (1.3121)
(c) Oxygen numbers vs. tensile strengths (Thorvaldson data)			
52 hr. control	-0.1105	0.1571	-0.2516
52 hr. autoclave	0.1496	0.6105	-0.3561
52 hr. + 14 month	-0.2300	0.2792	-0.4071
Δ 52 C - 52 A	0.2042	0.5396	-0.2503
Δ 52 C - 14 m	-0.1797	0.2283	-0.3258

approaches this minimum.

The multiple product correlations of Table 14(b) approach significant values, particularly the correlations between the effective oxygen ions and the 28 day average tensile strengths, and the gains in strengths from 7 to 28 days; and between the oxygen atoms and the gains in strength from 7 to 28 days. These values are 0.6599, 0.6598, and 0.6651, respectively. For six degrees of freedom (n-3 for three variates), Snedecor tabulates a minimum significant multiple correlation coefficient of 0.795 (25a, Table 13.5, p. 214). The correlation between the effective valence oxygen atoms and the gains in strength from 7 to 28 days, 0.5818, is large enough to be of slight significance.

The multiple product correlations of the previous paragraph all reflect not only the effect of the oxygen numbers, but also the effect of the rates of absorption. In order to separate these two variables, the t values of Table 14(b) were computed to test the significance of the oxygen numbers alone, in each case. For this check only the relationship between the effective oxygen ions and the average tensile strength at 28 days approaches significance. For six degrees of freedom Snedecor tabulates a minimum significant t value of 2.447 (25a, Table 3.8, p. 55), against which the t value noted is 2.0636. The t values for oxygen atoms and for effective oxygen ions, both

compared with the gains in strength from 7 to 28 days, 1.7793 and 1.7452, respectively, are large enough to be of slight significance.

Most of the product moment correlations of Table 14(c) are so low as to be of slight if any significance. However, values for correlation between effective oxygen ions and strengths at 52 hours with autoclave, and gains in strength from 52 hour control to 52 hour with autoclave, 0.6105 and 0.5396, respectively, are within the range of significance. For 14 degrees of freedom (n-2), Snedecor tabulates a minimum significant correlation coefficient of 0.497 (25b, Table 7.2, p. 125). The correlation between effective valence oxygen atoms and strengths at 14 months, -0.4071, is large enough to be of some significance.

Snedecor (25a) places the minimum significant value of the correlation coefficient or of the t value at that corresponding to the 5 per cent level under the conditions investigated. Thus samples having the indicated correlation or t value would be expected to occur only once in twenty trials if taken from a random population in which there were actually no correlation.

Thorvaldson's data, shown in Table 10, with the correlations among oxygen numbers and strengths as shown in Table 14(c), are in general comparable to the test data of this study. It is noted, however, that Thorvaldson's

specimen is a standard mortar briquet, containing aggregate in a matrix of water-cement paste. Its strength is therefore not only a function of the mortar-aggregate bond, but also of the cement paste strength. Results based on these data are thus subject to the qualification that, in addition to the direct effect of mineral composition on the strength of the bond, there may also be catalytic action between the aggregate and the water-cement paste. To the extent that such action has an effect upon the strength of the paste itself, it will have an unevaluated effect upon the correlations calculated as described above. It is suggested that this may account for the negative sign of the correlations between effective valence oxygen atoms and all strength values.

Based on the relatively favorable correlations obtained between the effective oxygen ion numbers and the various strength values, the strength data of Tables 12 and 13 are shown against the effective oxygen ion numbers in Figures 23 and 24, respectively. The open symbols of Figure 23 indicate the calculated average strengths. The broken lines connect points on the same abscissas whose ordinates have been calculated for the effective oxygen ion-average tensile strength plane. The values of the rates of absorption for the several points would be measured normal to the plane of the graph. The straight line for each

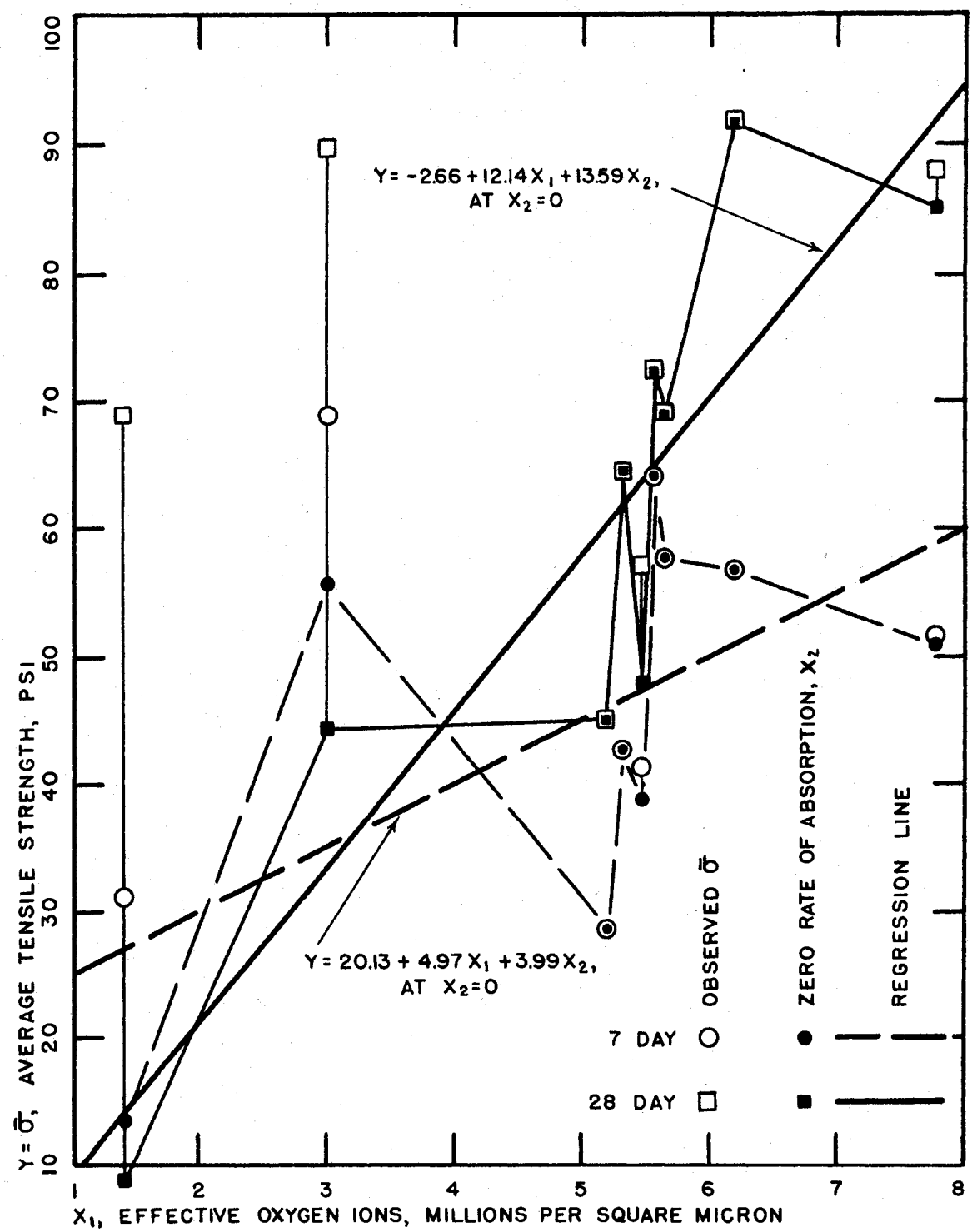

FIG 23 - EFFECTIVE OXYGEN IONS VS AVERAGE TENSILE STRENGTH

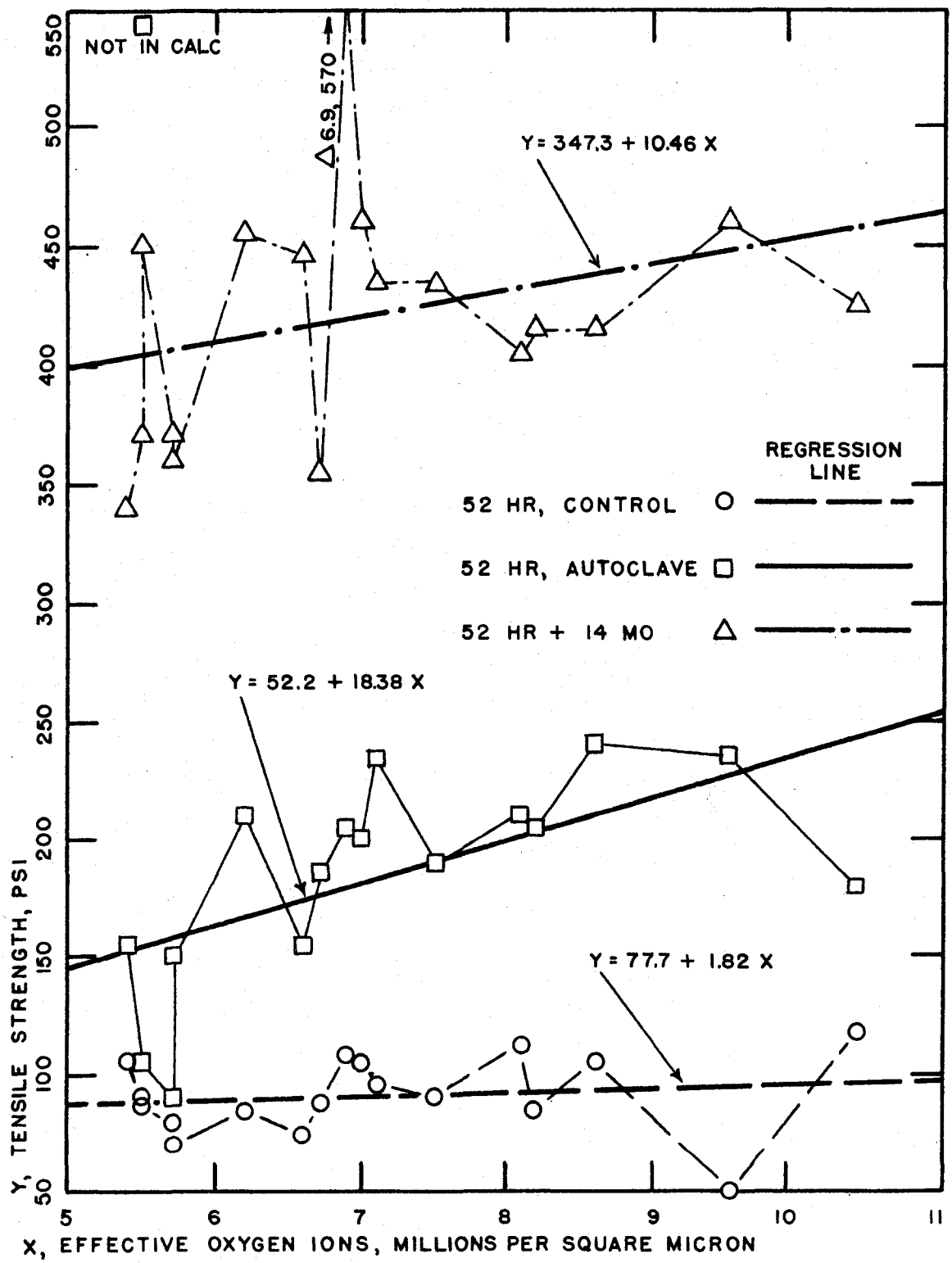

FIG 24 - EFFECTIVE OXYGEN IONS VS TENSILE STRENGTH (THORVALDSON'S DATA)

group of values is the trace of the calculated regression plane on the coordinate plane described above.

Figure 24, involving only two variates, is a simple two-dimensional representation. The straight lines are the calculated regression lines for each group of points.

Tensile Test Stress Component/Modulus of Rupture Ratio

The elongated prism section of the test specimens afforded an opportunity to evaluate the mortar strength of each specimen in flexure, which was intended as a basis of control for the correction of tensile test strengths in the event of curing variation. However, as noted above, a high proportion of these moduli of rupture were of no value due to the formation of gross flaws in the specimens. Hence no adjustment on the basis of such values was attempted. However, there were calculated ratios between the tensile test stress components and the moduli of rupture. These ratios were calculated for the flexure test results of the particular specimen involved where such results were available. In other cases, they were calculated on the basis of the root mean square value of the moduli of rupture for all useful values of the same age specimen. Averages of these ratios for the various aggregate materials and wafer orientations are tabulated in Table 15 and shown in Figure 25.

Table 15. Average tensile test strength/modulus of rupture ratios

Aggregate	Surface angle	7 day strength ratios		28 day strength ratios	
		σ/MR	τ/MR	σ/MR	τ/MR
Sepiolite	Normal	0.056	--	0.080	--
	30° to N	0.044	0.029	0.065	0.037
	60° to N	0.028	0.048	0.072	0.124
Mortar	Normal	0.055	--	0.066	--
	30° to N	0.096	0.056	0.060	0.034
	60° to N	0.107	0.186	0.105	0.182
Glass	Normal	0.048	--	0.043	--
	30° to N	0.044	0.025	0.052	0.030
	60° to N	0.022	0.038	0.038	0.066
Calcite	Normal	0.066	--	0.082	--
	30° to N	0.051	0.029	0.034	0.019
	60° to N	0.054	0.093	0.079	0.137
Chert	Normal	0.054	--	0.058	--
	30° to N	0.060	0.034	0.056	0.032
	60° to N	0.065	0.113	0.044	0.076
Feldspar	Normal	0.042	--	0.082	--
	30° to N	0.112	0.065	0.075	0.043
	60° to N	0.084	0.146	0.059	0.097
Quartz	Normal	0.059	--	0.082	--
	30° to N	0.091	0.053	0.064	0.037
	60° to N	0.066	0.115	0.059	0.102
Beryl	Normal	0.085	--	0.080	--
	30° to N	0.070	0.040	0.114	0.066
	60° to N	0.070	0.122	0.093	0.161
Spodumene	Normal	0.076	--	0.085	--
	30° to N	0.048	0.028	0.094	0.052
	60° to N	0.086	0.149	0.092	0.160

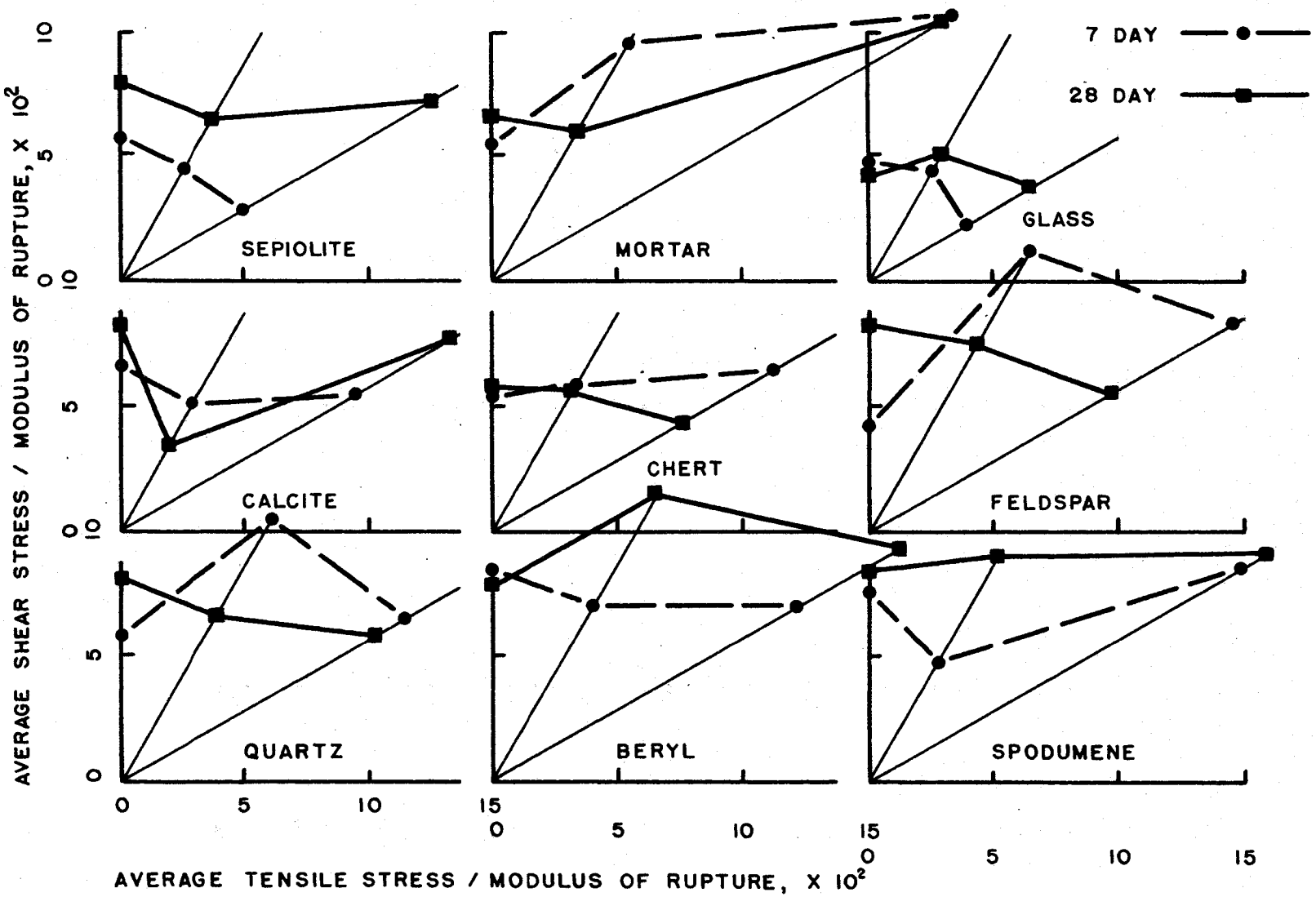

FIG 25 - AVERAGE TENSILE TEST STRENGTH / MODULUS OF RUPTURE RATIOS

Of the same general shape as the corresponding tensile test stress component graphs of Figures 14 through 22, the 7 and 28 day lines of Figure 25 are drawn together by the calculation of the ratio with the modulus of rupture, which later value appears to increase with time at approximately the same rate as the tensile test strength. The relatively uniform tensile strength value, independent of shear, as noted above, is also evident here. Another interesting pattern appears in these graphs. In the cases of mortar, chert, quartz, and feldspar the ratios at 28 days are distinctly lower than at 7 days. This indicates that early strength gain is more rapid for these aggregate materials. It was noted above, in discussion of Handy's hypothesis of bonding (13), that the crystal structures having a larger proportion of cations in the lattice would be expected to have a lower polarization screening effect, which would result in a more rapid early strength gain. It will be noted that the ratios for feldspar and quartz display this relative behavior. However, chert, quartz, and feldspar, all being tectosilicates, would, by this reasoning, all have higher polarization screening than the other materials, which contain more cations in their lattices. The effect of this consideration alone would be the opposite of that which is observed.

It is suggested that not only the number, but also the

character of the cations present is of great importance. In the tectosilicate lattices, the predominant cation is the silicon, with its fourfold, tetrahedral coordination. The silicon is replaced in this position, in the tectosilicates, only by the aluminum, in a similar coordination. As noted above, both of these elements have powerful bonds with oxygen. The other cations have relatively weaker bonds with oxygen.

The rapid early strength gain on the bond surface with the mortar wafer is perhaps due to the fact that the mortar of which the wafer was made was only a matter of weeks old, so that the cement of the wafer itself was still capable of developing bond linkages with the new gel structures of the fresh mortar.

One further observation is made. In the case of each of the three tectosilicates there is a distinct crossing of the 7 and 28 day lines. The same phenomenon, although not so distinct, is also present in the case of the mortar aggregate. No explanation for this pattern has been developed. It may not be significant, but its occurrence with each tectosilicate, and substantial absence in all other cases, is considered worthy of note.

Effect of Surface Smoothness

The bond strength developed on the polished feldspar surfaces averages just over three tenths of that developed on the sawn surface wafers at the same orientation. The tensile stress component averages almost 45 per cent of the average tensile stress component for all feldspar wafers with sawn surfaces. An examination of the electron micrographs of Figures 11 to 13 suggests a tentative explanation.

A brief outline of the technique of making these electron micrographs will assist in their interpretation. The original plate reacts under a real image of electron rays, which have been transmitted through the specimen. Since feldspar is not transparent to electron rays, the preparation of a replica is necessary. It was found that such a replica may be prepared using collodin. An initial, thin film of relatively dilute collodin is spread on the surface and allowed to dry to hardness. It is given a back up coat of a thicker collodin, which in turn is allowed to dry. The entire hardened collodin replica is then peeled off, using water which, due to its high wetting power on feldspar, assists in freeing the film. The collodin is then secured, replica side out, to a glass slide, and gold shadowed in vacuum from an angle of about 30°. The gold is in turn coated by a vacuum deposited layer of silica from an angle

of approximately 90°. The replica is then cut into pieces approximately one-sixteenth of an inch square, and the collodin is dissolved off in a solution of one part anhydrous ether to two parts absolute alcohol. There remains the gold shadow of the replica, which was a cast of the original surface, on a thin film of silica. This thin film is lifted from the ether-alcohol solution on a one-eighth inch circle of 200 mesh screen (74 micron opening). When dry, it is ready for insertion in the specimen holder of the microscope.

Thus the gold shadow is a negative picture of the replica surface, so that the negative of the image is a true picture of the replica surface. The figures have been printed from an intermediate negative film, so that they are true pictures also, of the replica surface. Depressions in the replica are protrusions on the original surface.

It must be noted that, although numerous replicas were examined in the selection of representative areas for micrographs, the entire area studied under these magnifications was really quite small, and represented only three separate sawed surfaces, and two separate polished surfaces. Thus to the uncertainties of visual interpretation there must be added qualifications concerning coverage.

The sawn surfaces were carefully aligned with the basal cleavage plane of the feldspar. Hence it is considered probable that the plane surfaces of the micrographs are

essentially cleavage planes. Their general appearance is consistent with this view. The sawn specimens are characterized by relatively wide steps, or shelves, with fracture surfaces, more or less vertical, between them. There is, in any one replica, a vague directional orientation of these fracture surfaces, suggesting that they may be related to the orientation of the specimen against the saw blade. Other than this, there is no evidence of saw marks. The polished specimens are characterized by a more uniform general surface, interrupted at numerous intervals by small mesa-like projections bordered by more or less vertical fracture surfaces, similar to but not as high as those separating the shelves of the sawn specimens. No directional pattern appears. There appears to be considerably less relief on the polished surface.

Thus it appears that, on the sawn surface, there is a considerable surface area approaching a perpendicular to the general surface. Any bonding developed on this surface would be able to resist a substantial stress normal to the general surface before the tensile stress across the inclined surface reached critical levels. Concurrently, exposed corners extend in more or less continuous lines for considerable distances across the mineral. Polarization and structural screening along such edges would be relatively ineffective, leaving a high potential demand for

chemisorption screening. In view of the discussion above, this chemisorption should promote bond strength gain.

On the other hand, the polished surface has relatively much less of this steeply inclined surface, and relatively fewer well defined edges. None of the edges on the polished surfaces was observed to extend for any appreciable distance across the mineral.

It is accordingly suggested that the improved bonding of the sawn surface is due to a larger proportion of favorably oriented surface, and to a structure favoring chemisorption, with resultant acceleration of bond strength gain.

Spherical Inclusion

The overall average modulus of rupture of the specimens of the supplemental tensile test series, Table 9, was computed at approximately 550 psi. By first entering Figure 7, Long et al. (18b), relationship of dynamic modulus of elasticity and flexural strength, and then Table 1, Long et al. (18b), listing a series of companion values of dynamic and static moduli of elasticity of concrete, the static modulus of elasticity of the mortar of these specimens was estimated at 3.33×10^6 psi.

Experimental Glass No. 7, referred to above as the basis for the oxide composition of the glass of Table 11,

is described by Philips (22, Table 4.1, p. 64) as having a modulus of elasticity of 7320 kg/sq. mm., or 10.40 x 10^6 psi. The ratio of the moduli of rupture of the glass and of the mortar is then approximately three. Entering Figure 3 of Edwards (11), for the stress at the pole of an ellipsoidal inclusion in a material subject to uniform axial tension parallel to the polar axis considered, and assuming that the values of Poisson's ratio are the same, this ratio of the shear moduli indicates a polar tension normal to the inclusion surface of approximately 1.40 σ_x, where σ_x is the value of the uniform axial tension at a distance from the inclusion. Applying this factor to the average mortar tension value computed for the supplemental test series specimens containing glass marbles, a tensile stress value of approximately 250 psi is indicated. This is a very rough approximation, since Edwards (11) develops his solution of the stresses around an ellipsoidal inclusion for the case of a finite inclusion in a uniform material of infinite extent, whereas the marble was approximately nine sixteenths inch in diameter (individual marbles varied slightly), and this spherical inclusion was contained in a prism only one inch square.

The magnitude of the variation between the average tensile stress for the specimens of the supplemental test series which failed on the aggregate wafer surfaces, 121.19

psi, and the tensile stress on the spherical inclusion, estimated at 250 psi, is so large as to indicate that the approximation noted above fails to yield useful values. The necessity for a greater ratio between specimen thickness and inclusion diameter is indicated. The effect of the inclusion is essentially nil at three diameters from its surface, in the case of an absolutely rigid inclusion, which suggests a minimum ratio of 7:1.

CONCLUSIONS

On the basis of the studies described and the experimental data reported, it is concluded that:

1. The Portland cement paste-aggregate surface fails in accordance with the maximum normal stress, or Rankine's theory of failure, at a limiting value of the normal tensile unit stress for each aggregate material.

2. The concentration of effective oxygen ions in the crystal structure of an aggregate has a significant effect on the bond strength between Portland cement paste and that aggregate.

3. The concentration of effective valence atoms of oxygen in the crystal structure of an aggregate has an observable effect on the bond strength between Portland cement paste and that aggregate.

4. The hypothesis of the mechanism of bond strength development through the progressive polymerization of ionic silicate groups on the surfaces of hydrating cement grains, aggregate particles, and spontaneous aggregations of colloidal size in the interstitial voids, together with the incorporation of calcium into calcium silicate hydrates, provides a coherent explanation of the data supporting conclusions 2 and 3.

RECOMMENDATIONS FOR FURTHER STUDY

In connection with further study relating to Conclusion 1, it is recommended that:

1. The study of tensile strength specimens in which an aggregate surface provides the sole stress transfer medium be continued. This will guard against possible catalytic side effects of the aggregate on the mortar, and limit the number of variables affecting specimen strength.

2. The tensile strength specimens be smaller. A cross sectional area of one square centimeter is considered adequate, and the provision of aggregate wafers will be much simplified.

3. The surface of the aggregate wafers be protected from all materials prior to placement of the mortar. In particular, the use of oil as a cooling lubricant for sawing should be avoided. Mold lubricants, skin oils, and other such substances should be kept from the aggregate surface.

4. The molds be designed to provide for uniform casting of the fresh mortar bearing down on the horizontal aggregate surface. This will tend to eliminate the effect of the adsorbed film of moisture observed in the specimens of the current study.

5. The use of vibration to consolidate the mortar be investigated. A low amplitude, moderately high frequency, obtainable by the use of solenoid powered equipment, is suggested as an initial possibility.

6. The molds be fabricated of metal not attacked by the cement mortar, and of sufficient rigidity to avoid distortion in use. This will tend to eliminate one of the more serious extraneous variables of the current study.

7. The general geometry of the tensile test specimen be retained. Casting the specimens on end as recommended above will permit the support of the aggregate wafer by a removable member in the initial mortar placement, obviating the need for notches in the mold walls to hold the wafer in place, and eliminating surface irregularity. The long uniform section will reduce stress concentration and provide the possibility of moduli of rupture tests for additional control.

8. The crystal orientation of the aggregate wafer be controlled, either through care in the orientation of monocrystalline aggregates, or through the selection of essentially random, fine grained microcrystalline aggregates. Ultimately the effect of variation of orientation in monocrystalline aggregates should be investigated.

9. The effect of aging of the aggregate surface prior to placement of mortar be investigated. Such aging should

take place in a variety of environments, including dry air, moist air, and vacuum, as preliminary suggestions.

10. The use of aggregate materials of appreciable porosity be avoided in planning investigations of other factors. This will tend to eliminate a potentially vexatious variable.

11. The effect of porosity upon the bond strength characteristics be investigated. Essentially pure limestones and cherts will provide wide ranges of porosity. Care must be taken to identify and evaluate side effects which are likely to accompany porosity in minerals such as, for example, prior ion adsorption.

12. The molding and storing of test specimens be carried on with materials and equipment meeting the requirements of ASTM Designation C 190-49, Test for Tensile Strength of Hydraulic-Cement Mortars (2, p. 188), or equivalent. This will tend to eliminate fortuitous variation.

13. The study of aggregate surfaces by high power microscopy be continued, both as control of surface smoothness, and as an aid to analysis. A variety of techniques are available in this field.

14. The applicability of sonic test methods to the study of bond strengths be investigated. The techniques of Long et al. (18b) are recommended as an initial approach.

15. The possibility of controlled reduction of the bond strength be investigated to permit development of critical normal tensile stress values before failure due to mortar tension, with substantial angles of inclination of the aggregate surface from the normal. Lea (17) reports reasonably consistent, reduced strengths upon regrinding hydrated cement. Dilution with non-reactive materials is an alternative possibility. Such methods would probably require reinforcement of the mortar.

16. The behavior of inclusions be studied under conditions more comparable to the usual assumptions of analytical studies. This would require small inclusions, or large mortar specimens.

In connection with further study relating to Conclusion 2, in addition to applicable comments above, especially 1, 8, 9, 10, 11, 13, and 14, it is recommended that:

17. The bond strength of the mortar-aggregate surface be determined at more frequent time intervals, especially during early ages. This will permit a more accurate evaluation of the time relationships of the various bonding effects.

18. The orientation of the aggregate wafers be restricted to that normal to the direction of the applied tensile force. This will further simplify the preparation of aggregate wafers, and will make casting of the specimens

less subject to variation.

In connection with further study relating to Conclusion 3, in addition to applicable comments above, especially 1, 8, 9, 10, 11, 13, 14, and 17, it is recommended that:

19. The zone structure of the aggregate crystals be analyzed. This will tend to restrict the study to materials of simple structure, but will be necessary for substantial progress in this area.

In connection with further study relating to Conclusion 4, in addition to applicable comments above, especially 1, 8, 9, 10, 13, 17, and 19, it is recommended that:

20. The study of aggregate surfaces recommended in 13 above be extended to include electron diffraction techniques. By careful examination of clean aggregate wafer surfaces, followed by similar examination of the same surface after fracture as a mortar-aggregate specimen, the identification of cement products involved and the checking of epitaxic structures may well be accomplished.

21. The formation of calcium silicate hydrate polymers be investigated by the application of thermodynamic principles, in extension of the work of M. von Glasenapp (27a, and in 12, p. 1217). The energy levels of the system should be affected by, and have an effect upon, the stability of the components and the hydration products.

22. The existence of colloidal analogues to Portland

cement paste among other types of materials, such as the organic gels, be investigated. The establishment of useful analogs of this type would be expected to accomplish great savings of time and effort in exploratory testing of hypotheses.

REFERENCES CITED

1. American Society for Testing Materials. 1930 Book of ASTM Standards, including Tentatives, Part II. The Society, Philadelphia. 1930.

2. _____. 1955 Book of ASTM Standards, including Tentatives, Part 3. The Society, Philadelphia. 1955.

3. _____. 1956 Supplement to Book of ASTM Standards, including Tentatives, Part 3. The Society, Philadelphia. 1956.

4. Bogue, Robert Herman. The Chemistry of Portland Cement, 2nd ed. Reinhold Publishing Corp., New York. 1955.

5. Bragg, Sir Lawrence. The Crystalline State--A General Survey. Vol. 1. G. Bell and Sons, Ltd., London. 1949.

6. Buckley, H. E. Crystal Growth. John Wiley & Sons, Inc., New York. 1951.

7. Cartmell, E., and G. W. A. Fowles. Valency and Molecular Structure. Academic Press, Inc., New York. 1956.

8. Coulson, Charles Alfred. Valence. Oxford University Press, London. 1952.

9. Dean, Robert B. Modern Colloids. D. van Nostrand Co., Inc., New York. 1948.

10. Desch, Cecil H. Discussion on the setting of cements and plasters. Trans. Faraday Society 14: 1-7, 67-69. 1919.

11. Edwards, R. H. Stress concentrations around spheroidal inclusions and cavities. J. Appl. Mech. 18: 19-30. 1951.

12. Eitel, Wilhelm. The Physical Chemistry of the Silicates. The University of Chicago Press, Chicago. 1954.

13. Handy, Richard L. Stabilization of Iowa loess with Portland cement. Unpublished Ph. D. Thesis. Iowa State College Library. Ames, Iowa. 1956.

14. Hauser, Ernst Alfred. Silicic Science. D. van Nostrand Co., Inc., New York. 1955.

15a. Houwink, R. Elasticity, Plasticity, and Structure of Matter, 2nd ed. Harren Press, Washington, D. C. 1953.

15b. Jeffery, J. W. The Crystal Structure of Tricalcium Silicate. Acta Cryst. 5: 26-35. 1952.

16. Kühl, Hans. Zementchemie in theorie und praxis. (Original not available for examination; English translation: Cement Chemistry in Theory and Practice, translated by J. W. Christelow. Concrete Publications, Ltd. London. 1931?

17. Lea, F. M. The Chemistry of Cement and Concrete, rev. ed. of Lea and Desch. St. Martin's Press, Inc., New York. 1956.

18a. Le Chatelier, Henri. Recherches experimentales sur la constitution des ciments et la theorie de leur prise. Compt. rend. 94: 867-869. 1882.

18b. Long, Bartlett G., Henry J. Kurtz, and Thomas A. Sandenaw. An instrument and a technic for field determination of the modulus of elasticity, and flexural strength, of concrete (pavements). J. Am. Conc. Inst. 16: 217-231. Jan. 1945.

19a. Marshall, C. Edmond. The Colloid Chemistry of the Silicate Minerals. Vol. 1, Agronomy Monographs. Academic Press, Inc., New York. 1949.

19b. Megaw, Helen D. The Structure of Afwillite, $Ca_3(SiO_3OH)_2 \cdot 2H_2O$. Acta Cryst. 5: 477-491. 1952.

20. Palache, Charles, Harry Berman, and Clifford Frondel. The System of Mineralogy of James Dwight Dana and Edward Salisbury Dana, Yale University, 1837-1892. 7th ed., Vol. 1. John Wiley & Sons, Inc., New York. 1944.

21. Pauling, Linus. The Nature of the Chemical Bond, 2nd ed. Cornell University Press, Ithaca, New York. 1942.

22. Phillips, C. J. Glass, the Miracle Maker. Pitman Publishing Corp., New York. 1941.

23. Seifert, H. Epitaxy. In Gomer, Robert, and Cyril Stanley Smith, eds. Structure and Properties of Solid Surfaces. pp. 318-372. The University of Chicago Press, Chicago. 1953.

24. Seitz, Frederick. The Modern Theory of Solids. McGraw-Hill Book Co., New York. 1940.

25a. Snedecor, George W. Statistical Methods. Collegiate Press, Inc., Ames, Iowa. 1937.

25b. Thorvaldson, T. Effect of chemical nature of aggregate on strength of steam-cured Portland cement mortars. Proc. Am. Conc. Inst. 52: 771-780, 1403-1413. 1955-56.

26. Trömel, G. Die Modifikationen des Kalziumorthosilikates Ca_2SiO_4. Naturwissenschaften 36: 88. 1949.

27a. von Glasenapp, M. Zur Petrographie des neuzeitlichen Portland-Zement-Klinkers. Zement 12: 133-136. 1923.

27b. Weiser, Harry Boyer. A Textbook of Colloid Chemistry, 2nd ed. John Wiley & Sons, Inc., New York. 1949.

28. Weyl, W. A. Wetting of solids as influenced by the polarizability of surface ions. In Gomer, Robert, and Cyril Stanley Smith, eds. Structure and Properties of Solid Surfaces. pp. 147-181. The University of Chicago Press, Chicago. 1953.

29. Winchell, Alexander N. Elements of Mineralogy. Prentice-Hall, Inc., New York. 1942.

30. Wyckoff, Ralph W. G. Crystal Structures. Vol. 1. Interscience Publishers, Inc., New York. 1948.

31. _____. The Structure of Crystals, Supplement for 1930-1934 to the Second Edition. American Chemical Society Monograph Series. Reinhold Publishing Corp., New York. 1935.

ACKNOWLEDGMENTS

The writer acknowledges with deep gratitude the counsel and encouragement of Dr. Glenn Murphy in the conduct of this study and in the presentation of the results.

The writer is also grateful to Prof. Charles M. Dodd, Professor and Head of Ceramic Engineering, for the use of that department's facilities, and for helpful advice; and to Dr. Percy H. Carr, Professor of Physics, for the use of the electron microscope, and for instruction and assistance in such use.